



(Chamier, 2014)

## Chapter 4

# Sensing by Acoustic Biosignals

**Abstract** After the interface between physiologic mechanisms and the resultant biosignals has been examined (Volume I), the subsequent interface between acoustic biosignals and the associated sensing technology is discussed here. A large variety of acoustic biosignals—permanent biosignals—originates in the inner human body, including heart sounds, lung sounds, and snoring sounds. These biosignals arise in the course of the body’s vital functions and convey physiological data to an observer, disclosing cardiorespiratory pathologies and the state of health. The genesis of acoustic biosignals is considered from a strategic point of view. In particular, the introduced common frame of hybrid biosignals comprises both the biosignal formation path from the biosignal source at the physiological level to biosignal propagation in the body, and the biosignal sensing path from the biosignal transmission in the sensor applied on the body up to its conversion to an electric signal. Namely, vibrating structures in the body yield acoustic sounds which are subject to damping while propagating through the thoracic tissues towards the skin. Arrived at the skin, different body sounds interfere with each other and induce mechanical skin vibration which, in turn, is perceived by a body sound sensor and then converted into the electric signal. It is highly instructive from an engineering and clinical point of view how sounds originate and interact with biological tissues. Discussed phenomena teach a lot about the physics of sound (as engineering sciences), and, on the other hand, biology and physiology (as live sciences). Basic and application-related issues are covered in depth. In fact, these issues should remain strong because these stand the test of time and mine knowledge of great value. Obviously, the highly interdisciplinary nature of acoustic biosignals and biomedical sensors is a challenge. However, it is a rewarding challenge after it has been coped with in a strategic way, as offered here. The chapter is intended to have the presence to answer intriguing “Aha!” questions.

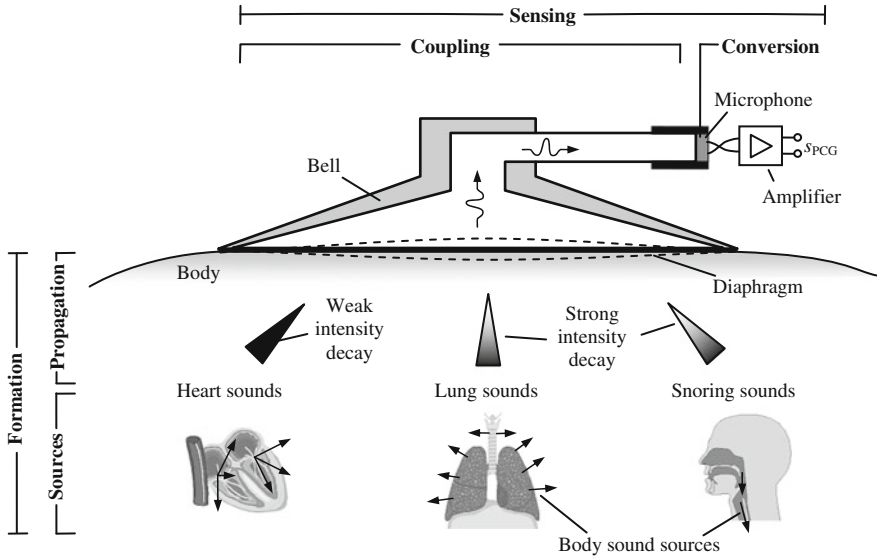


**Fig. 4.1** The stethoscope chestpiece is applied at the chest for the auscultation of various body sounds. The formation and sensing path of an acoustic biosignal phonocardiogram  $s_{PCG}$  is depicted; compare Fig. 4.2. The formation path includes sources of body sounds and the damping of sounds during their propagation through the body tissues, whereas the sensing path includes coupling and conversion of sounds

A large variety of *acoustic biosignals*, i.e., *permanent biosignals* according to their classification (Sect. 1.3), originates in the inner human body, including heart sounds, lung sounds, and snoring sounds. The *auscultation* of these *body sounds* is a timeless classic for diagnosis of health status, especially since Dr. Laennec, the inventor of the stethoscope, fundamentally improved the auscultation technique (Sect. 1.2). The body sounds convey numerous meaningful signals to the physician, disclosing *cardiorespiratory* pathologies or the state of health; compare with multiparametric monitoring (Sect. 1.4).

Traditionally, the auscultation of *heart sounds* is applied to detect cardiac pathologies. Auscultation of *lung sounds* and snoring sounds is applied to detect respiratory disturbances. Recently, medical interest has also focused on *snoring sounds* as an important symptom of the sleep apnea syndrome, i.e., a temporal and repetitive cessation of effective respiration during sleep at night (Sect. 3.1.2).

Figure 4.1 demonstrates a *body sound sensor* on the skin, which is basically given by the *chestpiece of the stethoscope* combined with a microphone. *Vibrating structures* in the body yield acoustic sounds which are subject to damping while *propagating through the thoracic tissues* towards the skin. Arrived at the skin, different body sounds interfere with each other and induce mechanical skin vibration which, in turn, forces the chestpiece diaphragm to oscillate. This oscillation creates acoustic *pressure waves* travelling into the chestpiece bell and down

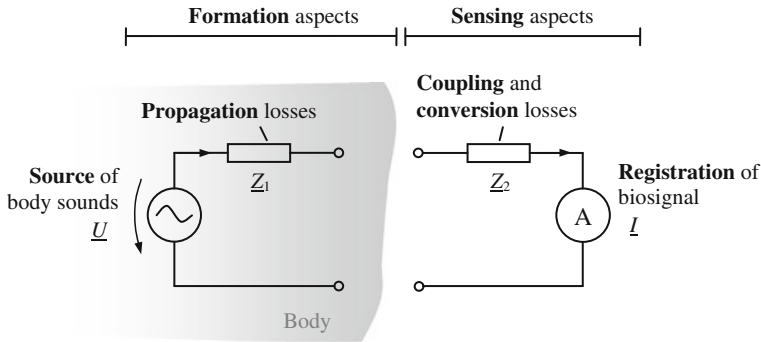


**Fig. 4.2** Model of permanent acoustic biosignal, including its generation, propagation, coupling, and registration; compare Fig. 1.3

to the microphone. The microphone serves as an acousto-electric converter to establish an *acoustic biosignal*  $s_{PCG}$ .

The *formation of body sounds* up to their registration can be simplified as an *electrical circuit model*, as illustrated in Fig. 4.2 (compare Sect. 1.1). In accordance with this model and in analogy with Fig. 4.1, we start with *sources of body sounds* (represented by voltage source  $\underline{U}$  in Fig. 4.2) and go over the *propagation* of generated sounds (propagation losses represented by electrical impedance  $\underline{Z}_1$  in Fig. 4.2) throughout biological tissue. As a certain portion of sounds leaves the body and thus is available for its auscultation, we continue with the sound *coupling* (coupling represented by electrical impedance  $\underline{Z}_2$  in Fig. 4.2) into an acoustic sensing device, i.e., a body sound sensor applied on the skin. Lastly, the sounds *conversion* (conversion losses as an additive part of electrical impedance  $\underline{Z}_2$  in Fig. 4.2) into an electric signal is modelled, preceding the *registration* of acoustic biosignals (modelled as ampere meter in Fig. 4.2).

## 4.1 Formation Aspects

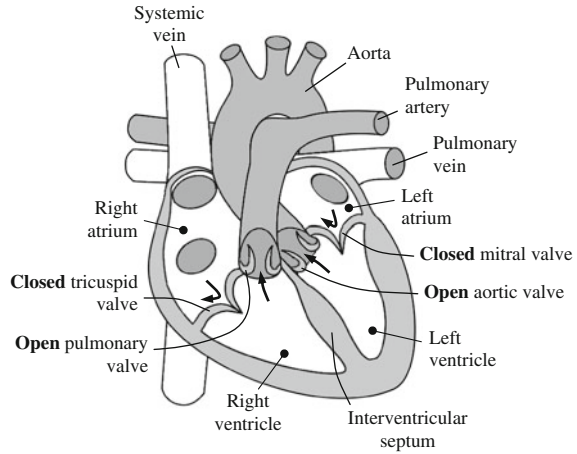
According to Figs. 4.1 and 4.2, *formation aspects* include

- the *genesis of body sounds* and
- their *transmission* in the body

towards the sensing device applied on the skin. The formation aspects reveal not only *clinically relevant correlations* between physiological phenomena of interest and recorded acoustic biosignals but also facilitate a proper understanding of the *biosignal's diagnostical relevance*.

In particular, distinctive types of *sources of body sounds* are reviewed, commenting on their mutual interrelations. It will be shown that body sounds, i.e., *mechanical waves* within the body, originate in the course of *mechanical vibrations*

**Fig. 4.3** Anatomic structure of the heart relevant for the generation of heart sounds; compare Fig. 2.32. Image data partly taken from Wikipedia (2010)



of *tissues and blood*, vibrations of *heart valves*, oscillation of *airway walls*, and air *turbulences* in the airways. From an acoustical point of view, body sounds comprise *impure tones or noises* and thus are composed of multiple spectral components of varying intensity and frequency. Later, the *transmission of body sounds* in the human body is discussed in the time and spatial domain, focussing on the sound's interaction with the biological medium.

## 4.1.1 Body Sounds—An Overview

### 4.1.1.1 Heart Sounds

*Heart sounds* are probably the most familiar body sounds which auscultation was fundamentally improved by the invention of the stethoscope (Sect. 1.2.1). In general, these sounds are related to the contractile activity of the cardiac system, including the heart and blood together,<sup>1</sup> and the *blood's turbulence* in atria and ventricles of the heart (Fig. 4.3). The sounds yield direct information on *myocardial contractility* and the *valve's closure* in the heart (Sect. 2.4.1).

In particular, heart sounds are generated within or close to the heart (Fig. 4.1). These sounds can be roughly classified into (Kaniusas 2007; Walker et al. 1990; Rangayyan 2002; Lessard and Jones 1988; Amit et al. 2009)

- normal heart sounds and
- abnormal heart sounds.

<sup>1</sup> The *heart and blood* together is comparable to a thin-walled and fluid-filled *balloon* which, when stimulated at any location, starts to vibrate as the whole and to *emit sounds* (Rangayyan 2002).

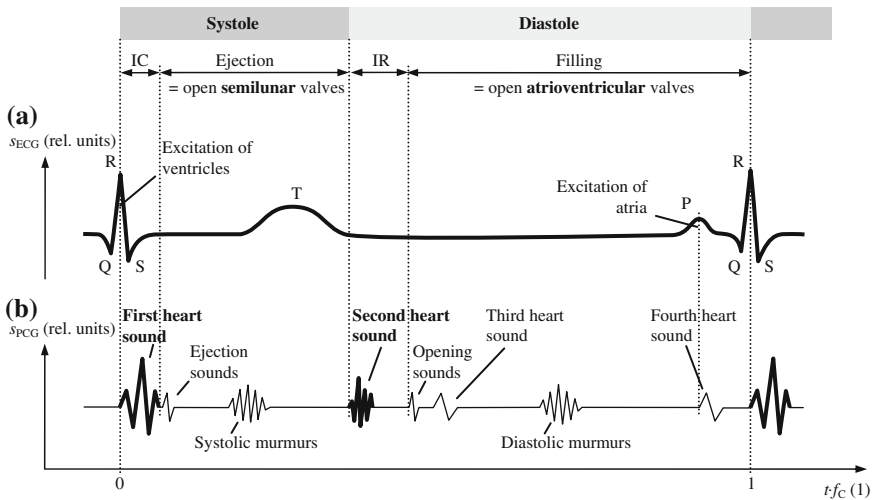


**Fig. 4.4** Schematic waveforms of (a) electric biosignal electrocardiogram  $s_{\text{ECG}}$  with typical waves and peaks in relation to (b) acoustic biosignal phonocardiogram  $s_{\text{PCG}}$  during the cardiac cycle with the duration  $1/f_c$ ; compare Fig. 2.38. Typical phases of the cardiac cycle are denoted including the isovolumetric contraction phase (IC) and the isovolumetric relaxation phase (IR). Different heart sounds are depicted with normal sounds drawn in *bold*, i.e., the first and second heart sounds. The frequency and amplitude of the respective heart sounds are qualitatively indicated

Within a single cardiac cycle, the following *normal heart sounds* can be observed, as illustrated in Fig. 4.4b (compare Fig. 2.38):

- The *first heart sound*: it is associated with the *closure of atrioventricular valves*, i.e., the tricuspid and mitral valves, preventing the backward flow of blood (from ventricles into atria). Abrupt tension changes of atrioventricular valves, deceleration of the blood flow, and jerky contraction of the ventricular myocardium induce mechanical vibrations (with reverberations) of the involved structures, which manifest as the first heart sound. This sound occurs at the onset of the ventricular *systole* immediately after the R wave of the electrocardiogram (Fig. 4.4a). The first sound is usually composed of *two components* (sound *splitting*), caused by the closure of the right-sided tricuspid valve and the left-sided mitral valve, respectively (Fig. 4.3). The mitral valve closes slightly earlier than the tricuspid valve,<sup>2</sup> so that the left-sided sounds slightly precede by about

<sup>2</sup> The *asynchronous closure of atrioventricular valves* can be attributed to several factors (Brooks et al. 1979). In particular, the left ventricle contracts slightly before the right ventricle, yielding an earlier closure of the mitral valve (Fig. 4.3). In addition, the mitral valve is more (nearly) closed when the contraction of the left ventricle begins than is the tricuspid valve when the contraction of the right ventricle begins; the asynchronous closure also greatly depends on the contraction and relaxation of both atria. The *inspiration* also delays the closure of the tricuspid valve because of increased venous return (see section “Normal Respiration” in Sect. 3.2.1.1), which enhances the splitting of the first heart sound (see section “Normal Respiration” in Sect. 3.2.1.2).

20 ms (Walker et al. 1990). Normally, the first heart sound is the *loudest and longest* of all heart sounds, including spectral components of *relatively low frequency* (Footnote 150 in Sect. 2). The sound's duration is about 140 ms with the spectral peak at about 30 Hz, whereas the intensity decreases by about 40 dB in the range of 10–100 Hz.

- The *second heart sound*: it is associated with the *closure of semilunar valves*, i.e., the pulmonary and aortic valves, preventing the backward flow of blood (from arteries into ventricles). In analogy with the first heart sound, the valve's closure and abrupt deceleration of the blood flow yield *vibrations of the valve's cusps* and blood in the great vessels. In particular, when the elastic limits of the tensed valve leaflets are met oscillations of the leaflets are initiated. Atria and ventricles vibrate in concert with the valves and blood because of their anatomical vicinity. This sound occurs at the onset of the ventricular *diastole*, beginning at the end of the T wave of the electrocardiogram (Fig. 4.4a). The second sound is usually composed of *two components* (sound *splitting*), caused by the closure of the right-sided pulmonary valve and the left-sided aortic valve, respectively (Fig. 4.3). Typically the aortic valve closes earlier than the pulmonary valve because of *respiration effects* (see section “Normal Respiration” in Sect. 3.2.1.2), so that the left-sided sounds precede by about 40 ms during *inspiration* (Walker et al. 1990); with *expiration* the left-sided and right-sided sounds may be superimposed or even still slightly split by < 30 ms. The left-sided sounds are usually louder<sup>3</sup> than the right-sided sounds due to a much higher blood pressure in the aorta at the onset of diastole. The second heart sound shows shorter duration of about 110 ms (< 140 ms), lower intensity, *higher frequency components*, and a more *snapping quality* than the first heart sound. Its short duration and dominant high frequency components result from the fact that semilunar valves are much tauter than atrioventricular valves and thus close more rapidly. In contrast to the first heart sound, the second sound does not show a consistent spectral peak and is not limited to a relatively narrow frequency bandwidth, whereas the intensity decreases more slowly by about 30 dB (< 40 dB) in the range of 10–100 Hz.

Normally, the *first and second heart sounds* are audible only. Figure 4.4 depicts that the time period between the first heart sound and the second heart sound defines the *duration of the ventricular systole*. Early studies found that the *spectral components* are negligible above 110 Hz in normal heart sounds (Rappaport and Sprague 1941) or reside in the approximate range of 20–120 Hz (Abella et al. 1992).

---

<sup>3</sup> The significantly higher pressures on the left side of the heart cause the *left-sided valves* to shut harder and faster than the closure of the *right-sided valves*. Therefore, the majority of auscultated heart sounds originates from the left-sided valves; though this can not be generalised and depends strongly on the auscultation location (compare section “Normal Respiration” in Sect. 3.2.1.2).

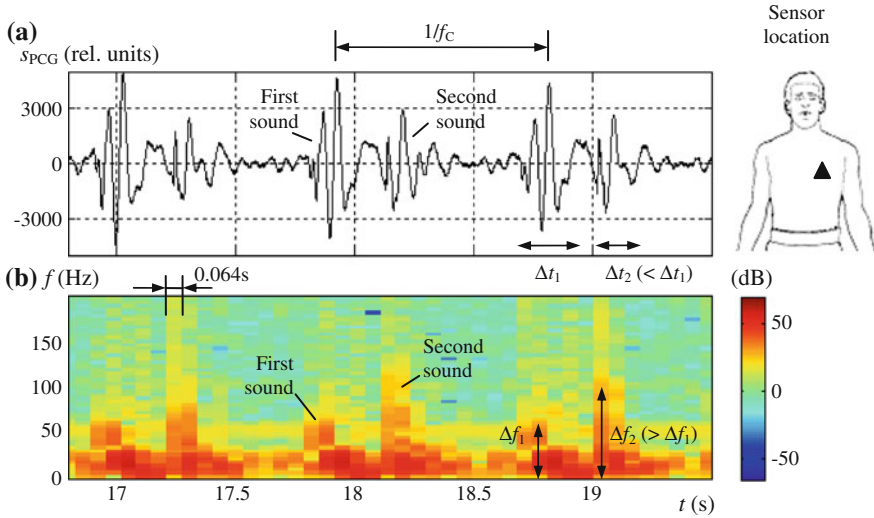


**Fig. 4.5** Normal heart sounds while holding breath. (a) Acoustic biosignal phonocardiogram  $s_{PCG}$  from the heart region at the chest with indicated heart rate  $f_C$ . (b) The corresponding spectrogram (see Footnote 4) shows differences between the first and second heart sound ( $\Delta t_1 > \Delta t_2$  and  $\Delta f_1 < \Delta f_2$ )

Figure 4.5 illustrates normal heart sounds while holding breath, which reoccur with the heart rate  $f_C$ ; for *sensing aspects* of body sounds see Sect. 4.2. It can be observed in Fig. 4.5a that the first heart sound exhibits a larger signal deflection and is a bit longer in duration than the second heart sound ( $\Delta t_1 > \Delta t_2$ ). The corresponding spectrogram<sup>4</sup> in Fig. 4.5b demonstrates that both *normal heart sounds* are characterized by short-term frequency components mainly in the frequency range of *up to about 100 Hz*, with weak contributions up to 400 Hz (Kaniusas et al. 2005); compare Fig. 4.8b. However, the second heart sound includes spectral components of higher frequency than the first heart sound ( $\Delta f_1 < \Delta f_2$  in Fig. 4.5b). In addition, the *50 Hz interference* from power lines can be recognised. The discussed *splitting* of the second heart sound is illustrated in Fig. 3.32.

<sup>4</sup> A *spectrogram* provides information of how signal power (i.e., signal variance) is distributed as a function of *frequency and time*; compare Footnote 193 in Sect. 3. Likewise, the spectrogram shows how the *power spectral density* varies with time. As illustrated in Fig. 4.5b, the horizontal axis represents *time t* while the vertical axis *frequency f*. The dot color in the image (i.e., the third dimension) reflects the signal power in a *logarithmic scale* for a particular frequency and at a particular time instant, see the color bar to the right of Fig. 4.5b. The striped pattern of the spectrogram in the vertical direction results from the fact that the power spectral density was calculated for time intervals of 0.128 s duration with 50 % overlap, yielding a time resolution of 0.064 s (Fig. 4.5b) and a frequency resolution of about  $1/0.128 \text{ s} \approx 7.8 \text{ Hz}$ .

Numerous *other heart sounds* originate within the scope of cardiac activity, which prevalence and audibility depend on age or indicate abnormality. As illustrated in Fig. 4.4b, the following sounds can be distinguished (Walker et al. 1990; Kaniusas 2007):

- The *third heart sound*: it is associated with the *rapid ventricular filling* (i.e., *passive* ventricular filling) when the *compliant* ventricular walls (mainly the left ventricular walls) twitch and generate sounds. This sound occurs in the early diastole after the second heart sound (Fig. 4.4b); compare with the rapid filling phase from Fig. 2.38b. It is relatively short and includes spectral components of *very low frequency* in the range of 25–50 Hz because walls are relaxed. The third heart sound is also known as *ventricular gallop* which refers to the cadence of the three heart sounds (i.e., first, second, and third sounds), occurring in rapid succession.
- The *fourth heart sound*: it is associated with the *contraction of atria*, displacing blood into ventricles (i.e., *active* ventricular filling). If the ventricular *compliance is decreased* (abnormal on the left or right side of the heart), the blood strikes the ventricles which start to vibrate and produce audible sounds. This sound occurs in the late diastole just before the first heart sound (Fig. 4.4b). It includes spectral components of *very low frequency* in the range of 20–30 Hz. The fourth heart sound yields an auscultatory cadence that resembles the canter of a horse, thus this sound is also designated as *atrial gallop*.
- *Ejection sounds* (or ejection clicks): they are associated with the (maximal) *opening of semilunar valves*, in which a sudden tensing or an abrupt opening of valves generates sounds. Also the *rapid distention of the aortic root or pulmonary artery* (abnormally dilated) at the onset of ejection may contribute to these sounds (Fig. 4.3). In particular, these sounds arise when either the aortic or pulmonary valve is diseased (e.g., stenotic valves are present). The ejection sounds occur shortly after the first heart sound with the onset of ventricular ejection during *systole* (Fig. 4.4b). The sounds are *high frequency* clicky sounds.
- *Opening sounds* (or opening snaps): constitute the diastolic correlate of the ejection sounds. They are associated with the (maximal) *opening of atrioventricular valves* provided that the mitral or tricuspid valve is diseased and its opening is pathologically arrested. These sounds occur after the second heart sound with the onset of ventricular filling during *diastole* (Fig. 4.4b). The sounds are *high frequency* clicky sounds.
- *Murmurs*: these abnormal sounds are mainly associated with the induced turbulent blood flow in the course of backward regurgitation through leaking valves and forward flow through narrowed or deformed valves (e.g., stenotic valves are present); in addition, vibrations of loose structures within the heart may contribute to murmurs. These sounds may occur either during *systole* (systolic murmurs) or during *diastole* (diastolic murmurs). Murmurs are *high frequency* noisy sounds, whereas the frequency is roughly proportional to the velocity of blood flow; compare the discussion about (4.1) and Footnote 5.

Consequently, heart sounds offer information on *valvular*, *myocardial*, and *hemodynamic activities*, deterioration of which leaves audible traces within heart sounds.

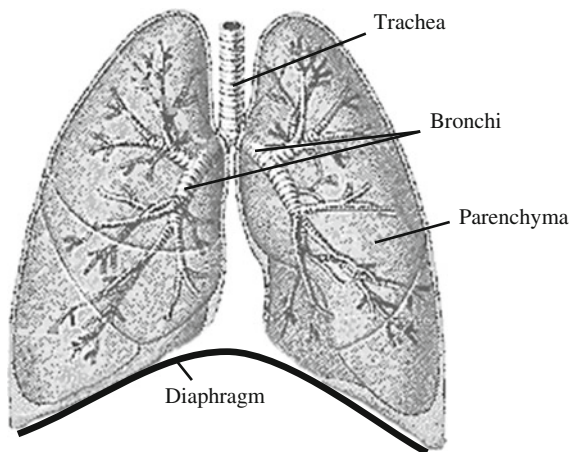
#### 4.1.1.2 Lung Sounds

*Lung sounds* comprise another type of body sounds which can be auscultated on the skin (Fig. 4.1). In general, these sounds are related to *turbulent air flow* in relatively large airways, located outside and inside the lungs (Fig. 4.6). *Vibrations of the air and airway walls* are induced, which propagate through the lung tissue (lung parenchyma) and the thoracic tissue towards the skin, the site of the sound's auscultation. Lung sounds yield direct information on the dynamics and ventilation of the *upper airways*, e.g., for the diagnosis of apneas (Sect. 3.1.2), and on the dynamics and ventilation of the *lower airways*, e.g., for the diagnosis of asthma (an inflammatory disease of airways).

In contrast to heart sounds (Sect. 4.1.1.1), *lung sounds* are much more *versatile* and *variable over time*. The status of the lung sounds nomenclature can be best viewed by the Laennec's notice—Laennec is the inventor of the stethoscope (Sect. 1.2.1)—that lung sounds heard were easier to distinguish than to describe (Sect. 1.2.2). Ironically, some physicians devaluated lung sounds as “the sound repertoire of a wet sponge such as the lung is limited” more than 30 years ago (Pasterkamp et al. 1997b).

In particular, lung sounds are generated in the large airways and the lungs (Fig. 4.6). These sounds can be roughly classified into (Dalmay et al. 1995; Loudon and Murphy 1984; Pasterkamp et al. 1997b; Kompis et al. 2001; Hadjileontiadis and Panas 1997a; Fachinger 2003; Kaniusas 2007)

**Fig. 4.6** Lungs and adjacent airways relevant for the generation of lung sounds



- normal lung sounds and
- abnormal (adventitious) lung sounds.

The common *classification* of the normal lung sounds is based on the *location of the sound's source*. In particular, the following *normal lung sounds* can be distinguished:

- *Tracheobronchial sounds*: these are the sounds originating in bronchial and tracheal tracts and are heard over or close to large airways (with > 4 mm in diameter), e.g., heard at the chest over the trachea, over the larynx, or on the lateral neck. The sound's source is *centrally situated* and is given by the *turbulent air flow in the bronchi and trachea*, i.e., in the upper airways. The turbulences are due to high *velocity of the air flow*,<sup>5</sup> causing *vibrations of the air and airway walls* during *inspiration* and *expiration*. The propagation distance of sounds towards the skin is relatively short so that sounds, particularly those originating in the trachea, experience only a relatively *weak damping*. As a result, the emitted sounds (at the skin level) are relatively loud and have a tubular (hollow) sound quality as if the air was blown through a tube. The sounds contain frequency components of up to 1 kHz while the component's amplitudes reach baseline levels in the range of 1.2–1.8 kHz (Dalmay et al. 1995); likewise, frequency components are in the approximate range of 100–1,000 Hz (Fachinger 2003). The tracheobronchial sounds are abnormal when heard further away from large airways; it would indicate a consolidation

---

<sup>5</sup> Streamlined flow or smooth *laminar flow* occurs when air tends to move in parallel layers as if adjacent layers would slide past one another *without lateral mixing*. In a *tube*, the air travelling at the same velocity will be symmetrically arranged around the tube axis, forming cylindrical lamina; the maximum velocity arises at the centre of the tube (Sect. 2.5.2.2). However, the laminar flow can be maintained when it is sufficiently slow or it happens on a sufficiently small scale. Otherwise, rough *turbulent flow* occurs with eddies *leading to lateral mixing* and not contributing to the volume flow rate. The onset of the turbulent flow is roughly determined through the tube's geometry and the *Reynolds number*

$$R = \frac{\langle u \rangle \cdot 2r \cdot \rho}{\mu}$$

Here  $\langle u \rangle$  is the average flow velocity of air—with its density  $\rho$  and its dynamic viscosity  $\mu$ —through the tube with the radius  $r$ . In an approximation, the turbulent flow starts to develop with  $R > 2000$ .

Interestingly, the *pressure gradient* scales linearly with the volume *flow rate* in the case of the *laminar flow*, as shown in (2.18). In contrast, the *pressure gradient* is approximately proportional to the *square of the flow* in the case of the *turbulent flow*. Because of the lateral mixing and vortices formed in the turbulent flow, extra energy is required (i.e., disproportionately higher pressure gradient) to maintain the increased movement of air that does not directly contribute to the net flow.

Likewise, the air flow of low  $u$  is *laminar* and thus is *silent*. With increasing  $u$  (or  $r$ ) *turbulences* start to occur causing *vibrations* of air and airway walls, which constitute *sound sources*. The arising sound is a *noise-like* signal with a relatively *wide spectrum*, whereas the particular frequency range of noise depends on the level of  $u$ .

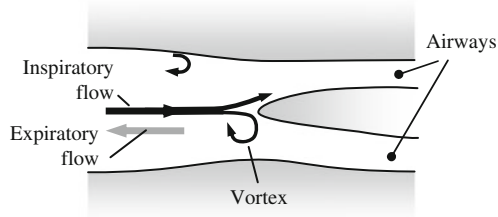


**Fig. 4.7** Generation mechanisms of vesicular sounds, i.e., normal lung sounds. Narrowing and branching of small bronchial airways in the lungs constrict and hinder inspiratory air flow, inducing local air turbulences. These turbulences comprise local and distributed (diffuse) sources of lung sounds

of the lung tissue (lung disease) because the consolidation facilitates the sound propagation (i.e., reduces damping of sounds, Sect. 4.1.2.2).

- *Vesicular sounds*: these sounds are heard at sites which are distant from large airways; e.g., at the chest in the peripheral lung fields. The sound's sources are *distributed* throughout the lungs and originate in *air turbulences along bronchi* outside alveoli.<sup>6</sup> The air turbulences are induced by *branching* and *narrowing* of airways, leading to directional changes of the local air flow. The inner surface of airways is *uneven*, which also contributes to the turbulences. In particular, vesicular sounds mainly originate when the air moves into increasingly smaller airways (towards alveoli) during *inspiration*. As shown in Fig. 4.7, airways branch into smaller and smaller airways, whereas the inspiratory air flow hits these branches and air turbulences are created. In contrast, the air moves into increasingly larger airways during expiration, in the course of which the air flow is less confined and it has only a loose contact with the surface of airways. Consequently, less turbulences are created and thus *less sound is generated during expiration* (Fig. 4.7). Vesicular sounds propagate through alveolar tissue (lung parenchyma) towards the skin, experiencing a relatively *large damping*. These emitted sounds (at the skin level) have a soft sound quality as if the air was blown through leaves of a tree. The sounds contain frequency components clearly distinguishable at about 100 Hz (in the range of 100–400 Hz (Fachinger 2003)); the amplitude's *fall-off to baseline levels* at about 1 kHz is much more rapid than for tracheobronchial sounds (Dalmay et al. 1995). In contrast to tracheobronchial sounds, vesicular sounds show *lower intensity* and *narrower spectral range*; e.g., the frequency components above 1 kHz were more clearly auscultated over the trachea than at the chest (Loudon and Murphy 1984). In fact, these differences are due to a strong filtering of vesicular sounds when

<sup>6</sup> In *alveoli* the velocity of the air flow is very low because of a very large total cross-sectional area of the airways. Consequently, the *air flow is laminar* and air turbulences are missing; compare Footnote 5.

propagating to the chest skin. Vesicular sounds tend to have longer transmission paths with more damping (inertial) components involved.

- *Bronchovesicular sounds*: these sounds are intermediate in their characteristics between tracheobronchial and vesicular sounds.

Figure 4.8 illustrates *normal lung sounds* auscultated on the *neck* in comparison with the sounds from the *chest*. Tracheobronchial sounds dominate on the neck (Fig. 4.8a) while vesicular sounds dominate at the chest (Fig. 4.8b). It can be observed that lung sounds can not be recognised in the time domain, only *heart sounds* (Fig. 4.5a) are easily discernable here because of their relatively high intensity. For instance, heart sounds are approximately 30 dB stronger than lung sounds if auscultated on the chest, as discussed in Sect. 4.2.2.3. However, the discussed behaviour of tracheobronchial and vesicular sounds is disclosed in the corresponding *spectrograms*. In fact, the *non-linear logarithmic scaling* (dot color) in the spectrograms accentuates *weak lung sounds* in the presence of *strong heart sounds*. As expected, *tracheobronchial* sounds (Fig. 4.8a) occur during both *inspiration and expiration*, whereas *vesicular* sounds (Fig. 4.8b) dominate only during *inspiration*. It can also be observed that tracheobronchial sounds include a wider range of *frequency components up to about 1 kHz* in comparison to vesicular sounds with components *up to about 500 Hz*, which is in good agreement with the sound descriptions from above.

The *abnormal lung sounds* (adventitious lung sounds) are heard in pathological cases only. Their common classification is based on the *sound's duration*, i.e., continuous sounds with a duration of more than 250 ms can be distinguished from discontinuous sounds with a duration of less than 20 ms (Loudon and Murphy 1984; Pasterkamp et al. 1997b; Rappaport and Sprague 1941; Hadjileontiadis and Panas 1996, 1997b; Iyer et al. 1989; Mikami et al. 1987).

- *Abnormal continuous sounds*: these sounds extend over a relatively long period of time of more than 250 ms and have musical character. A further subdivision is commonly used:
  - *Wheezes*: they seem to arise in the course of interaction between walls of central and lower airways and, on the other hand, the air flow passing these airways. In particular, *narrowed and constricted airways* favour *elastic oscillation* of airway walls (i.e., gradual opening and closure of airways in the radial direction) provided that the *air flow* is limited and non-zero at the constricted site; compare Sect. 4.1.1.3 and Fig. 4.12a. In extreme cases, the narrowing can go to the point where opposite walls touch each other. Arising *vibrations* of the air and airway walls as well as induced *turbulences* contribute to wheezes.<sup>7</sup> These sounds are *high frequency* sounds resembling musical noise.

---

<sup>7</sup> A very short musical wheeze is also known as *squawk*. Squawks are a combination of wheezes and crackles; they are thought to occur from an explosive opening of airways and fluttering of unstable airway walls.

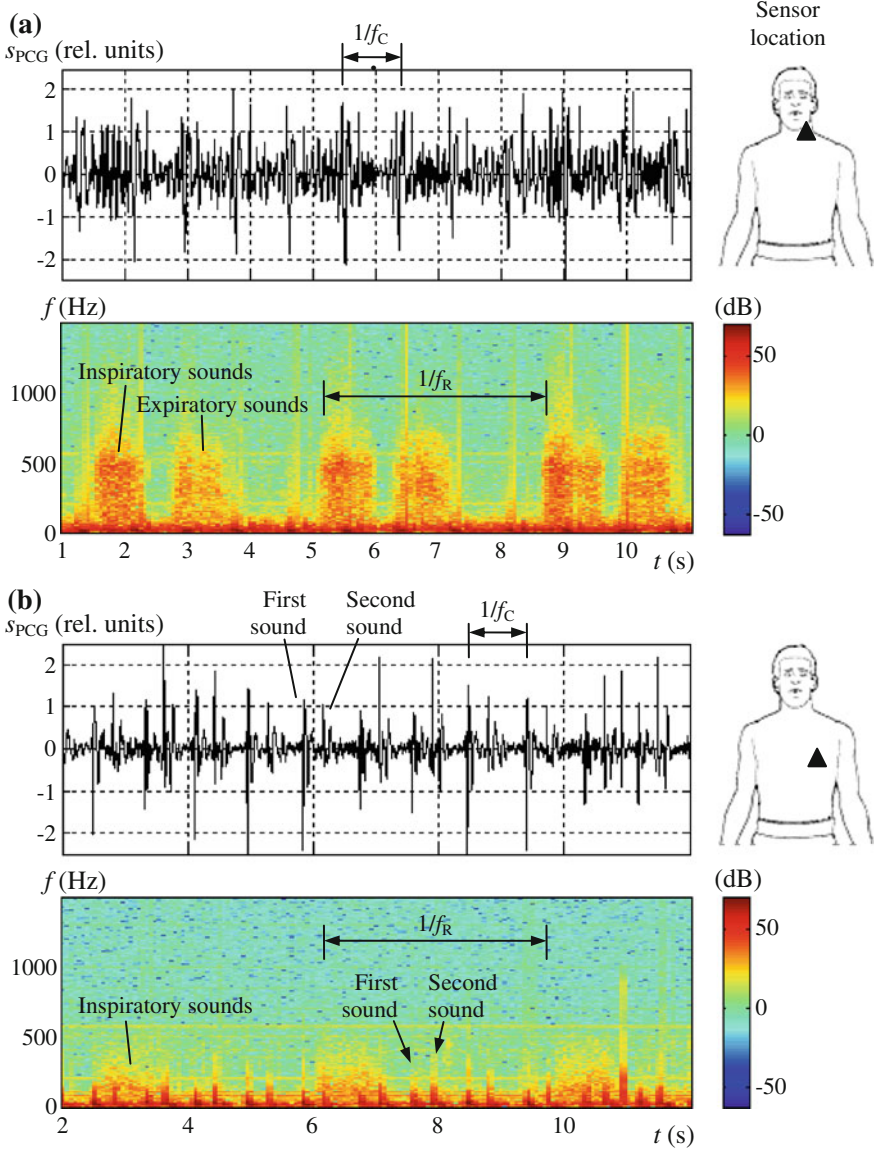


**Fig. 4.8** Normal lung sounds while breathing at rest. **(a)** Tracheobronchial sounds, as illustrated by an acoustic biosignal phonocardiogram  $s_{PCG}$  from the neck region. **(b)** Vesicular sounds, as illustrated by  $s_{PCG}$  from the chest region. The heart rate  $f_C$  and respiratory rate  $f_R$  are indicated. The corresponding spectrograms (*lower subfigures*) show differences between the tracheobronchial and vesicular sounds. For parameters of the spectrograms see Footnote 4

- *Rhonchi*: these sounds originate in the relatively large airways such as bronchi or bronchioles which are *partially obstructed*. The narrowing is usually due to excessive mucous *secretions* or local swellings. An increased velocity of air flow through thick mucous secretions and the rupture of fluid films contribute to the sound's generation, similar to the generation mechanism of wheezes. Rhonchi are *low frequency* sounds and have a sonorous snoring sound quality.
- *Stridors*: these are intense monophonic wheezes indicating *obstruction of the upper airways* such as of trachea or larynx.
- Abnormal *discontinuous* sounds: these sounds extend over a relatively short period of time of less than 20 ms and have implosive noise-like character. These are due to *explosive reopening* of small airways or fluid-filled alveoli during respiration, previously closed by excessive fluid or lack of aeration. In addition, *bubbling* of the air through copious secretions may contribute to discontinuous sounds. In all cases a rapid equalisation of gas pressures (downstream and upstream) and a rapid release of tensions of airway walls occur; it results in a series of distinct vibrations of the air and airway walls, generating intermittent explosive sounds. Excessive accumulations of secretions in airways or diseased lungs (e.g., inflammation or swelling in tissues surrounding airways) yield discontinuous sounds which can be further subdivided into:
  - *Coarse crackles*: these sounds exhibit a relatively long duration and *low frequency* components, and are mainly indicative of large fluid accumulation and bubbling of the air.
  - *Fine crackles*: in contrast to coarse crackles, fine crackles show short duration and *high frequency* components, and are mainly indicative of airway reopenings.

Figure 4.9 illustrates *vesicular lung sounds* in more detail, which were auscultated at the *chest* while normally breathing. In the time domain (Fig. 4.9a), vesicular sounds can be hardly recognised, as already mentioned. However, if the time axis is stretched out and the amplitude resolution is increased so that signal details can be examined—as depicted in the upper subfigures of Fig. 4.9a—vesicular sounds become uncovered. During *inspiration*, an oscillation with the fundamental harmonic frequency  $f_{R1}$  of about 260 Hz can be observed, whereas at the end of expiration oscillatory contributions are absent; this is in full agreement with the discussed generation mechanisms (Kaniusas et al. 2005).

Likewise, the *cardiac component*  $s_{PCG}^C$  of the auscultated biosignal (Fig. 4.9a) is almost constant within the zoomed region of 10 ms duration because heart sounds dominate up to about 100 Hz, i.e., 100 Hz = 1/10 ms. Conversely, the *respiratory component*  $s_{PCG}^R$  of the biosignal can be observed within this time resolution because vesicular sounds go up to about 500 Hz, i.e., numerous oscillatory periods of respiratory sounds fit into 10 ms. The *relative amplitude* of vesicular sounds in relation to that of heart sounds can be easily estimated from Fig. 4.9a, yielding

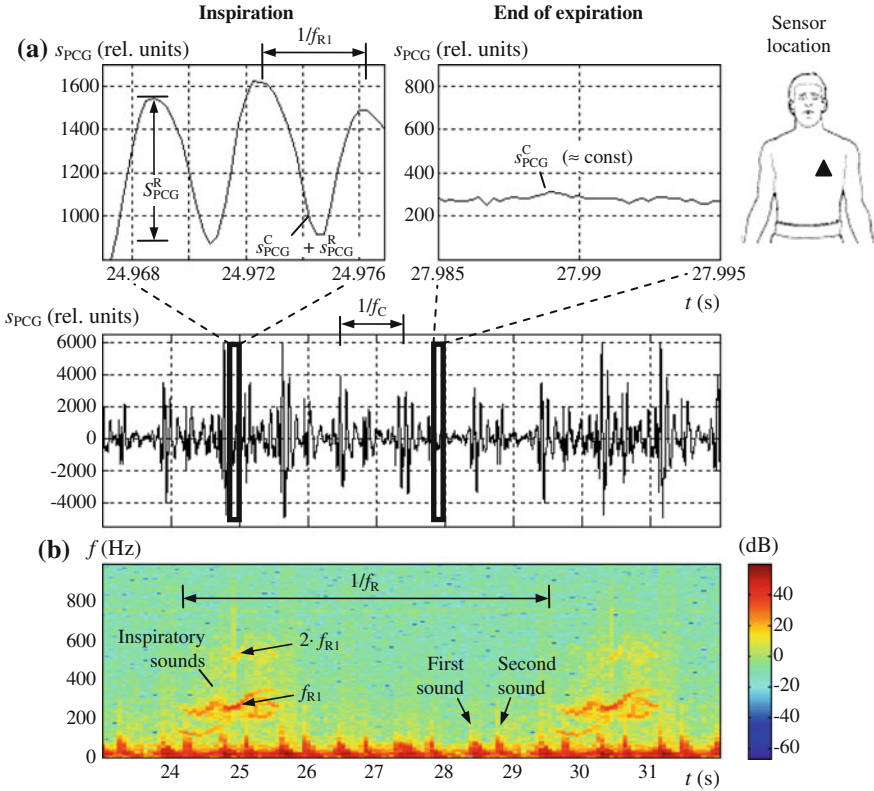


**Fig. 4.9** Vesicular lung sounds while breathing at rest. **(a)** Acoustic biosignal phonocardiogram  $s_{PCG}$  from the chest region with indicated heart rate  $f_C$ . A zoomed region of  $s_{PCG}$  with the duration of 10 ms is given at the time of inspiration, including the cardiac component  $s_{PCG}^C$  and respiratory component  $s_{PCG}^R$  (left upper subfigure), in comparison to the end of expiration including only  $s_{PCG}^C$  (right upper subfigure). **(b)** The corresponding spectrogram with indicated respiratory rate  $f_R$  and fundamental harmonic frequency  $f_{R1}$ . For parameters of the spectrogram see Footnote 4

about  $-24$  dB ( $= 20 \cdot \log(700/11000)$ ); that is,  $s_{PCG}^R$  exhibits much smaller oscillation amplitude than  $s_{PCG}^C$ ; compare Sect. 4.2.2.3.

Again, vesicular sounds manifest in the *spectrogram* during inspiration (Fig. 4.9b). In particular, the fundamental harmonic with  $f_{R1}$  can be seen, the same as already disclosed in the expanded waveforms of Fig. 4.9a. Additionally, a second harmonic appears at  $2 \cdot f_{R1}$ .

As can be derived from the origin of normal lung sounds, at the *chest wall* expiratory sounds originate from a more central source than inspiratory sounds (Earis 1992; Dalmy et al. 1995). Likewise, *central compact sources* of tracheobronchial sounds (located in the upper large airways) contribute more to the auscultated sounds during *expiration*, whereas *local distributed (diffuse) sources* of vesicular sounds (located in the distal bronchial airways) contribute more during *inspiration*.

In consequence, the inspiratory sounds show a relatively large amplitude (intensity) and include components of high frequency due to close vicinity of the auscultation site to inspiratory (distributed) sound sources. In contrast, the expiratory sounds are relatively weak due to distant (central) sound sources, long sound transmission paths, and thus strong accumulated damping of sounds. For instance, author in Fachinger (2003) report that the inspiratory sounds on the anterior chest showed twice as large intensity as that of the expiratory sounds.

An important characteristic of *normal lung sounds* is that their spectra are clearly linked to the strength of the respiratory *air flow*  $q^A$  (Dalmay et al. 1995). In an approximation, the sound intensity or the *lung sounds amplitude*  $S_{PCG}^R$  of normal lung sounds—as illustrated in Fig. 4.9a—increases exponentially with increasing  $q^A$ , that is

$$S_{PCG}^R = c \cdot (q^A)^\alpha. \quad (4.1)$$

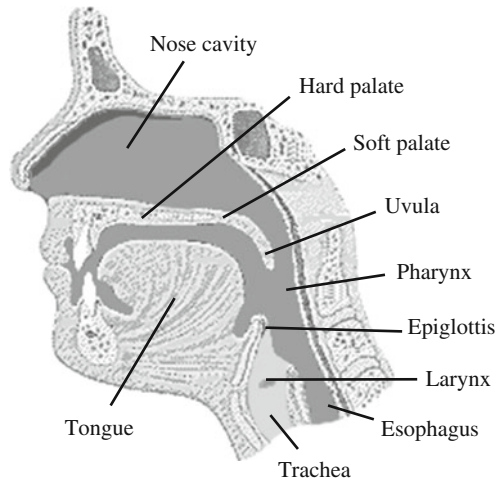
Here  $c$  is a positive constant and  $\alpha$  is another constant representing the power index of  $q^A$ . In the case of

- *tracheobronchial sounds*, frequency components shift upward in frequency and their amplitudes increase in proportion to  $q^A$ , this relationship being more marked during *inspiration* (Dalmay et al. 1995). Likewise,  $\alpha = 1$  applies in (4.1).
- The regional intensity of *vesicular sounds* correlates with increasing level of regional ventilation (Loudon and Murphy 1984; Jones et al. 1999). Similarly, the amplitude of vesicular sounds linearly increases and frequency components shift upwards as  $q^A$  rises, which is particularly pronounced during *inspiration* (Dalmay et al. 1995). In the case of the *linear relationship*,  $\alpha = 1$  applies; however, *non-linear relationships* were also reported with  $\alpha = 1.75$  (Fachinger 2003) or  $\alpha = 2$  (Pasterkamp et al. 1997b; Earis 1992).

It should be noted that reduced *intensity of vesicular sounds* was reported to be a strong indicator of *obstructive pulmonary disease* (Pasterkamp et al. 1997b), i.e., to be an indicator of impaired local ventilation of the lungs. In contrast, an increase in the intensity of vesicular sounds is considered indicative of *lung expansion* (Jones et al. 1999). For the *typical intensity levels* of normal lung sounds see Sect. 4.1.1.3.

Lastly, *large variability of lung sounds* should be addressed in some depth (Dalmay et al. 1995; Jones et al. 1999; Kompis et al. 2001). The content of lung sounds in the time and frequency domain—such as demonstrated in Fig. 4.9—greatly depends on the particular site of auscultation within *one subject* (Sect. 4.2.2.3), the degree of voluntary control that the subject is able to exert over breathing, body position (e.g., sitting or lying), and, of course, the actual respiration phase, i.e., inspiration or expiration. The temporal variability of lung sounds is more pronounced during expiration than inspiration (Dalmay et al. 1995). In fact, this variability is mainly due to strong influence of individual morphology of airways (Pasterkamp et al. 1997b) and lung-muscle-fat ratios (Kompis et al. 2001). Lung sounds vary greatly *among subjects* ventilating even at similar  $q^A$  (4.1),

**Fig. 4.10** Pharyngeal airways and surrounding structures of the upper airways relevant for the generation of snoring sounds



whereas the variability is still considerably high after introduction of corrections for diverse physical characteristics of subjects such as body weight, body height, the subject's age, and body surface area.

#### 4.1.1.3 Snoring Sounds

While heart and lung sounds have been in the focus of clinical investigations for centuries, only recently medical interest has focussed on *snoring sounds*<sup>8</sup> while sleeping (Fig. 4.1). In general, these sounds are related to *vibrations of instable structures* in the upper airways (such as the soft palate or uvula), *radial oscillation* of (pharyngeal) *flexible airway walls* and *oscillatory narrowing* of airways (up to their complete occlusion), and *turbulences of the air*<sup>9</sup> (Fig. 4.10). Snoring sounds

<sup>8</sup> Epidemiological studies have shown that nearly 40 % of males and about 20 % of females are snorers (Saletu 2001). The *prevalence* of habitual snoring rises markedly after the age of 40, whereas more than 60 % of males and more than 40 % of females are snorers in this aged population (Beck et al. 1995).

<sup>9</sup> In fact, the physics of sound formation in *snoring* is very similar to that in *speech* (Perez-Padilla et al. 1993). For instance,

- voiced sounds are related to *vibrations* of vocal cords,
- fricative sounds are related to the friction of *turbulent air flow* through a narrow orifice, and
- explosive sounds are related to sudden *release of pressure*.

are favoured by various *physiologic and social factors*,<sup>10</sup> whereas these sounds yield direct information on the dynamics and ventilation of the *upper airways*, e.g., for the diagnosis of apneas (Sects. 3.1.2 and 4.1.1.4). Snoring could be related to sleep deprivation and thus to other *severe pathologies*.<sup>11</sup>

In particular, the *snoring is proceeded* by a temporal decrease in the *diameter* of the oropharynx (Fig. 4.10), which can be even reduced to a slit<sup>12</sup> (Liistro et al. 1991; Cirignota 2004). Figure 4.11a, b demonstrates the narrowing of the pharynx by video images. Likewise, the (supraglottic) *resistance of the airway* to the air flow increases—by a factor of about 3, estimated from Liistro et al. (1991)—which in the case of heavy and obstructive snoring (i.e., *spontaneous snoring* during sleep) leads to initial *flow limitation* before onset of the snoring. In particular, the flow first increases as the driving pressure increases but then it saturates, i.e., the air flow becomes limited.

As the *snoring begins* and continues—mainly during *inspiration* (Liistro et al. 1991)—fluttering of loose structures in the upper airways occur, especially *vibrations* of the soft palate and pharyngeal walls (Perez-Padilla et al. 1993; Beck et al. 1995). Likewise, the appearance of *repetitive and steady sound* structures in the time domain during snoring coincides with the time course of airway wall motions and the time course of the air flow oscillation.

---

<sup>10</sup> *Snoring* is favoured by *physiological factors* such as small pharyngeal area and increased pharyngeal floppiness, i.e., excessive change in pharyngeal area occurs in response to applied air pressure (Saletu and Saletu-Zyhlarz 2001; Brunt et al. 1997). In addition, the supine sleep posture (i.e., retroposition of the tongue), obesity (i.e., high body mass index *BMI*, Footnote 202 in Sect. 3), large neck circumference (Sergi et al. 1999), presence of space occupying masses which block airways (e.g., hypertrophy of the soft palate or uvula), or a pathological narrowing of the nasal airway facilitate (disadvantageously) the generation of snoring. Among *social factors* contributing to the occurrence of snoring, mental stress, tiredness, and alcohol intake can be mentioned. Interestingly, *subjective factors* as familiar home settings or less familiar sleep labs also seem to influence the severity of nocturnal snoring which, in fact, tends to be heavier while sleeping in a sleep lab (Series et al. 1993).

<sup>11</sup> From the *physiological* point of view, the snoring, especially *obstructive snoring*, may be connected to increased morbidity, systemic hypertension, cerebrovascular disease, stroke, and even impaired cognitive functions (Saletu and Saletu-Zyhlarz 2001; Series et al. 1993; Wilson et al. 1999). In addition, obstructive and loud snoring is a major cause of disruption to other family members besides the snorer himself; it represents a disadvantageous *social* impact of snoring.

<sup>12</sup> The *narrowing of the pharyngeal airway* (or even its partial and *passive collapse*) can be due to negative oropharyngeal pressure generated during *inspiration*, relaxation of the pharyngeal muscles, or even sleep-related fall in the tone of the upper airway muscles (Liistro et al. 1991). The pharyngeal muscle tone is reduced not only during sleep, but also under the influence of alcohol or drugs (Saletu and Saletu-Zyhlarz 2001).

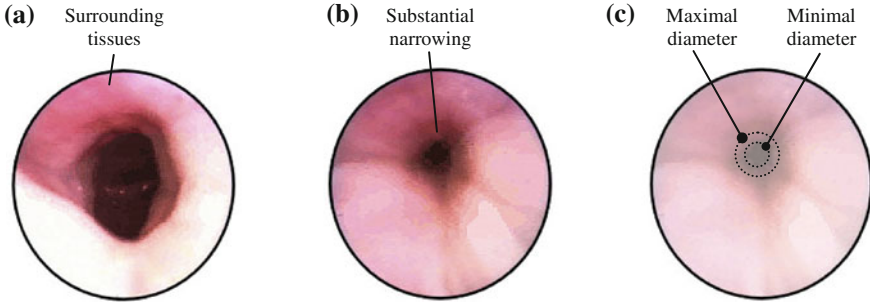


**Fig. 4.11** Video images of the pharynx as recorded from the mouth cavity (Hohenhorst 2000). (a) Before inspiration. (b) During inspiration. (c) During inspiration with schematically indicated oscillation of the airway diameter

Figures 4.11c and 4.12a illustrate such *elastic oscillations* of airway walls provided that a local narrowing (*flow-limiting segment*) is present within the depicted *highly compliant airway*. *Aeroelastic interactions* occur between the air flow and the airway wall. At the constriction, the air flow is confined to a smaller cross sectional area  $A$  (Fig. 4.12a). Consequently, the velocity  $u$  of the air flow increases at the constriction site ( $u_2 > u_1$ ) because the net flow

$$q^A = \langle u \rangle \cdot A \quad (4.2)$$

does not change along the airway (i.e.,  $q^A$  is assumed to be constant); compare (2.17). The lateral pressure  $p$  of the air flow must correspondingly decrease ( $p_2 < p_1$ ),<sup>13</sup> favouring the narrowing of the constriction even more. Likewise, radial forces keeping the airway open are reduced and thus there is an *inward* swing of airway walls<sup>14</sup>; the constricted site becomes more pronounced and unstable (collapsible) at

<sup>13</sup> The *Bernoulli's equation* governs the behaviour of  $u$  and  $p$  in an ideal flow, which is deduced from the principle of the conservation of energy (Nichols and O'Rourke 2005). According to Fig. 4.12, the total energy, i.e., the sum of potential and kinetic energies, at a non-constricted site with  $p_1$  and  $u_1$  is equal to the total energy at a constricted site with  $p_2$  and  $u_2$ , considering a single horizontal airway. It yields

$$p_1 - p_2 = \frac{1}{2} \cdot \rho \cdot (u_2^2 - u_1^2),$$

where  $\rho$  is the air density. The latter equation demonstrates that  $p_2 < p_1$  if  $u_2 > u_1$ , i.e.,  $p$  is decreased at the constricted site if a constant  $q^A$  along the airway is given. In other words, the opening pressure at the constricted site is decreased, which promotes the airway collapsibility at its constriction even more.

<sup>14</sup> It seems that the critically *low cross-sectional area* and critical *limitation of the flow*  $q^A$  initiate the oscillation of airway walls (Liistro et al. 1991; Perez-Padilla et al. 1993). In general, the limitation of  $q^A$  appears when  $u$  equals the velocity of propagating pressure pulse waves along the airway. Likewise, the oscillations occur more readily at a lower  $q^A$ , provided that the *compliance of the airway* is high.

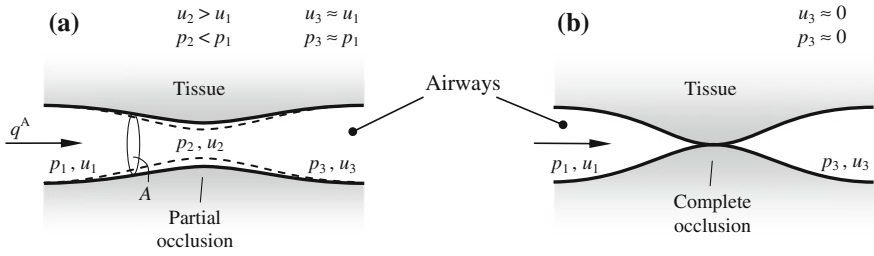


**Fig. 4.12** (a) Generation of continuous snoring sounds because of an oscillatory narrowing and local constriction of large upper airways; compare widened (*bold*) and narrowed (*dashed*) airways. The relations of the pressure  $p$  and velocity  $u$  of the air flow  $q^A$  along the depicted airway are indicated; compare Footnotes 13 and 15. (b) Generation of obstructive snoring sounds due to a repetitive and temporal occlusion of large upper airways. The walls of the airways show a high compliance with excessive masses involved, which favours the collapsibility of airways and reduces their permeability to air; compare Footnote 16

$q^A \neq 0$ . However, *elastic forces* appear progressively in airway walls, which are directed *outwards* and cause the deflected walls to swing back to their neutral position; an oscillatory vibration of airway walls results<sup>15</sup>; the latter mechanism dominates also the *generation of wheezes* in obstructed sites (Sect. 4.1.1.2).

On the other hand, a *collapsible airway* experiencing a local pressure decrease (Fig. 4.12a) can even collapse and completely occlude the lumen for a brief period of time (Fig. 4.12b). In particular, large amplitude oscillations of airway walls can yield partial or complete occlusion of the airway, with the point of maximum constriction moving upstream along the airway. Repetitive openings of the occluded airway generate *abrupt pressure equalizations* (popping openings) and *tissue vibrations*, which emit series of *explosive and discontinuous sound* structures—reoccurring with the frequency of the openings—in the time domain.<sup>16</sup>

*Further narrowing of the oropharynx* during snoring may lead to even louder snoring and laboured breathing. In extreme cases, progressive narrowing can yield a *sustained and complete occlusion* of the upper airway, which then manifests as the obstructive *sleep apnea* (Sect. 3.1.2).

<sup>15</sup> This theory is called “*flutter theory*” (Perez-Padilla et al. 1993); compare Footnote 16. That is, it explains the *continuous form* of snoring sounds in the time domain. These sounds arise in the course of oscillations of airway walls when the airflow is forced through a highly compliant airway and can interact with the elastic walls (Fig. 4.12a). The resulting *oscillation frequency* tends to decrease with increasing wall thickness and decreasing longitudinal tension in the walls, this tension being also affected by the activity of pharyngeal muscles.

<sup>16</sup> This theory is called “*relaxation theory*” (Perez-Padilla et al. 1993); compare Footnote 15. That is, it explains the *discontinuous form* of *explosive snoring sounds* in the time domain, which are due to repetitive openings of local occlusions of the airway (Fig. 4.12b). The resulting *oscillation frequency* is relatively low because of *large radial deflection* of airway walls.

In addition, local *turbulences of the air* in the upper airways seem to contribute to the emission of snoring sounds; compare Sect. 4.1.1.2. That is, the (increased) level of  $u$  in the (narrowed) airway (Fig. 4.12a) determines if *noise-like broadband sounds* will be emitted, whereas the frequency range of these sounds depends on this level of  $u$ ; compare Footnote 5.

Likewise, *fricative turbulent quality* of snoring sounds is related to *air turbulences* in the pharyngeal airway which is narrowed and the air flow within the airway is limited at a lower value than during rattling snoring (Perez-Padilla et al. 1993). In contrast, *regular rattling quality* of snoring sounds is due to *oscillating structures* such as the pharyngeal walls or soft palate. Relatively small oscillations yield steady continuous waveforms (according to the “flutter theory”, Footnote 15) while relatively large oscillations with recurring reopenings yield series of repetitive explosive structures in the sound waveform (according to the “relaxation theory”, Footnote 16).

In general, *characteristics of snoring sounds* are mainly determined by the air pressure and air flow in the upper airways in combination with the compliance and collapsibility of airways (Series et al. 1993). Usually the energy of snoring sounds is limited to their frequency components *below 2 kHz* (Perez-Padilla et al. 1993).

Like lung sounds (Sect. 4.1.1.2), *snoring sounds* show high diversity and are subjected to large *variability*. The footprints of snoring sounds in the time and frequency domains can even change from one breath to the other. Consequently, there are numerous possibilities to classify snoring sounds. The most commonly used *classifications* are based on (Kaniusas 2007)

- the location of the sound source,
- the diagnostically relevant type of snoring, and
- the waveform of snoring sounds in the time domain.

In accordance with the location of the *sound source*, the following snoring sounds can be distinguished (Liistro et al. 1991):

- *Nasal snoring*: during simulated nasal snoring (breathing exclusively through the nose) the resulting mainly inspiratory sounds originate in the course of the *uvula* vibrations (Fig. 4.10) while the soft palate and the back of the tongue remain in close contact (Liistro et al. 1991). On the other hand, spontaneous nasal snoring is also due to the *palate* or *pharyngeal wall* vibrations (Perez-Padilla et al. 1993). For instance, the oscillation frequency of the uvula is about 80 Hz (Liistro et al. 1991). In the frequency domain, the nasal snoring shows discrete sharp peaks below 500 Hz, i.e., a peak at a fundamental harmonic frequency and subsequent peaks at its harmonics. These peaks correspond to the resonant peaks (formants) of the *airway’s resonating cavities* and suggest that a *single sound source* dominates nasal snoring<sup>17</sup> (Perez-Padilla et al. 1993).

---

<sup>17</sup> In general, *spectral characteristics* of emitted sounds result from both the *source of sound* and *filtering properties* (or resonant properties) of the airway (Perez-Padilla et al. 1993). For instance, the *source properties* change when a different segment starts to oscillate or the mechanical

- *Oral snoring*: this snoring through the open mouth (breathing exclusively through the mouth) is characterized by vibrations of the whole *soft palate* and a dramatic decrease in the cross-sectional area of the oropharynx (Fig. 4.10), yielding a lower oscillation frequency of about 30 Hz in comparison with the nasal snoring (Liistro et al. 1991). This difference may be attributed to a larger oscillating mass of the soft palate than that of the uvula, yielding a lower oscillation frequency for a larger oscillating mass.
- *Oronasal snoring*: these snoring sounds (breathing through the nose and mouth) exhibit a mixture of sounds similar to *nasal snoring* and fricative *noisy sounds* characteristic of a source in the *turbulent flow* (Perez-Padilla et al. 1993); compare Footnote 5. Likewise, in the frequency domain a mixture of discrete sharp peaks and broad-band (white) noise dominate in the range of up to about 1,300 Hz. The large number of peaks may reflect two or more segments (e.g., the *uvula* and *soft palate*) oscillating with different frequencies. Figure 3.6c demonstrates an oscillation of the air flow during snoring with the rate of about 40 Hz.

Considering the diagnostically relevant *types of snoring*, the following snoring sounds can be distinguished (Liistro et al. 1991; Perez-Padilla et al. 1993; Series et al. 1993; Beck et al. 1995):

- *Normal snoring*: spontaneous snoring is always preceded by the *limitation of the air flow* and the *narrowing of the pharyngeal airway* (Liistro et al. 1991; Perez-Padilla et al. 1993; Series et al. 1993). The oscillation of airway walls occurs in line with the “*flutter theory*” (Footnote 15), as illustrated in Fig. 4.12a. The supraglottic pressure<sup>18</sup> if depicted over  $q^A$  forms a *hysteresis loop*, i.e., oscillations of the supraglottic pressure and  $q^A$  are 180° out-of-phase. The latter behaviour can be explained by consecutive (partial) closings and openings of the pharynx by the soft palate, yielding opposite changes in the supraglottic pressure and  $q^A$  (Liistro et al. 1991). Normal snoring sounds show a *regular rattling character* (Perez-Padilla et al. 1993) with dominant frequency components in the range of 100–600 Hz and minor components up to 1 kHz (Beck et al. 1995). Spectral peaks in the frequency domain occur at regular distances and represent *harmonic waves*.

---

(Footnote 17 continued)

characteristics of the other *oscillating segment* are different. In analogy, the *filtering properties* change when geometric dimensions of the pharynx or mouth cavity vary over time (i.e., dimensions of resonating cavities in front of the source location, cavities acting as *band-pass filters*; compare Fig. 4.24), or dimensions of neighbouring apertures for the air escape vary over time. In fact, *emitted sounds* are determined by a *product of the sound source* (usually broadband source) and the *filtering function* (band-pass filters) of the airway.

<sup>18</sup> *Supraglottic pressure* is the pressure drop along the upper airway above the epiglottis, see Fig. 4.10.

- *Obstructive snoring*: this pathological type of snoring (dominating in humans with the *obstructive sleep apnea*, Sect. 3.1.2) is associated with *repetitive temporal occlusion* and opening of a strongly *narrowed and collapsible airway*. This is due to high compliance of airway walls, as illustrated in Fig. 4.12b, and corresponds to the “*relaxation theory*” (Footnote 16). In addition, obstructive snoring is related to oscillations of the *soft palate*. The hysteresis loop is larger in size compared to normal snoring. Obstructive snoring sounds are *louder* than normal snoring sounds and have *fricative high-pitched quality*. In the time domain, the sounds exhibit *intermittent bursts of noise* at regular intervals—related to the fundamental harmonic frequency—and dramatically variable sound patterns. Typically, regular discrete peaks, i.e., spectral *harmonics*, can be observed in the frequency domain with the frequency components extending up to 2 kHz; compare Sect. 4.1.1.4. Obstructive snoring sounds have a higher cumulative power above 800 Hz relative to the power below 800 Hz when compared to normal snoring (Perez-Padilla et al. 1993). In an approximation, the intensity of frequency components decreases with increasing frequency less strongly in obstructive snoring than in normal snoring.
- *Simulated snoring*: this kind of an intentionally provoked snoring is *not preceded by flow limitation*, even though preceded by an increase in the supraglottic resistance of the airway, at variance with the spontaneous snoring during sleep (Liistro et al. 1991). The narrowing of the pharyngeal airway is probably produced by voluntary contraction of the pharyngeal constrictor muscles. The presence of the *hysteresis loop* has also been reported (Liistro et al. 1991). Simulated snoring sounds resemble complex-waveform snoring (as described below) with multiple equally-spaced peaks of power in the frequency domain ranging up to 800 Hz (Beck et al. 1995).

If the distinct *waveform patterns* of snoring sounds in the time domain are taken as the classification basis, the following snoring sounds can be distinguished (Beck et al. 1995):

- *Simple-waveform snoring*: this type of snoring shows a nearly *sinusoidal waveform* or a *periodic waveform* (with a secondary deflection) over time with minor secondary oscillations. Consequently, only one up to three equally-spaced peaks (i.e., only a few harmonics) dominate in the frequency domain in the range of about 100–240 Hz while the first peak (at the lowest frequency) is usually the most prominent. The simple-waveform snoring probably results from the *vibration of airway walls* around their neutral position without the actual closure of the lumen (compare Fig. 4.12a).
- *Complex-waveform snoring*: it is characterized by *repetitive, equally-spaced segments* in the time domain, whereas each segment starts with a large deflection and ends with a decaying wave. The repetitive segments arise with the frequencies in the range of about 60–140 Hz, thus the frequencies are lower than in the simple-waveform snoring. More rapid, secondary *oscillations within each*

*segment* occur in the range of up to about 1,000 Hz. Therefore, a comb-like structure with multiple peaks of different amplitudes can be observed in the frequency domain, whereas the frequency interval between the peaks is equal to the arousal frequency of the repetitive segments. In contrast to the simple-waveform snoring, the complex-waveform snoring probably results from *repetitive collisions of airway walls* with intermittent brief closures of the lumen.<sup>19</sup> It should be noted that the simple-waveform and complex-waveform snoring can be found in a single subject, whereas one type of snoring can change to the other even within a single snore.

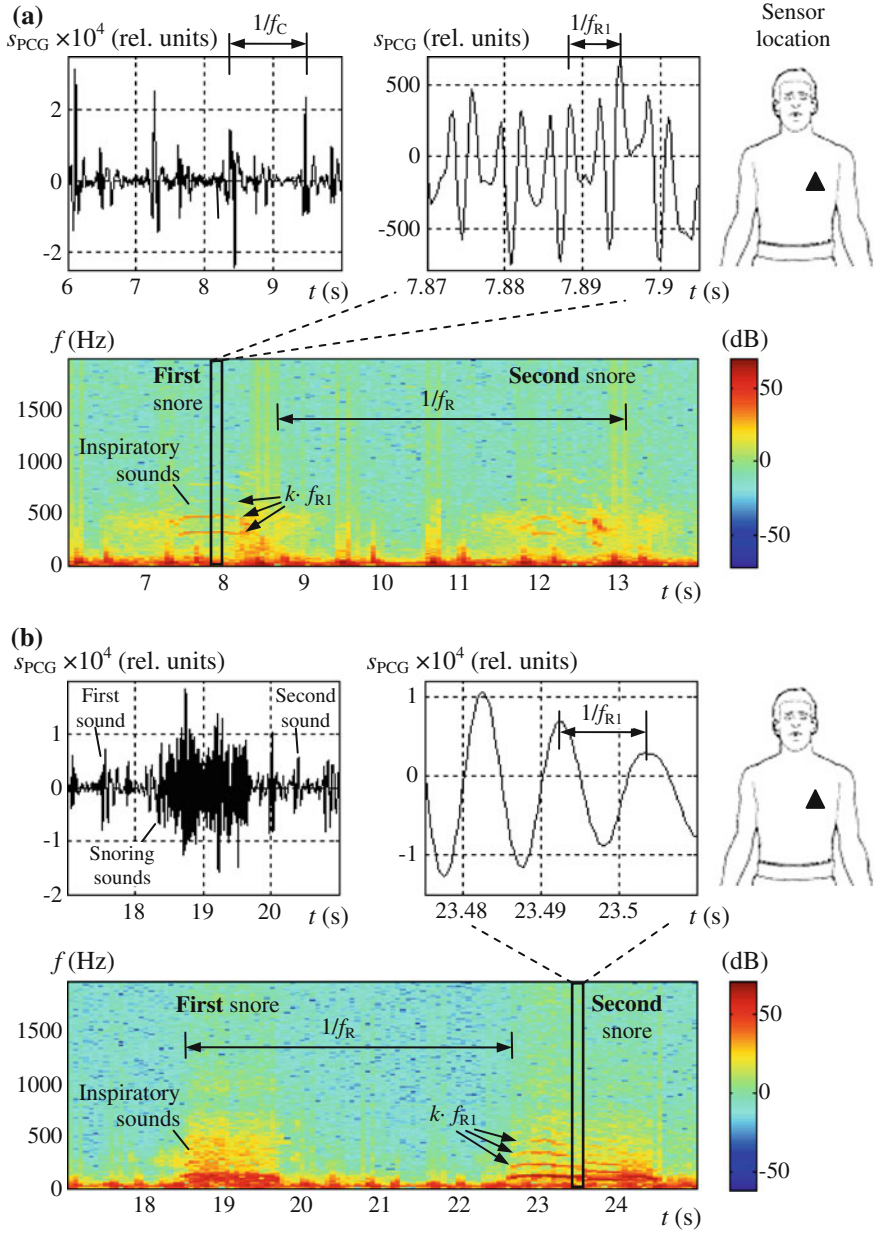
Figure 4.13 illustrates *normal snoring sounds* in more detail, which were auscultated at the *chest* during sleep. Provided that the snoring is relatively *silent* (Fig. 4.13a), snoring sounds can be hardly recognised in the time domain (Kaniusas et al. 2005); only heart sounds are easily discernable here (compare Fig. 4.9). However, if the time axis is stretched out during an *inspiratory snoring* event and the amplitude resolution is increased—as depicted in the right upper subfigure of Fig. 4.13a—the waveform pattern of snoring sounds becomes uncovered. That is, a *periodic waveform* with the fundamental harmonic frequency  $f_{R1}$  of about 160 Hz can be observed. The *relative amplitude* of these snoring sounds in relation to that of heart sounds can be easily estimated and yields  $-32$  dB ( $= 20 \cdot \log(1000/40000)$ ); likewise, the *silent normal snoring sounds* are much *weaker than heart sounds*; compare Sect. 4.2.2.3. Again, normal snoring sounds clearly manifest in the *spectrogram* during inspiration (Fig. 4.13a). In particular, a series of *harmonics* at integer multiples of  $f_{R1}$ , i.e., at  $k \cdot f_{R1}$  with  $k$  as the integer index, can be seen, whereas the fundamental harmonic located at  $f_{R1}$  was already disclosed in the right upper subfigure of Fig. 4.13a.

In the case of the relatively *loud normal snoring* (Fig. 4.13b), snoring sounds start to dominate in the time domain (Kaniusas et al. 2005). A nearly *sinusoidal waveform* can be observed in the expanded waveform with  $f_{R1} \approx 95$  Hz. The *relative amplitude* of these snoring sounds in relation to that of heart sounds amounts to  $+2.5$  dB ( $= 20 \cdot \log(20000/15000)$ ); likewise, the *loud normal snoring sounds* are already a little bit *stronger than heart sounds*. In the *spectrogram*, the footprint of snoring sounds is more dense and includes more high frequency components as compared with either the relatively silent snoring (Fig. 4.13a) or vesicular lung sounds (Fig. 4.9b).

Specific sound patterns related to *obstructive snoring* are shown in Fig. 4.14, illustrating an evident difference between normal and obstructive snoring. These *snoring sounds* clearly *dominate over heart sounds* in the time domain, whereas the expanded waveform pattern shows *interfering oscillations* with  $f_{R1} \approx 85$  Hz (Fig. 4.14a). The *relative amplitude* of obstructive snoring sounds in relation to that

---

<sup>19</sup> Interestingly, the largest and sharpest deflection of the sound wave coincides with the peak of the air flow, considering the complex-waveform snoring (Beck et al. 1995). It indicates the relevance of the *air flow* for the generation of *snoring sounds*, according to discussed mechanisms shown in Fig. 4.12.



◀**Fig. 4.13** Normal snoring sounds during sleep (compare Fig. 4.14). (a) Relatively silent snoring from a male subject (body mass index  $BMI$  of  $23.6 \text{ kg/m}^2$ , see Footnote 202 in Sect. 3), as illustrated by an acoustic biosignal phonocardiogram  $s_{PCG}$  from the chest region. (b) Relatively loud snoring from another male subject ( $BMI = 24.7 \text{ kg/m}^2$ ). A zoomed region of  $s_{PCG}$  with the duration of 35 ms is given in each case at the time of a snoring event (*right upper subfigure*). The heart rate  $f_C$  and respiratory rate  $f_R$  are indicated. The corresponding spectrograms (*lower subfigures*) with shown fundamental harmonic frequency  $f_{R1}$  are given for comparison. For parameters of the spectrograms see Footnote 4

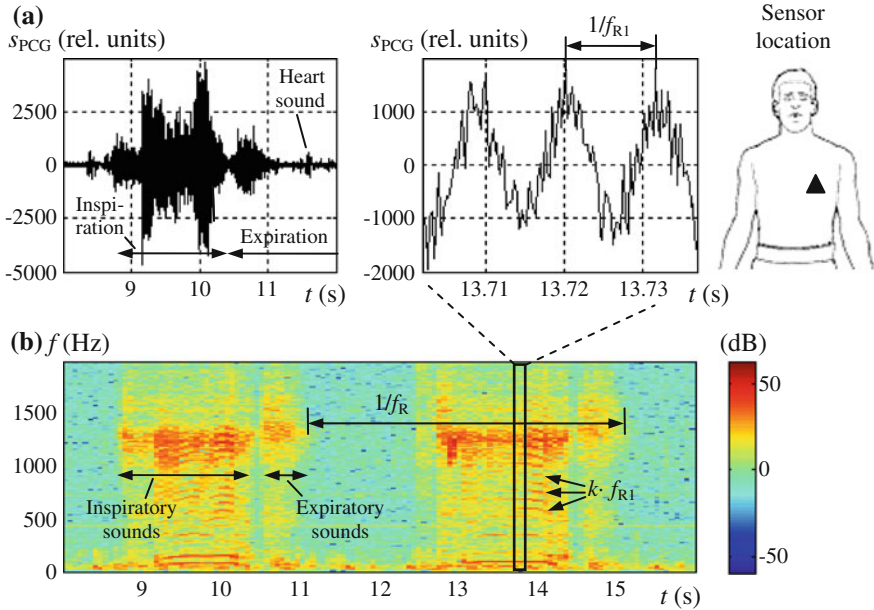


**Fig. 4.14** Obstructive snoring sounds during sleep, recorded from a male patient with the obstructive sleep apnea ( $BMI = 35.5 \text{ kg/m}^2$ ); compare Fig. 4.13. (a) Acoustic biosignal phonocardiogram  $s_{PCG}$  from the chest region. A zoomed region of  $s_{PCG}$  with the duration of 35 ms is given at the time of an obstructive snoring event (*right subfigure*). (b) The corresponding spectrogram with indicated respiratory rate  $f_R$  and fundamental harmonic frequency  $f_{R1}$ . For parameters of the spectrogram see Footnote 4

of heart sounds amounts to  $+12 \text{ dB}$  ( $= 20 \cdot \log(5000/1300)$ ); compare Sect. 4.2.2.3. A series of *harmonics* can be observed in the spectrogram, extending up to  $1,500 \text{ Hz}$  (Fig. 4.14b). A noise-like structure is visible above  $1,000 \text{ Hz}$ , which also appears in the course of expiratory snoring sounds but with smaller amplitude. As the dominant feature, the cumulative power of *high frequency components* above  $800 \text{ Hz}$  seems to be larger than that below  $800 \text{ Hz}$ .

*Simulated snoring sounds* are depicted in Figs. 3.5 and 3.6 (Sect. 3.1.2). The corresponding oscillations of the air flow with the frequency  $f_{R1} \approx 40 \text{ Hz}$  can be clearly recognised in Fig. 3.6c. In fact, the air flow oscillates with the oscillation

frequency of the sound waveform, as also shown in Beck et al. (1995); compare Footnote 19.

Considering the different ways of the snoring sound classification, the illustrated (silent and loud) normal snoring from Fig. 4.13 seems to correspond to the oronasal and simple-waveform snoring. On the other hand, the obstructive snoring from Fig. 4.14 resembles the oronasal and complex-waveform snoring.

In analogy with lung sounds, there are indications that the *amplitude of snoring sounds* depends strongly on—or, as a first approximation, is proportional to—the level of the *air flow*  $q^A$ ; see Footnote 19. However, this relationship seems to be *non-linear* because different generation mechanisms (i.e., oscillations, reopenings, and turbulences) are involved in the origination of snoring sounds. In addition,  $q^A$  is a function of both  $u$  and  $A$  (4.2) which are important non-linear parameters of these mechanisms.

Similar to lung sounds (Sect. 4.1.1.2), *snoring sounds* are subjected to *strong variability* in their loudness and frequency. The strong variability can be observed in the time and frequency domains, in which sound patterns may change from one snore to another or even experience changes within a single snore (Kaniusas 2007; Moerman et al. 2002; Perez-Padilla et al. 1993). The variability of obstructive snoring is particularly high (Beck et al. 1995). This *variability* in sound patterns may arise due to

- altering (geometric, physical) characteristics of *resonating cavities* in the upper airways such as the pharynx or mouth cavity. The geometry and apertures of cavities significantly change when airways temporarily occlude or fully dilate.
- Movement of the *site of collapse* upstream or downstream the airway also contributes to the sound variability.

The *spectrogram* in Fig. 4.13b clearly demonstrates the *variability* of snoring sounds. In the depicted case, noise-like structure during the first snore (with *fricative quality*) transforms into a series of harmonics during the second snore (with *rattling quality*). Even frequencies of harmonics markedly decrease during the second snore.

Lastly, *intensity levels* of snoring sounds should be shortly discussed, especially in comparison to normal lung sounds (Sect. 4.1.1.2). To begin with, the *background noise* level in rooms could reach 50 dB *sound pressure level* (SPL).<sup>20</sup>

---

<sup>20</sup> The abbreviation *dB SPL* refers to a logarithmic measure of the sound pressure level relative to a reference pressure level (of 20  $\mu\text{Pa}$ ), i.e., relative to the *threshold of human hearing*. For instance, a normal conversation yields about 60 dB SPL, whereas a pneumatic drill—in a distance of a few meters—yields 100 dB SPL.

However, the human ear does not equally respond to all frequencies and it is highly sensitive to sounds in the frequency range of about 1–5 kHz; likewise, the ear is less sensitive to very low or very high frequencies of sounds. To accommodate this behaviour, sound meters use frequency filters which mimic this non-linear frequency response of the ear. In this context, the abbreviation *dBA* stays for a logarithmic measure of the sound pressure level employing the so-called *A-weighting filter*. This filter disproportionately attenuates very low frequencies, e.g., an attenuation of –30 dB is applied at 50 Hz while no attenuation (of 0 dB) is applied at 1 kHz.

The *lung sound level* is normally in the range of 40–45 dB SPL (Schäfer 1988) or 17–26 dBA (Schäfer 1996), and could go up to 54 dB SPL (Series et al. 1993).

The *snoring sound level* is greater than 60 dB SPL in line with (Series et al. 1993; Itasaka et al. 1999) or greater than 68 dB SPL according to Schäfer (1988), and can temporarily reach values of more than 100 dB SPL in a distance less than 1 m from the head of the snorer (according to diverging reports). The *obstructive snoring* yields levels in the range of 50–70 dBA, the levels increasing by > 5 dBA from nonapneic snoring patients to apneic snoring patients (Wilson et al. 1999). Similarly, *maximum snoring sound levels* of up to 80 dBA were reported in a distance of 1 m for nonapneic snoring patients, whereas maximum levels of up to 94 dBA were reported during postapneic snores in apneic snoring patients (Schäfer 1996). In fact, loud snoring may constitute an excessive noise exposure which can even cause *hearing problems* (Wilson et al. 1999).

#### 4.1.1.4 Apneic Sounds

There is strong evidence that *obstructive snoring* during sleep (Sect. 4.1.1.3) may be an intermediate symptom<sup>21</sup> in the history of the sleep apnea syndrome (Sect. 3.1.2). In particular, the *obstructive sleep apnea* is characterised by a complete occlusion of the upper airways and ceased breathing, as illustrated in Fig. 3.8b. The intermittent respiratory arrest is marked by intermittent absence of breathing sounds, i.e., lung and snoring sounds, which yields a unique *acoustical fingerprint of apneas* among body sounds.

When an obstructive *apnea terminates*, a gasp for the air follows and very loud, high frequency, explosive *apneic sounds* are usually induced by reopening of the collapsed airways at the tongue base. These *inspiratory sounds* appear to be highly different from *regular, rattling snoring sounds in nonapneic subjects* (Perez-Padilla et al. 1993); compare Sect. 4.1.1.3.

Even though snoring sounds greatly vary from one respiration cycle to another, the *first postapneic inspiratory snore* (at the end of an apnea) is distinctive because the *airway is at its narrowest*. That is, instead of rattling and repetitive quality, continuous *turbulent and fricative quality* can be heard such as can be simulated by producing a consonant “h” sound. The *air turbulences* from the air flowing through a *narrow orifice*—with a relatively *high flow velocity* (Footnote 5)—appear to contribute much to the inspiratory noise; the momentary airway geometry filters and modifies this noise (i.e., resonances in the airway acting as band-pass filters to the noise, Footnote 17). That is, this postapneic snore consists of irregular high frequency *noise* with poorly formed and variable *bursts* in the time domain (Perez-Padilla et al. 1993). In the frequency domain, this snore shows a broad spectral peak at around

---

<sup>21</sup> Namely, *obstructive snoring* is considered as a primary symptom for *sleep apnea* (Brunt et al. 1997). However, the noisy respiration during sleep, as actually the snoring corresponds to, can not be used as a sole indicator of breathing abnormalities, such as sleep apnea (Wilson et al. 1999). Likewise, snoring lacks *specificity* for diagnosis of apneas.

450 Hz and another one at around 1 kHz; both peaks probably raised by filtering and modification of the noise in the airway. The latter bursts of sound—superimposed on the noise—also indicate additional sound sources other than air turbulences (*turbulent mechanisms*), such as intermittent opening and closing of the airway (*vocal mechanisms*), all sources contributing to the first postapneic snore.

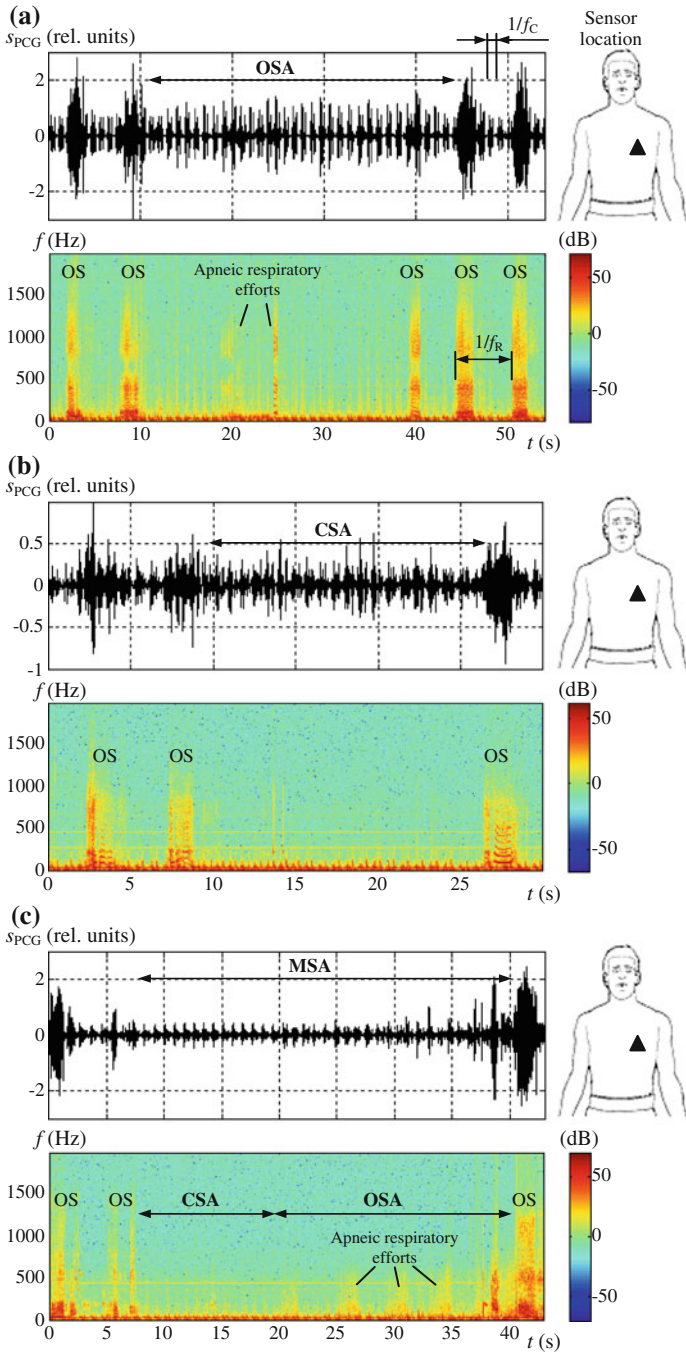
In the course of *subsequent breaths* after the first postapneic snore, apneic sounds become like obstructive snoring sounds. The *high-pitched sounds* may possibly fade into the *low-pitched sounds* in the ventilatory interval between two neighbouring apneas. In fact, postapneic sounds exhibit very high variability in the time and frequency domains because of highly pronounced morphological variations of the pharyngeal airway from fully occluded to fully dilated (Perez-Padilla et al. 1993).

Figure 4.15 illustrates *apneic sounds* and their variability considering different types of apneas. The *obstructive sleep apnea* (Fig. 4.15a) is surrounded by obstructive snoring events because this type of apnea is characterised by obstructive occlusions of the upper airway. In analogy to Fig. 4.14b, high frequency components above 800 Hz can be clearly distinguished, which is a typical feature of obstructive snoring (Sect. 4.1.1.3). Brief high-pitched sounds can be observed in the middle of this obstructive apnea, which indicate *apneic respiratory efforts* during the apnea. These acoustically noticeable efforts denote time intervals during which the airway is incompletely occluded. Distinct snoring surrounds the depicted *central sleep apnea* (Fig. 4.15b), which composition in the time and frequency domains is similar to that of loud snoring from Fig. 4.13b. In the case of the *mixed sleep apnea* (Fig. 4.15c), a preceding central segment without apneic respiratory efforts can be seen, followed by an obstructive segment with numerous apneic respiratory efforts; in fact, this observation complies with the definition of the mixed sleep apnea (Sect. 3.1.2).

The acoustical fingerprint of an *obstructive sleep hypopnea*—characterised by a mere reduction of the respiratory airflow (Sect. 3.1.2)—is demonstrated in Fig. 4.16. Temporal reduction of the amplitude (or the intensity) of the obstructive snoring sounds can be observed in the time domain; compare the depicted envelopes in Fig. 4.16a. In the spectrogram, the power of high frequency components above around 800 Hz decreases temporarily during the hypopnea (Fig. 4.16b). However, snoring events during the hypopnea still remain as obstructive snoring events because of the obvious spectral gap around 800 Hz in the obstructive events; compare with Fig. 4.14b.

#### 4.1.1.5 Mutual Interrelations

As shown in Sects. 4.1.1.1–4.1.1.3, *heart sounds* arise in the course of cardiac activity while *lung, snoring, and apneic sounds* arise in the course of respiratory activity. Since *cardiac and respiratory activities* are intimately and conclusively related to each other (Sect. 3), body sounds originating from cardiac and respiratory activities (Fig. 4.1) exhibit various *mutual interrelations*. Likewise, sources of the



◀**Fig. 4.15** Apneic sounds during sleep, as illustrated by an acoustic biosignal phonocardiogram  $s_{PCG}$  from the chest region of sleep apnea patients. (a) Obstructive sleep apnea (OSA) with an apneic respiratory effort, surrounded by obstructive snoring (OS) events (male patient,  $BMI = 29 \text{ kg/m}^2$ ); compare Fig. 4.14. (b) Central sleep apnea (CSA) delimited by OS events (female,  $BMI = 28.2 \text{ kg/m}^2$ ). (c) Mixed sleep apnea (MSA) with successive segments of CSA and OSA (male,  $BMI = 35.5 \text{ kg/m}^2$ ). The heart rate  $f_C$  and respiratory rate  $f_R$  are indicated. The corresponding spectrograms (*lower subfigures*) disclose intermittent respiratory activity in more detail. For parameters of the spectrograms see Footnote 4

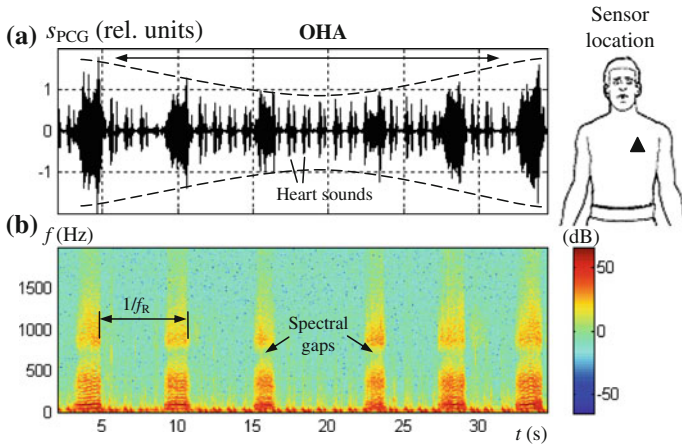


**Fig. 4.16** Apneic sounds during obstructive sleep hypopnea (OHA), recorded from a patient with the obstructive sleep apnea (male patient,  $BMI = 29 \text{ kg/m}^2$ ); compare Fig. 4.15. (a) Acoustic biosignal phonocardiogram  $s_{PCG}$  from the chest region. (b) The corresponding spectrogram with indicated respiratory rate  $f_R$ . For parameters of the spectrogram see Footnote 4

corresponding body sounds—in terms of the sound’s formation in the electrical circuit model, see Fig. 4.2—are tightly related to each other. On the other hand, mutual interrelations among body sounds originating from *respiratory activity* only, such as lung, snoring, and apneic sounds, also exist because all these sounds have the same origin—the respiration.

Figure 4.17 illustrates the latter relationships of sources of the different body sounds. In fact, *mechanic, neurogenic, and hormonal* control mechanisms are involved here, as described below (compare Sect. 3.2).

To begin with mutual interrelations, the *respiration-induced effects on heart sounds* will be considered first (A and B in Fig. 4.17). During *inspiration* these modulation effects can be summarized as follows:

- intensification of sounds from the right side of the heart, i.e., intensification of *right-sided heart sounds* which are generated by closure of the right-sided valves, the tricuspid and pulmonary valve (Fig. 4.3);
- attenuation of *left-sided heart sounds*, generated by closure of the left-sided valves, the mitral and aortic valve (Fig. 4.3);

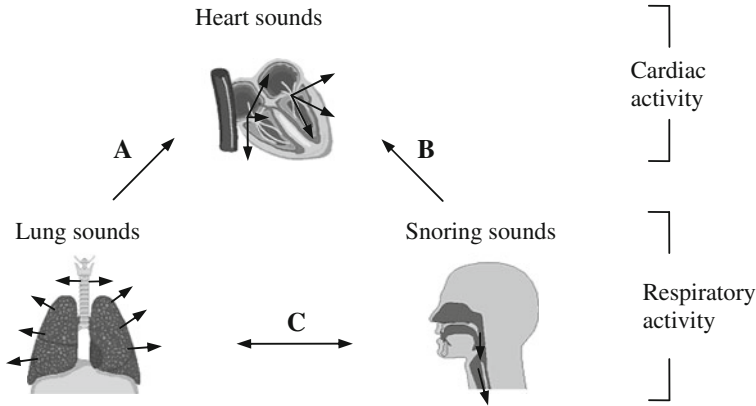


**Fig. 4.17** Mutual interrelations of the sources of the different body sounds with indicated direction of the physiological influence

- (intensified) *splitting* of the first and second heart sound; and
- increased *repetition rate* of heart sounds, i.e., increased  $f_C$ .

Obviously, modulation effects reverse during expiration and disappear when *holding breath*. Generally, the changing volume of the lung influences the pressure conditions within the heart and those close to the heart, which in turn mechanically influences *intensity and timing* of the *valve's closure*.

As described in section “Normal Respiration” in Sect. 3.2.1.2 in more detail and illustrated in Fig. 3.31, during *inspiration* the *right ventricular stroke volume* increases temporarily and rises the volume of the *decelerated blood* in the right side of the heart at the valve's closure. Thus, the vibration intensities of the corresponding *right-sided valves* (Fig. 4.3) and the involved right-sided blood volumes increase, which intensifies the *right-sided heart sounds*; compare generation mechanisms of heart sounds in Sect. 4.1.1.1. Conversely, during inspiration the left ventricular stroke volume decreases temporarily, which causes the *left-sided heart sounds* to decrease in their intensity.

Likewise, authors in Amit et al. (2009) report that the decreased left ventricular stroke volume and the correspondingly decreased left ventricular *contraction force* (compare Footnote 225 in Sect. 3) contribute to the attenuation of the first heart sound during inspiration. In analogy, an increased *pressure difference* between aortic pressure and left ventricular pressure (i.e., increased *afterload*) accentuates the second heart sound. Therefore, *mechanical mechanisms* are responsible for the rhythmic changes in the sound intensity within the respiration cycle.

Similar *mechanical mechanisms* are responsible for an audible separation between consecutive sound components within the first heart sound and those within the second heart sound (Sect. 4.1.1.1), i.e., responsible for an intensified *splitting* of these heart sounds during *inspiration*. As described in section “Normal Respiration” in Sect. 3.2.1.2 and illustrated in Fig. 3.32, the tricuspid valve and

pulmonary valve (Fig. 4.3) stay open longer in the course of the ventricular systole during inspiration in comparison with expiration; this is because the right ventricular stroke volume increases during inspiration. In addition, the mitral valve closes a bit earlier than the tricuspid valve due to mechanisms described in Footnote 2. The aortic valve closes earlier than the pulmonary valve because of both the decreased left ventricular stroke volume and increased right ventricular stroke volume. As a result, the gap between the early sound contribution from the closure of the mitral valve and the late sound contribution from the closure of the tricuspid valve widens within the *first heart sound* at inspiration. In analogy, the gap between the early sound contribution from the closure of the aortic valve and the late sound contribution from the closure of the pulmonary valve widens within the *second heart sound* at inspiration.

In addition to the discussed mechanisms, the *first and second heart sound* was observed to be slightly *delayed and advanced*, respectively, during inspiration (Amit et al. 2009). The latter observation corresponds to the dominance of the right-sided sounds in the first heart sound and the dominance of the left-sided sounds in the second heart sound, given the discussed changes in stroke volumes; compare Fig. 4.18a.

*Neurogenic mechanisms* account for *increased  $f_C$*  at *inspiration*, whereas  $f_C$  decreases at expiration. As described and illustrated in Sect. 3.2.1.1, respiratory sinus arrhythmia occurs from the influence of breathing on the autonomic nervous system which governs the heart beat (Sect. 3.1.1).

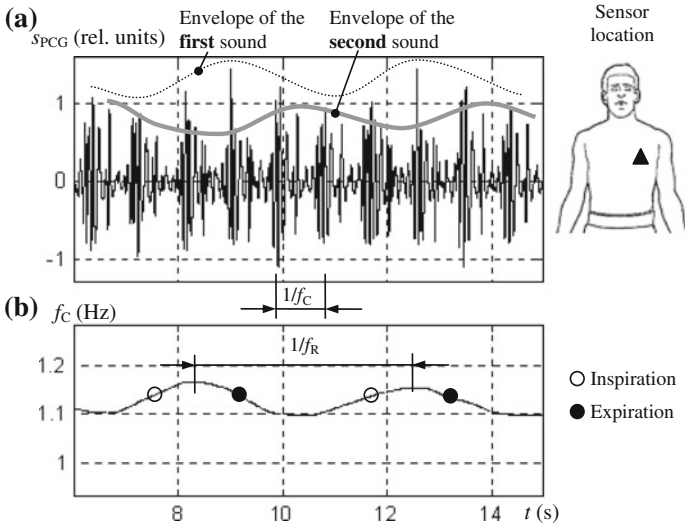


**Fig. 4.18** Influence of breathing on heart sounds. **(a)** Acoustic biosignal phonocardiogram  $s_{PCG}$  from the chest region with an added envelope which indicates the amplitude modulation of  $s_{PCG}$  with the respiratory rate  $f_R$ . **(b)** The instantaneous heart rate  $f_C$  derived from  $s_{PCG}$

In fact, the aforementioned mechanisms rather apply for *normal breathing* (A in Fig. 4.17). However, in the case of *obstructive snoring* the long-term impact of the snoring sound sources on the heart sound sources becomes more intricate and less direct (B in Fig. 4.17). The persistent obstruction of the upper airways may overload the heart in the long-term, involving also hormonal mechanisms, favouring *cardiovascular diseases* (Sect. 4.1.1.3) and thus causing malfunction of valves and vibrating structures (i.e., sound sources) in and close to the heart. In particular, impact on the heart is strong if the obstruction occurs with an intermittent and complete closure of the airway lumen, i.e., with intermittent apneas (Sect. 3.1.2).

*Body sounds of the respiratory origin* arise in synchrony, yielding an identical respiratory rate (C in Fig. 4.17). Nonetheless, signal properties of lung, snoring, and apneic sounds remain very different; see Sects. 4.1.1.2–4.1.1.4. In addition, it can be expected that laboured breathing or heavy obstructive snoring (with an intermittent occlusion of the upper airways) could temporarily alter resonance (spatial) characteristics of airways in which lung sounds originate. This would lead to snoring-related changes in spectral components of lung sounds; compare Footnote 17 and section “Specific Issues” in Sect. 4.1.2.1.

Figure 4.18 illustrates *respiration-induced effects on heart sounds*. It can be observed that the amplitude of the *first heart sound* increases during *inspiration* while that of the *second heart sound* decreases, see the corresponding envelopes in Fig. 4.18a. That is, the amplification of the right-sided heart sounds is stronger in the first heart sound than the concurrent attenuation of the left-sided heart sounds, i.e., the right-sided sounds dominate in the first heart sound. The reverse is true for the second heart sound. However, as noticed in section “Normal Respiration” in Sect. 3.2.1.2, the illustrated behaviour in Fig. 4.18a *is not generally valid*, as also reported in Amit et al. (2009). For instance, Fig. 3.31b shows decreasing amplitude of the first heart sound and increasing amplitude of the second heart sound during inspiration; Figs. 4.9a and 3.5b demonstrate increasing both first and second heart sounds during inspiration; Fig. 3.32b discloses decreased intensities of both heart sounds during inspiration, as also reported in Ishikawa and Tamura (1979). In addition, Fig. 4.18b illustrates a temporal *increase of  $f_C$*  (i.e., the reoccurrence rate of heart sounds) at *inspiration*, as expected from respiratory sinus arrhythmia.

Lastly, *overlapping frequency ranges of the different body sounds* should be addressed. As can be extracted from Sects. 4.1.1.1–4.1.1.3,

- *heart sounds* reside in the approximate frequency range up to 100 Hz,
- tracheobronchial *lung sounds* in the range of 100–1,000 Hz,
- vesicular *lung sounds* 100–500 Hz,
- normal *snoring sounds* 100–800 Hz, and
- obstructive *snoring sounds* 100–2,000 Hz.

Besides the above approximations of the frequency ranges, the frequency components of heart sounds overlap with that of breathing sounds (such as lung sounds and snoring sounds). In particular, the relatively *strong heart sounds* overlap with

the low frequency components of the relatively *weak breathing sounds*. For instance, the *interference of heart sounds* in *breathing sounds*—as recorded on the neck—was quantitatively reported in Lessard and Jones (1988). The authors showed that the contribution of heart sounds can not be neglected even at frequencies above 100 Hz because of their relatively high intensity (Sect. 4.1.1.2). The first heart sound was shown to contribute to the acoustic power in the frequency range of 175–225 Hz during inspiration and 75–125 Hz during expiration. In parallel, the second heart sound—with spectral components of even higher frequencies (Sect. 4.1.1.1)—appeared to contribute to the acoustic power in a more extended range of 75–425 Hz during inspiration and 75–325 Hz during expiration.

### 4.1.2 Transmission of Body Sounds

The *transmission of body sounds* throughout the tissue, in addition to their genesis (Sect. 4.1.1), comprises *formation aspects* of body sounds, according to the model of acoustic biosignals (Fig. 4.2). As illustrated in Fig. 4.1, the acoustical path of body sounds begins within the respective *sound source* which is given by oscillating (biological) structures, vibrating blood volumes and turbulent air. The induced *mechanical waves*<sup>22</sup> propagate through the tissue along multiple paths and are subjected to changes in their intensity (mostly damping) because of *absorption, scattering, diffraction, reflection, refraction, and resonance* phenomena. In fact, a large percentage of the sound energy dissipates on the way and never reaches the skin surface where an acoustic *sensing device* is usually located (Fig. 4.1).

---

<sup>22</sup> Sound is provided by *mechanical oscillations* in an *elastic medium*, as illustrated in Fig. 4.19a for longitudinal waves. Under influence of a transient external force, composing *particles* of the medium (e.g., molecules in the air or tissue) are dislocated from their equilibrium (rest) position and are then left to their own devices. Inertial and elastic forces (restoring forces) are induced, which force these particles to move back, so that the particles start to swing around their equilibrium positions with a certain *particle velocity* in terms of mechanical oscillations. Consequently, as demonstrated in Fig. 4.19, the mechanical *overpressure* (positive *sound pressure*) arises in the regions of increased medium density while the *underpressure* (negative sound pressure) arises in the regions of decreased density, as compared with the resting state of the medium without propagating sounds; compare Footnote 26. Please note that

- the spatial *wave of the sound pressure*  $p(x)$  propagating in the direction  $x$  (Fig. 4.19b) is in-phase with the *wave of the particle velocity*  $u(x)$  in *unlimited elastic medium* (but not in the limited resonating cavity such as in Fig. 4.24), whereas
- the corresponding *wave of the particle deflection* is dislocated by  $90^\circ$  with respect to  $p(x)$  or  $u(x)$ .

In fact, the *particle velocity* strongly differs from the *sound propagation velocity* (4.3). The particle velocity (4.6) is usually by many orders lower than the propagation velocity; e.g.,  $5 \cdot 10^{-8}$  m/s versus 343 m/s in the air (Table 4.1) at the human auditory threshold at 1 kHz (Veit 1996). In addition, the particle velocity increases with increasing loudness (sound intensity) while the propagation velocity usually does not.

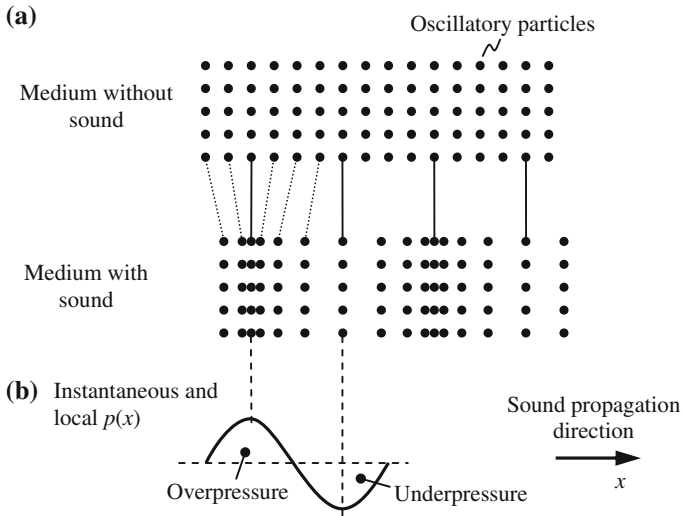


**Fig. 4.19** Sound waves or mechanical deformation propagating in an elastic medium. (a) Oscillatory particles in medium—elastically bound to each other—are transiently dislocated from their equilibrium position by the propagating pressure wave. (b) The associated sound pressure  $p$  indicates local regions of overpressure and underpressure. In fact, a longitudinal density wave is demonstrated here, while the wave  $p$  oscillates in the direction of the sound propagation

#### 4.1.2.1 Propagation of Sounds

##### General Issues

Body sounds propagate in a biological medium with the sound propagation velocity  $v$  (a *time-space* characteristic), oscillate with the sound frequency  $f$  in the time domain (a *time* characteristic), and oscillate with the wavelength  $\lambda$  along their propagation path (a *space* characteristic) according to

$$v = \lambda \cdot f . \quad (4.3)$$

In fact, the above equation applies for any type of wave propagation, including the propagation of pulse waves along arteries, as discussed in section “Pulse Propagation” in Sect. 2.5.2.3.

The value of  $v$  is determined by (macroscopic) physical properties of the propagation medium, such as biological tissue or air, according to

$$v = \sqrt{\frac{\bar{\kappa}}{\rho}} = \sqrt{\frac{1}{\rho \cdot D}} . \quad (4.4)$$

**Table 4.1** Typical and approximate sound velocities  $v$  in the air, water, muscle, bone (Veit 1996), large airways (i.e., with diameter  $> 1$  mm), biological tissue (Kompis et al. 2001), tallow (Trendelenburg 1961), and lung tissue (Kompis et al. 2001; Rice 1983; Wodicka et al. 1989)

Propagation medium	Sound velocity $v$ (m/s)	Sound wavelength $\lambda$ (m)	Absorption coefficient $\alpha_F + \alpha_T$ (1/m)
Air	343	0.34	$10^{-5}$
Water	1,440	1.44	$10^{-8}$
Sea water	1,533	1.53	$10^{-8}$
Fat	1,450	1.45	$> 10^{-8}$
(Olive) oil	1,420	1.42	$> 10^{-6}$
Tallow	390	0.39	$10^{-4}$
Large airways	270	0.27	$10^{-5}$
Tissue	1,500	1.5	$> 10^{-8}$
Muscle	1,560	1.56	$> 10^{-8}$
Bone	3,600	3.6	$> 10^{-4}$
Lung tissue	50	0.05	$> 10^{-4}$

The corresponding wavelengths  $\lambda$  are estimated for the sound frequency 1 kHz by (4.3). Typical and approximate sound absorption coefficients  $\alpha$  (considering only  $\alpha_F$  and  $\alpha_T$ , see (4.14)) are also given for the frequency 1 kHz, according to the classical sound absorption theory (Meyer and Neumann 1975; Trendelenburg 1961). Data has been accumulated from different sources (Kaniusas 2007)

In analogy to 2.22 and 2.23,  $\kappa$  is the module of volume elasticity,  $\rho$  the density, and  $D$  ( $= 1/\kappa$ ) the compliance (or adiabatic compressibility) of the propagation medium.

Table 4.1 summarizes  $v$  and  $\lambda$  for the most relevant types of *physical and biological media* involved in the transmission of body sounds. For the sake of simplicity, only approximate values are given without considering effects of varying  $f$ , temperature, humidity, and the type of acoustical waves (e.g., longitudinal or transverse wave).<sup>23</sup>

<sup>23</sup> The influence of temperature and humidity on  $v$ —and thus also on  $\lambda$  (4.3)—should be discussed shortly from a physiological point of view. It is well known that  $v$  in the air tends to increase with increasing temperature, yielding an increase rate of about 0.6 m/s per degree Celsius. During *inspiration* the air at room temperature (usually  $< 37$  °C) enters the respiratory airways, whereas during *expiration* the warmed up air at body temperature ( $\approx 37$  °C) leaves the airways. Consequently, the level of  $v$  in the large airways decreases with inspiration by a few percent and correspondingly increases with expiration.

Regarding the influence of humidity, it should be noted that the inspired air is saturated with water vapour (relative humidity of 100 %) as it flows over the wet and warm mucous membranes lining the respiratory airways (Sect. 2.6.2). The effective value of  $v$  is very slightly influenced by the air humidity, e.g., a change in the relative humidity from 50 % at *inspiration* to 100 % at *expiration* increases  $v$  by only about 0.5 % at 37 °C.

In fact, the more *compressible* is the propagation medium, i.e., the larger is  $D$  (4.4), the lower is  $v$ . Consecutively, the air, large airways, and lung tissue exhibit relatively low values of  $v$ , whereas incompressible liquids like (sea) water show relatively high values of  $v$ . Solid substances such as *bone* tend to show even higher values of  $v$ . *Biological tissues* (including blood) yield  $v$  comparable with that in the (sea) *water* because tissues have a relatively high (salt) water content of about 60 % (Silbermagl 2007); compare Table 2.1. The *lung tissue*, given by a mixture of a compliant tissue and the air,<sup>24</sup> yields the lowest  $v$  in the order of 50 m/s, or in the range of 23–60 m/s (Kompis et al. 2001). It can also be observed in Table 4.1 that fat (e.g., fat layers in tissue) tends to slow down the sound propagation; for instance, the level of  $v$  in porcine muscle and skin (1,620 and 1,680 m/s) were reported as being higher than in the outer (skin) fat layer (1,435 m/s) (Koch et al. 2010).

### Specific Issues

The calculated values of  $\lambda$  for  $f = 1$  kHz (Table 4.1) indicate that they are in the range of average *body dimensions* of less than 2 m but are significantly larger than the *auscultation distance*  $r$  from sources of inner body sounds to typical auscultation sites. Figure 4.20 demonstrates that typical values of  $r$  are in the range of 5–30 cm. That is, the acoustical *near field*—satisfying the inequality  $r < 2 \cdot \lambda$  (see Sect. 6)—dominates in typical *auscultation sites* on the skin. In particular, this near field condition is fulfilled in *solid* and *liquid* media (with relatively high  $\kappa$ , (4.4)) while in the *air*  $r$  and  $\lambda$  become comparable in size. However, the *lung tissue* is an exception with  $\lambda$  in the

<sup>24</sup> The value of  $v$  in the *lung tissue* depends strongly on the air content in the lung. Provided that the volumetric portion of the air is 75 % and the rest is tissue (Wodicka et al. 1989), the effective  $\rho$  and  $D$  of the composite mixture can be estimated as

$$\rho = 0.75 \cdot \rho_A + 0.25 \cdot \rho_T \approx 0.25 \cdot \rho_T$$

and

$$D = 0.75 \cdot D_A + 0.25 \cdot D_T \approx 0.75 \cdot D_A$$

where  $\rho_A$  ( $= 1.2 \text{ kg/m}^3$ ) and  $\rho_T$  ( $= 1,040 \text{ kg/m}^3$ ) are approximate densities of the air and tissue, respectively. In analogy,  $D_A$  ( $= 7,083 \text{ GPa}^{-1}$ ) and  $D_T$  ( $= 0.43 \text{ GPa}^{-1}$ ) are the corresponding compliances which are estimated using (4.4) with  $v$  (Table 4.1) and  $\rho$  as parameters. It can be observed that  $\rho_A \ll \rho_T$  and  $D_A \gg D_T$ . With the effective  $\rho$  and  $D$  from above equations, (4.4) yields  $v = 27 \text{ m/s}$  fitting well the reported range of 23–60 m/s (Kompis et al. 2001).

In fact, the above postulation of a *homogenous mixture of gas and tissue* assumes that the *size of  $\lambda$*  in the lung parenchyma is significantly larger than the alveolar size (diameter  $< 1 \text{ mm}$ ). In fact, this assumption is entirely met by body sounds in the frequency range up to 2 kHz (see section “Volume Effects” in Sect. 4.1.2.2).

range of only 5 cm (at  $f = 1$  kHz). Thus, the condition of the near field is hardly met in the lung tissue (and the far field conditions apply).

It should be stressed that the size of  $\lambda$  *decreases* with *increasing*  $f$  (4.3), so that the inequality  $r < 2 \cdot \lambda$  increasingly ceases to apply. In addition, as will be shown later (in Fig. 4.23), high frequency components of body sounds tend to take an airway bound route while propagating in the body; i.e., the branched structure of the (air-filled) respiratory airways is preferred over the lung parenchyma (or semi-solid tissue of the inner mediastinum) as the *propagation pathway* of body sounds.

In the case of *body sounds*, two types of their *sources* can be distinguished:

- *point source* of sound, i.e., the spatial extension of a single sound source is less than  $r$  and is limited to a particular region of the body;
- *diffuse source* of sound, i.e., distributed multiple sound sources dominate within a relatively large region of the body, which dimensions are in the range of  $r$  or even exceed  $r$ .

For instance, sound sources of *heart sounds*, tracheobronchial *lung sounds*, and *snoring sounds* can be approximated as point sources of sound (compare Sect. 4.2.2.3). In contrast, vesicular *lung sounds* yield a diffuse source of sound.

The type of sound source is relevant for a *qualitative understanding* of the propagation and absorption of body sounds, whereas the *sound attenuation* over a propagation distance is basically governed by both

- propagation *geometry* and
- propagation *medium*.

In the case of the *point source* of sound and thus *spherical waves* (Sect. 6), the sound intensity  $I$  at the distance  $r$  obeys the *geometry-related damping*, namely, the *inverse square law*<sup>25</sup>; here free and far field radiation is assumed, i.e., without sound absorption in the propagation medium and without sound reflections at any limiting boundary surfaces. Since  $I$  is inversely related to  $r^2$  (Fig. 4.21) and

$$I = p \cdot u = \frac{p^2}{Z} \quad (4.5)$$

---

<sup>25</sup> The *inverse square law* applies for *spherical waves* (Sect. 6) when *sounds* are radiated in *lossless media* outward radially from a point source, as illustrated in Fig. 4.21. Since the original *source power*  $P$  is spread out over an *area* ( $= 4\pi \cdot r^2$ ) of a sphere, which increases in proportion to  $r^2$  with the velocity  $v$ , the resulting *sound intensity*  $I$  at the distance  $r$  (passing through a unit area and facing directly the point source) is equal to

$$I = \frac{P}{4\pi \cdot r^2},$$

i.e., is inversely related to  $r^2$ . As demonstrated in Fig. 4.21, the level of  $I$  quadruples while  $p$  doubles when  $r$  is halved.

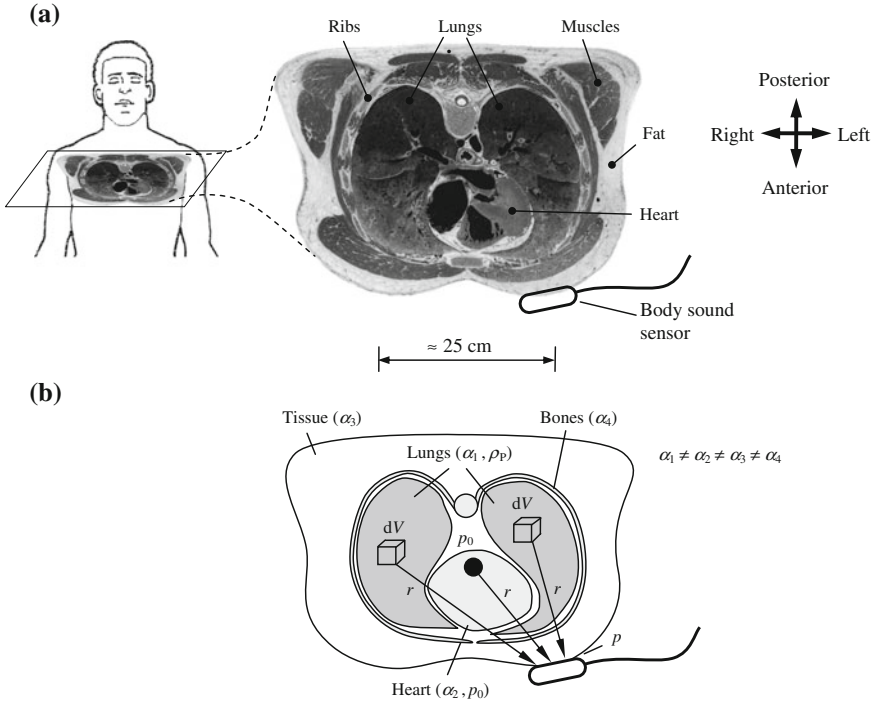


**Fig. 4.20** Propagation of body sounds in the thorax. **(a)** Photographic image of the cross-section of the thorax at the level of the heart (Bulling 1997), disclosing a highly heterogeneous propagation medium. **(b)** Schematic representation of the cross-section of the thorax at the level of the heart. Contributions of a point source of heart sounds (with the induced sound pressure  $p_0$  within the source, (4.7)) and diffuse (distributed) sources of lung sounds (with the volume density  $\rho_p$  of the induced sound pressure within the differential volume  $dV$ , (4.8)) to the sound pressure  $p$  are indicated at an auscultation site on the chest where an acoustic sensing device resides. The resulting level of  $p$  depends strongly on the source-sensor distance  $r$  and sound absorption coefficients  $\alpha$

with  $Z$  as the *characteristic acoustic impedance* (compare analogous concepts in Sect. 6), which is a (macroscopic) material property given by

$$Z = \frac{P}{u} = \rho \cdot v, \tag{4.6}$$

it can easily be derived that the effective magnitude of the *sound pressure*  $p$  is *inversely related to*  $r$  (Fig. 4.21) in a *spherical wave*. Here  $u$  denotes the effective magnitude of the *particle velocity* (around the particle's equilibrium), see Footnote 22. However, (4.5) strictly applies only under conditions of *far field* ( $r > 2 \cdot \lambda$ ) where the spatial fields of  $p$  and  $u$  oscillate *in-phase*; compare Sect. 6.

In addition to the aforementioned geometry-related damping, the propagation medium absorbs sounds, i.e., the absorbing medium reduces  $I$  with increasing  $r$ ,

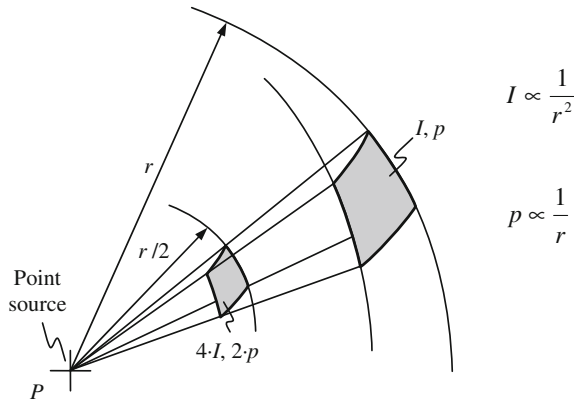


**Fig. 4.21** Illustration of the inverse square law for spherical waves with  $r$  as the distance from the point source to the auscultation site,  $P$  the source power (at  $r = 0$ ), and  $I$  the resulting sound intensity at the distance  $r$ ; compare Sect. 6

which will be referred to as the *medium-related damping*. Because of this absorption, the *medium is heated up* (see section “Volume Effects” in Sect. 4.1.2.2). In particular, the *envelope of the sound pressure*  $p^{26}$  experiences *exponential decay* in a *homogenous medium* (Sect. 6), which rate increases with the *sound absorption coefficient*  $\alpha$ . Likewise, the local decrease of  $p$  is proportional to the amplitude of  $p$  itself; see Footnote 19 in Sect. 5. Figure 4.22 demonstrates the spatial relationship between the envelope of  $p$ , the instantaneous  $p$ , and  $r$  considering only the medium-related damping. The medium with a higher  $\alpha$  ( $= \alpha_1$  and  $\alpha_1 > \alpha_2$ ) yields a steeper decrease of the envelope of  $p$  and thus a stronger damping of body sounds within this medium; see the corresponding tangents in Fig. 4.22.

Considering both mechanisms of the *sound attenuation* with  $r$  as parameter, the effective level of  $p$  at the distance  $r$ —provided that a *point source of sound* is given yielding *spherical waves*—can be approximated as

$$p = c \cdot \frac{P_0}{r} \cdot e^{-\alpha \cdot r} . \tag{4.7}$$

Here  $p_0$  describes the induced sound pressure within the point source (at  $r = 0$ ) and  $c$  is a positive constant; compare Fig. 4.20b. The factor  $1/r$  accounts for the geometry-related damping while the factor  $e^{-\alpha \cdot r}$  accounts for the medium-related damping. It is interesting to observe in (4.7) that the rate, with which  $p$  decays,

<sup>26</sup> It should be stressed that the *sound pressure*  $p$  is an *overpressure* (and the corresponding *underpressure*) related to the ambient atmospheric pressure; compare Fig. 4.19. Consequently, positive or negative  $p$  means pressure above or below the ambient pressure, respectively. In this context, Fig. 4.22 demonstrates the decay of this overpressure (or the decay of the underpressure), whereas Fig. 4.24 demonstrates periodic changes of the *instantaneous sound pressure* from values below the ambient pressure to that above the ambient pressure and vice versa.

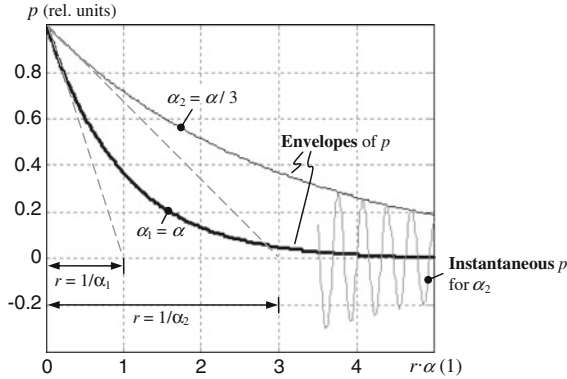


**Fig. 4.22** Spatial response of the envelopes of the sound pressure  $p$  (Footnote 26) in terms of the medium-related damping as a function of the propagation distance  $r$  at two different sound absorption coefficients  $\alpha_1$  and  $\alpha_2$  ( $\alpha_2 < \alpha_1$ ). The corresponding tangents are depicted at  $r = 0$  (dashed lines) to indicate the size of  $\alpha$  (compare Sect. 6)

decreases with increasing  $r$ . Likewise, *spherical waves* close to the point source mutate into *plain waves* distant to the source.

In analogy with (4.7), a *diffuse source* of sound yields

$$p = c \cdot \int_V \frac{\rho_P}{r} \cdot e^{-\alpha \cdot r} \cdot dV, \quad (4.8)$$

where  $\rho_P$  is the volume *density of the induced sound pressure* within the differential volume  $dV$  located in the diffuse source. The induced local (and differential) sound pressure  $dp_0$  in the diffuse source could be given as  $\rho_P \cdot dV$ , without considering pressure contributions from neighbouring regions. In general, the density  $\rho_P$  depends on  $r$ , i.e., on the spatial location of the volume  $dV$ .

Provided that a diffuse source of sound is given, it can be expected that the geometry-related damping dominates less than around a point source because the sound wavefront of the diffuse source resembles rather a *plane wave*. In consequence, the geometry-related factor should be less strong than  $1/r$ .<sup>27</sup>

<sup>27</sup> Generally, different *assumptions* regarding the *geometry-related damping factor*, i.e., the factor  $1/r$  from (4.7), can be found in literature. For instance, this factor was completely neglected in Wodicka et al. (1989), assuming plain wave conditions for the propagation of the intensity  $I$  in the lung parenchyma ( $I \propto p^2$ , (4.5)). In contrast, authors in Kompis et al. (1998, 2001) assumed an even stronger damping factor  $1/r^2$  for the assessment of the spatial distribution of the effective  $p$  in the thorax.

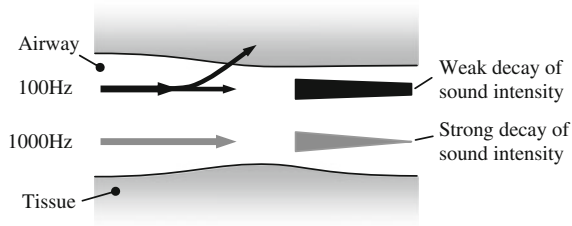


**Fig. 4.23** Sound propagation and attenuation as a function of the sound's frequency; compare Fig. 4.1

Figure 4.20 depicts photographically and schematically sources of body sounds and their respective distances  $r$  to an auscultation site on the chest wall. The geometrical dimensions of the thoracic cross-section, in combination with data from Table 4.1, prove the discussed inequality  $r < 2 \cdot \lambda$ . Figure 4.20b demonstrates also the integration procedure related to (4.8) for the highly heterogeneous medium in the thorax (Fig. 4.20a), whereas each medium has its own  $\alpha$  (Table 4.1). Provided that a point source and a diffuse source are simultaneously active, the resulting  $p$  at the auscultation site shows *additive contributions* from this point source with  $p_0$  (e.g., located in the heart) and this diffuse source with  $dp_0 = \rho_P \cdot dV$  (e.g., located in the lung).

It is interesting to observe that the *propagation pathway* of body sounds differs with the varying *sound frequency*. In particular, it applies for *lung sounds* and *snoring sounds* propagating in the highly heterogeneous medium which is basically composed of waterlike tissue and the air:

- *Low frequency sounds*, i.e., below 300 Hz (Pasterkamp et al. 1997b) or in the range of 100–600 Hz (Wodicka et al. 1989), tend to be coupled from the respiratory airways (including large airways such as trachea) into the surrounding lung parenchyma or inner *mediastinum* via induced mechanical *oscillations of airway walls*. The network of airway branches behaves as a network of *compliant tubes* which *non-rigid walls resonate* in response to the intraluminal sound at these relatively low frequencies; i.e., airway walls tend to absorb energy of low frequency sounds. Likewise, the travelling of low frequency sounds is impeded down the air-filled airways, whereas sounds bypass other airways.
- *High frequency sounds*, i.e., with frequencies above those of low frequency sounds (see above), experience *rigid walls* of airways because of their inherent mass. In other words, walls are too inert to follow fast mechanical vibrations of sounds so that these sounds remain mainly within the airway lumen and travel further along the network of *airway branches*.

In other words, *heart sounds*, i.e., low frequency sounds, tend to remain within the *mediastinum*. As illustrated in Fig. 4.23, *low frequency sounds* are primarily bound to the *lung parenchyma* or *inner mediastinum*, whereas these sounds exit respiratory airways. According to Rice (1983), translobar sounds tend to travel through the bulk of the lung parenchyma—a foamlike substance, a homogenous mixture of waterlike tissue and air (Footnote 24)—and not along airways or blood vessels because the parenchyma acts as an elastic continuum to audible sounds. In contrast, the propagation of *high frequency sounds* is primarily linked to *airway-bound routes* (Fig. 4.23).

Such observations suggest that *low frequency sounds* at the *chest wall* provide information mostly on the lung parenchyma and inner mediastinum, whereas *high frequency sounds* at the chest wall reflect mostly airway properties. This dependence of the *propagation pathway* on the sound frequency has *strong implications* on the composition of sounds registered by a room microphone or skin microphone (Sect. 4.2.1.2) and on the asymmetry of the sound transmission in the thorax (Sect. 4.2.2.3).

Provided that the propagation pathway of body sounds varies with the sound frequency, it can be deduced from Table 4.1 that the *sound propagation velocity*  $v$  will also *depend on the frequency*. For instance, low frequency components of lung sounds will propagate with lower  $v$  than high frequency components. This is because these low frequency components are mainly bound to the parenchymal tissue with  $v \approx 50$  m/s while the high frequency components are mainly bound to airways with  $v \approx 270$  m/s.<sup>28</sup>

The sound propagation in *spatially limited air volumes* such as the upper airways should be addressed in more detail. Provided that the axial dimensions of the airways are in the range of  $\lambda$  of a propagating sound wave (or even larger than  $\lambda$ ), which is easily met especially for higher sound frequencies (Table 4.1 and (4.3)), the upper airways act as *resonating acoustic filters*. Such filters attenuate the transfer of sound energy at certain frequencies while allowing maximal energy through at particular resonance frequencies, also known as *formant frequencies*.

---

<sup>28</sup> Various *experimental data* confirm the dependence of the propagation pathway on the sound frequency and thus the *dependence of  $v$  on the frequency*. The authors in Pasterkamp et al. (1997b) demonstrate that low frequency sounds at 200 Hz are transmitted from the trachea to the chest wall with a *phase delay* of about 2.5 ms, whereas high frequency sounds at 800 Hz traverse a faster route with a phase delay of only 1.5 ms. For an assumed propagation distance of 20 cm, it would yield  $v \approx 80$  m/s for low frequency sounds and  $v \approx 130$  m/s for high frequency sounds.

The hypothesis of parenchymal propagation of sounds at lower frequencies is also supported by the fact that the inhalation of a *helium-oxygen mixture* (80 % helium and 20 % oxygen) affects only weakly (i.e., reduces) the *phase delay* of the sound transmission from the trachea to the chest wall at *lower frequencies*, in comparison with the inhalation of air (Pasterkamp et al. 1997b). In contrast, this *phase delay* is significantly reduced at *higher frequencies* while inhaling the helium-oxygen mixture. In quantitative terms, a reduction by about 0.7 ms was observed at 800 Hz (i.e., from 1.5 ms for the air inhalation down to 0.8 ms for the gas mixture) with almost no reduction at 200 Hz (i.e., 2.5 ms for both the air and gas mixture). Since the helium-oxygen mixture shows higher value of  $v$  than the air, the discussed observation proves a predominantly airway-bound sound transmission of high frequency sounds in the thorax.

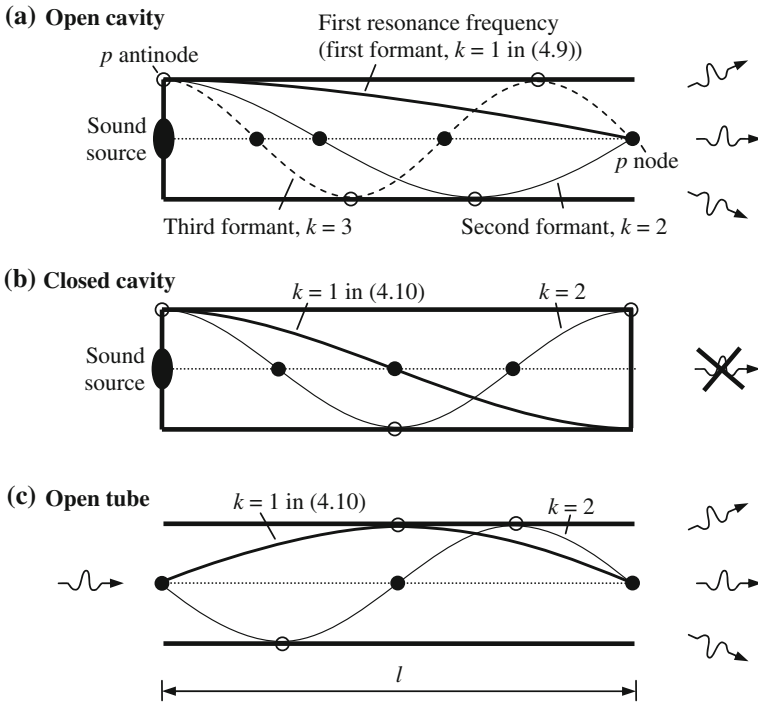


**Fig. 4.24** Resonating cavities and openings with the corresponding waveforms of the sound pressure  $p$ . (a) Resonance of the open cavity, e.g., the upper airway which is approximated as a tube of the length  $l$  with a sound source at its closed end and an opening at its opposite end (e.g., mouth opening). (b) Resonance of the closed cavity, e.g., the pulmonary airways. (c) Resonance of the open tube. Nodes of the sound pressure  $p$  (i.e., zero overpressure) are indicated by filled circles while antinodes of  $p$  (i.e., maximal overpressure and minimal underpressure) are indicated by empty circles; compare Footnote 26

This can be compared with the function of the vocal tract in speech production, in which the upper airways above and below the sound source (i.e., glottis) act as acoustic filters for the transmission of vowel sounds; compare Footnote 17.

In particular, an underlying vibration (or a *sound source*) generates a periodic wave of  $p$  at a specific *fundamental frequency*, whereas numerous higher harmonics usually dominate in the generated waveform (comparable with a broadband noise-like signal). As shown in Fig. 4.24a, the air-filled upper airways—in terms of *resonating cavities*—are closely attached to the sound source. The depicted *open resonating cavity* of the upper airways, i.e., *open to the outside* via open mouth and *closed* at the anatomical level of the sound source (reverberant and sound-reflecting site), *amplifies sound components* from the generated broadband signal at the particular *formant frequencies*. In fact, it is comparable with the source-filter

behaviour (from Footnote 17), where the final sound emitted is determined by a product of the *sound source* and the *transfer function* of the airways.

That is, only those acoustic waves fit into the resonating cavity—i.e., resonate within the cavity and, in turn, become amplified—which fulfil *boundary conditions* of this cavity (compare Footnote 161 in Sect. 2). The latter conditions imply that a sound *pressure node* (and an antinode of the sound particle velocity) occurs at the *cavity opening* while a *pressure antinode* (and velocity node) occurs at its *closed end* where the reverberant sound source resides. Figure 4.24a demonstrates the resulting phenomenon of *standing waves*<sup>29</sup> within the cavity of the length  $l$ . The standing waves arise only when the axial extension  $l$  matches  $\lambda/4$ ,  $3 \cdot \lambda/4$ , or  $5 \cdot \lambda/4$ , i.e., the sound waves fulfil the aforementioned boundary conditions. The resulting formant frequencies  $f_F^k$  of the standing waves with the index  $k$  ( $= 1, 2, 3, \dots$ ) indicating the presence of numerous *formant frequencies* amount to

$$f_F^k = \frac{v}{\lambda} = \frac{v}{4 \cdot l} \cdot (2k - 1) . \quad (4.9)$$

Thus, the *transmission efficiency* of the resonating cavity in Fig. 4.24a reaches its maxima at  $f_F^k$ . To give a quantitative example, an assumed (realistic) length  $l$  of about 17 cm would yield  $f_F^1$  of about 500 Hz and  $f_F^2$  of about 1,500 Hz. Likewise, cavity resonances and the level of  $f_F^k$  are influenced by the shape and size of the upper airways. For the sake of completeness, it should be pointed out that the corresponding waveform of the *sound particle velocity* in the resonating cavity exhibits a phase shift of  $\lambda/4$  (or  $90^\circ$ ) in relation to the waveform of  $p$  (Fig. 4.24); compare Footnote 22.

In terms of *snoring sounds*, the lowest formant frequency ( $= f_F^1$  in (4.9)) is related to the degree of *constriction in the pharynx*, the next higher ( $= f_F^2$ ) is related to the position and shape of the *tongue*, and the one after that ( $= f_F^3$ ) is correlated

<sup>29</sup> In fact, the *standing wave* within the *resonating cavity* is the sum of incident and reflected  $p$  waves which move in opposite directions (compare Footnote 170 in Sect. 2 and Sect. 6). However, the resulting standing wave oscillates only but does not propagate any more. For instance, at the closed end (*hard sound-reflecting surface*) the *incident pressure wave*  $p_I = P_I \cdot \cos(kx - \omega t)$ —propagating in the  $x$  direction with the pressure amplitude  $P_I$ , angular frequency  $\omega$  ( $= 2\pi \cdot f$ ), and wavenumber  $k$  ( $= 2\pi/\lambda$ )—is reflected *without phase change*. The *reflected pressure wave*  $p_R = P_R \cdot \cos(kx + \omega t)$  with the amplitude  $P_R = P_I = P$  interferes with  $p_I$ ; e.g., interferes constructively at the closed end; compare Footnote 161 in Sect. 2. The resulting standing wave  $p_I + p_R = 2P \cdot \cos(\omega t) \cdot \cos(kx)$  extends along  $x$ —with the closed end located at  $x = 0$ —and pulsates with  $t$ . Along the cavity in the  $x$  direction,

- *constructive interference*, i.e., amplitudes of the in-phase incident and reflected pressure waves *add*, and
- *destructive interference*, i.e., amplitudes of the out-of-phase incident and reflected pressure waves *subtract*,

occur. From a *physical point of view*, the pressure of air molecules reflecting off the closed end adds to that of air molecules approaching the closed end. In consequence, the total  $p$  doubles at the closed end, i.e.,  $p_I + p_R = 2P$  at  $x = 0$  and  $t = 0$ .

with the degree of *lip-rounding* (Ng et al. 2008). For instance, the level of  $f_F^1$  was shown to be higher in obstructive apneic snores (Sect. 4.1.1.3) than in benign snores, which illustrates increasing  $f_F^1$  with increasing degree of the pharynx constriction (Ng et al. 2008), i.e.,  $f_F^1$  increases with effectively decreasing  $l$  in (4.9).

As already mentioned, while sounds in the upper airways are intensified at *formant frequencies*, other sound components are damped in other specific frequency bands. For instance, *closed resonating cavities*, i.e., closed to the outside, such as closed pulmonary airways behind the sound source (Perez-Padilla et al. 1993) *absorb sounds* of specific frequencies and thus *reduce auscultatory sounds* emanating from the body. In an approximation, those sound components are damped, whose multiple half-wavelengths  $k \cdot \lambda/2$  match the axial extension  $l$  of the closed resonating cavity, i.e., *pressure antinodes* should occur at both ends of the cavity, as illustrated in Fig. 4.24b. In analogy to (4.9), the resulting resonance frequencies  $f^k$ —also known as *harmonic eigenfrequencies*—at which sounds are absorbed can be given as

$$f^k = \frac{v}{\lambda} = \frac{v}{2 \cdot l} \cdot k, \quad (4.10)$$

where the index  $k$  ( $= 1, 2, 3, \dots$ ) indicates the presence of *multiple frequencies*.

For the sake of completeness, Fig. 4.24c depicts an *open tube* as a *resonating chamber*, in comparison with the *open resonating cavity* (Fig. 4.24a) and the *closed resonating cavity* (Fig. 4.24b). In the course of the *resonance* in the open tube, the sound transmission throughout the tube is most efficient. In the resonance, *pressure nodes* occur at both ends of the tube and the resulting harmonic eigenfrequencies can be calculated according to (4.10).

#### 4.1.2.2 Effects on Sounds

After diverse propagation phenomena of body sounds have been discussed in Sect. 4.1.2.1, a highly instructive *interaction of sounds with biological tissue* should be discussed. In general, body sounds are subjected to

- *volume effects* such as *absorption*, which *attenuate* sound waves propagating in a *homogenous medium*; and
- *inhomogeneity effects* such as *scattering*, *diffraction*, *reflection*, *refraction*, and *resonance*, which *attenuate and redirect* sound waves heading in a particular direction. The latter effects are primarily caused by a *heterogeneous medium* in the sound propagation path (Fig. 4.20a).

Generally speaking, the above *effects are not fully independent* from each other. For instance, if a finite volume of tissue is exposed to ambient sounds, a part of the ambient *incident sounds* is already *reflected* back at the tissue boundary, another part of sounds is *absorbed* by tissue, and the rest is *transmitted* through this volume of tissue. In other words, the sum of reflected, absorbed, and transmitted portions of sounds should equal the ambient incident sounds. In addition, body sounds interact

with biological tissues in a rather complex way so that sounds are altered not only in their intensity but also tonal quality as they pass through tissues.

### Volume Effects

The aforementioned *medium-related damping* (see section “Specific Issues” in Sect. 4.1.2.1) accounts for the different *volume effects* in *homogenous medium*. That is, the absorption of sounds quantifies the *loss of sound energy* in a certain spatial direction as body sounds pass through biological tissue; consequently, *tissue is heated up*.

The process of *sound absorption* is represented by the coefficient  $\alpha$  ((4.7) and (4.8)) considering all three (Meyer and Neumann 1975; Wodicka et al. 1989; Trendelenburg 1961; Erikson et al. 1974):

- inner friction,
- thermal conduction, and
- molecular relaxation.

Propagating sound waves are tightly interrelated with propagating (spatial) waves of  $p$  and waves of the sound particle velocity. Because of resulting differences in local sound particle velocities, an *inner friction*<sup>30</sup> occurs between particles oscillating with different velocity. The friction is proportional to the ratio  $\mu/\rho$ . Therefore, propagation paths with stronger viscosity (or more inertial components) favour the friction and thus yield stronger damping of the propagating sound wave. The corresponding *friction-related contribution*  $\alpha_F$  to  $\alpha$  can be calculated as

$$\alpha_F = \frac{8\pi^2 \cdot \mu}{3 \cdot \rho \cdot v^3} \cdot f^2, \quad (4.11)$$

whereas  $\alpha_F$  *increases* disproportionately with the *sound frequency*  $f$ . The level of  $\alpha_F$  in water is extremely low and amounts to about  $10^{-8} \text{ m}^{-1}$  at 1 kHz; compare Table 4.1. It can be assumed that the latter value approximately applies also to biological tissue which mainly consists of water. In comparison with water,  $\alpha_F$  in the air is higher by three orders of magnitude<sup>31</sup> (Table 4.1).

In analogy with the inner friction, the propagating sound wave is linked with differences in local medium temperature. The balancing of these differences due to (finite) thermal conductivity withdraws energy from the sound wave. Likewise, the

---

<sup>30</sup> *Homogenous materials* tend to absorb the acoustic energy mainly because of the *inner friction*, i.e., because of local deformations and frictions within the propagation medium. In contrast, *porous materials* such as the lung parenchyma also absorb the acoustic energy in terms of the *outer friction* (Veit 1996), i.e., the friction between oscillating air particles in alveoli and semi-solid medium encircling alveoli.

<sup>31</sup> To give an example, if only very low values of  $\alpha_F$  are considered (Table 4.1), the *sound pressure*  $p$  at 1 kHz would decrease by about 1 dB either after 11,000 km while *sound travelling in water*, or after 11 km while *travelling in the air* (compare the exponential term in (4.7)).

*thermal conduction* can be interpreted as a spatial diffusion of kinetic energy, yielding the corresponding *temperature-related contribution*  $\alpha_T$  to  $\alpha$  according to

$$\alpha_T = \left( \frac{c_P}{c_V} - 1 \right) \cdot \frac{2\pi^2 \cdot v}{c_P \cdot \rho \cdot v^3} \cdot f^2. \quad (4.12)$$

Here  $v$  is the heat conductivity, whereas  $c_P$  and  $c_V$  are the specific heat capacities for constant pressure and constant volume, respectively. The level of  $\alpha_T$  in water is three orders of magnitude lower than  $\alpha_F$  in water. In the air,  $\alpha_T$  is comparable in size to  $\alpha_F$ .

The *molecular relaxation* is related to the fact that rapidly submitted sound energy—in terms of increasing local  $p$  in the propagation medium—is stored as *translational energy* of molecules, i.e., stored as increasing translational motion of molecules (solely responsible for the pressure itself). The translational energy is rapidly transferred into *rotational energy* (i.e., rotational motions of molecules) with almost no delay or, likewise, with zero *relaxation time constant*  $\tau$  ( $\approx 0$ ). In parallel, a part of the translational energy is converted into the *vibrational energy* (i.e., vibrational motions of molecules) with *time delay* or excitation time  $\tau$  ( $\gg 0$ ). When the local  $p$  starts to decrease within the time frame of  $\tau$  (i.e.,  $\tau \approx 1/(2\pi \cdot f)$  with  $f$  as the sound frequency), the vibrational energy is not timely converted back into the translational energy, resulting in an *apparent loss of the instantaneous translational energy* and thus an apparent attenuation of the instantaneous local  $p$ . Likewise, the translational energy and thus the level of  $p$  appear to be greater during *compression* than during subsequent *depression*. Therefore, a part of the *sound energy seems to be lost* due to delayed relaxation; or, in other words, some of the ordered energy of the sound is transformed into random motion of the medium particles. In analogy, for relatively high sound frequencies  $f \gg 1/(2\pi \cdot \tau)$ , the vibrational motion of molecules is not excited (i.e., molecules can not respond fast enough). For relatively low frequencies  $f \ll 1/(2\pi \cdot \tau)$ , a vibrational (thermal) *equilibrium* is reached at any time, i.e., the vibrational relaxation follows in step with the sound wave. In both cases of relatively high and low frequencies, there is *no sound attenuation* by the vibrational relaxation.

The corresponding *relaxation-related contribution*  $\alpha_M$  to  $\alpha$  amounts to

$$\alpha_M = \left( 1 - \frac{v_0^2}{v_\infty^2} \right) \cdot \frac{2\pi^2 \cdot \tau}{(1 + (2\pi \cdot f \cdot \tau)^2) \cdot v} \cdot f^2, \quad (4.13)$$

whereas  $v_0$  and  $v_\infty$  ( $> v_0$ <sup>32</sup>) are the sound velocities before the vibrational relaxation (i.e., for relatively low frequencies  $f \ll 1/(2\pi \cdot \tau)$ ) and after the vibrational relaxation (for  $f \gg 1/(2\pi \cdot \tau)$ ), respectively. It follows from the above discussion and (4.13)

---

<sup>32</sup> The *compressibility* of the propagation medium is higher at lower frequencies before the vibrational relaxation (i.e.,  $f \ll 1/(2\pi \cdot \tau)$ ) in comparison with higher frequencies after the relaxation ( $f \gg 1/(2\pi \cdot \tau)$ ). Thus the *relation*  $v_0 < v_\infty$  applies; compare the influence of  $D$  on the size of  $v$  in (4.4) (Meyer and Neumann 1975).

that sounds are subjected to a maximum loss at the *relaxation frequency*  $1/(2\pi \cdot \tau)$  where the product  $\alpha_M \cdot \lambda$ —or the sound attenuation per sound wave cycle  $\nu \cdot \alpha_M/f$ , (4.3)—becomes a maximum.

Obviously the size of  $\tau$  depends strongly on the propagation medium and tends to decrease with temperature. Complex relaxation phenomena—including chemical relaxation in terms of the ionic dissociation due to local pressure variations created by the acoustic wave—arise in liquids such as sea *water* with various dissolved substances involved. The relaxation frequency of fresh water (not sea water) is very high amounting to about  $1/(2\pi \cdot \tau) \approx 80$  GHz. This high value, in turn, yields a relatively low  $\alpha_M$  (in the range of  $3 \cdot 10^{-8} \text{ m}^{-1}$  at 1 kHz and 20 °C) and its strong frequency dependence ( $\alpha_M \propto f^2$ ) considering the absorption of body sounds with their (low) frequency components only up to 2 kHz ( $\ll 80$  GHz).<sup>33</sup>

The relaxation phenomena are responsible for most of the acoustic losses in the *air*, whereas relaxations of oxygen and nitrogen molecules are involved. The time constant  $\tau$  tends to decrease with increasing humidity because collisions of (diatomic) air molecules with water molecules favour fast transitions between different energy states; e.g., at the air humidity 70 % and temperature 20 °C the relaxation frequency is about 70 kHz for oxygen<sup>34</sup> and about 700 Hz for nitrogen (Rossing 2007). Likewise, the sound frequency of 1 kHz is above that associated with the relaxation of molecular nitrogen and below that associated with the oxygen relaxation. Typically, the level of  $\alpha_M$  in the air increases with increasing water content (air humidity) and increasing sound frequency, e.g., at the humidity 70 %, temperature 20 °C, and frequency 1 kHz, the sound attenuation is about 5 dB/km or  $\alpha_M = 6 \cdot 10^{-4} \text{ m}^{-1}$  ( $> \alpha_T, \alpha_F$  of the air); compare Footnotes 31, 33 and Table 4.1.

The *total absorption coefficient*  $\alpha$ —as used in (4.7) and (4.8)—can be given as

$$\alpha = \alpha_F + \alpha_T + \alpha_M. \quad (4.14)$$

It is important to observe from (4.11) to (4.13) that the level of  $\alpha$  increases with increasing  $f$ . In particular, the contributions  $\alpha_F$  and  $\alpha_T$  are even proportional to  $f^2$  while  $\alpha_M$  is proportional to  $f^2$  (only) below the relaxation frequency (i.e., for  $f \ll 1/(2\pi \cdot \tau)$  and constant  $\nu$ ).<sup>35</sup> That is, not only the propagation pathway of body sounds in the thorax

<sup>33</sup> In contrast, *sea water* shows a significantly higher  $\alpha_M$  because of two additional relaxation phenomena in it with one relaxation frequency above 1 kHz (ionic dissociation of boric acid  $\text{H}_3\text{BO}_3$ ) and another one above 100 kHz (ionic dissociation of magnesium sulphate  $\text{MgSO}_4$ ). For instance, at the sound frequency 1 kHz and temperature 20 °C the sound attenuation in sea water totals about 0.06 dB/km or  $\alpha_M = 7 \cdot 10^{-6} \text{ m}^{-1}$ .

<sup>34</sup> For instance, the *relaxation frequency of pure oxygen* is only about 10 Hz yielding a large  $\tau$  of about 16 ms.

<sup>35</sup> *Experimental data* confirm the frequency dependence of the *medium-related damping*. For instance, authors in Erikson et al. (1974) report that  $\alpha$  is approximately proportional to  $f$ , whereas individual tissues may yield a stronger frequency dependence up to  $f^2$ , e.g., hemoglobin has  $\alpha$  proportional to  $f^{1.3}$ . Studies in Loudon and Murphy (1984), Hadjileontiadis and Panas (1997a) show that the intensity of vesicular lung sounds (Sect. 4.1.1.2) declines exponentially with increasing  $f$ , which implies the proportionality between  $\alpha$  and  $f$ ; compare (4.7) and Fig. 4.22.

depends on  $f$  (Fig. 4.23) but also the medium-related damping within biological tissues increases with  $f$ , which have important practical consequences.

As illustrated in Figs. 4.1 and 4.23, the *frequency dependence of  $\alpha$*  causes that *high frequency sounds* do not spread as diffusely or, retain as much amplitude, as do *low frequency sounds* (across the thorax). Consequently, high frequency sounds are more localised around their source. Concerning the different body sounds, it can be concluded that

- *heart sounds*—as body sounds in the low frequency range up to 100 Hz (Sect. 4.1.1.1)—are subjected to lowest attenuation in tissue, which favours their auscultation almost everywhere on the thoracic skin (Sect. 4.2.2.3).
- *Lung sounds* and *snoring sounds* experience larger attenuations than heart sounds because breathing sounds contain more high frequency components. Among them, vesicular lung sounds tend to face lowest attenuation in tissue (frequency range up to 500 Hz, Sect. 4.1.1.2) while obstructive snoring sounds face highest attenuation (range up to 2,000 Hz, Sect. 4.1.1.3). Obviously, the resulting intensity of breathing sounds on the skin (i.e., at an auscultation site) depends not only on
  - their *attenuation* in tissue but also on
  - the *frequency dependence* of their propagation pathways towards the skin,
  - the *propagation distance* to the skin, and
  - the *intensities* of their sound sources.
- *Pathological sounds*, e.g., discontinuous lung sounds, exhibit mostly high frequency components—due to a transient occurrence of such sounds—and thus do not spread as widely as *normal sounds*.<sup>36</sup>

From an engineering point of view,<sup>37</sup> the frequency dependence of  $\alpha$  means that the transmission efficiency of the lung parenchyma and chest wall deteriorates with

---

<sup>36</sup> In fact, *high frequency sounds* exhibit *localising properties*, which are very useful in diagnosis. High frequency sounds do not spread as widely or with the intensity that low frequency sounds spread across the thorax (Ertel et al. 1966b). It means that as soon as high frequency sounds (usually pathological sounds) are heard, the corresponding sound source (or the site of pathology) is already close to the current auscultation site. This offers physicians an ability to localise pathological breathing sounds to their point of origin.

<sup>37</sup> *Sound transmission* through the thorax may be of high clinical value if altered transmission patterns correlate with *pathology* (Peng et al. 2014). For instance, changes in the lung structure due to the presence of *pneumothorax*—creating more barriers to the propagating acoustic waves—causes a drop in the intensity of the transmitted mechanical waves at *high frequencies* (above 100 Hz in humans (Peng et al. 2014)), which are subjected to relatively strong attenuation in tissue (see text). In contrast, sound waves at *lower frequencies* (below 100 Hz)—subjected to relatively low attenuation in tissue—can travel a longer distance (around the internal organs in the thorax) before these waves lose their energy. Consequently, structural changes of the internal organs may result in small effects on the propagation of these low frequency sounds.

Authors in Peng et al. (2014) showed that the presence of *pneumothorax* had smaller effects on the sound transmission through the thorax at *lower frequencies*. Likewise, it seems that *high frequency* mechanical waves (as could be introduced at the anterior chest surface by an actuator)

increasing  $f$ ; i.e., *biological tissue* acts as *low-pass filter* which transmits body sounds predominantly at relatively low  $f$  (Wodicka et al. 1989; Welsby and Earis 2001; Welsby et al. 2003). For instance, the sound attenuation in tissue has been shown to be negligible at 100 Hz and then to increase to about 1 dB/cm at 400 Hz and even to about 3 dB/cm at 600 Hz (Wodicka et al. 1989); the corresponding level of  $\alpha$  would amount to 11 and 34  $\text{m}^{-1}$  at 400 and 600 Hz, respectively (compare Table 4.1).

Table 4.1 compares  $\alpha_F + \alpha_T$  for different types of *physical and biological media*. It can be observed that air, adipose tissue, and lung parenchyma are strongest absorbers if the inner friction and thermal conduction are considered only. However, it should be stressed that effective values of  $\alpha$  (4.14) are usually larger by orders of magnitude than tabled values of  $\alpha_F + \alpha_T$ . The contribution  $\alpha_M$  (due to the molecular relaxation) to  $\alpha$  is highly significant, as discussed above with regard to water and the air. Furthermore, the real absorption mechanisms in *liquids* and *semi-solids* (such as biological tissue) are highly complex; these mechanisms are also determined by *interactions* between solvent and solute and, on the other hand, governed by local *structural relaxation*, i.e., by a periodic change in the molecular arrangement due to local pressure variations created by the (mechanical) acoustic wave.

Authors in Rappaport and Sprague (1941) suggest that if effects of the inner friction (4.11) are small, as in the case with water, air, and bone, the sound energy may be transmitted with remarkably little loss. In other media, such as (breast) *fatty tissue*, sound waves are almost immediately suppressed. The flesh of the chest also acts as a strong damping medium since *obesity* might completely mask (even) *heart sounds*, i.e., sounds composed of (even) low frequency components. Likewise, relatively low frequencies of heart sounds are subjected to weak attenuation. As demonstrated in Kaniusas (2007), an increase in the *body mass index BMI* (Footnote 202 in Sect. 3) from 24 to 38  $\text{kg}/\text{m}^2$ , i.e., an increase in obesity and amount of adipose tissue, reduced the peak amplitude of heart sounds by about 60 %.

The *attenuation of sounds* in the *lung parenchyma* deserves a few more comments. As shown in section “General Issues” in Sect. 4.1.2.1, the propagation speed  $v$  in the lungs is relatively slow because of the lung’s elasticity dominated by a mixture of tissue and the air (Pasterkamp et al. 1997b; Kompis et al. 2001); compare Footnote 24. The non-continuous porous structure of the lung parenchyma (Footnote 30) is of special importance regarding the frequency dependence of its  $\alpha$ . In fact, *alveoli* of the parenchyma act as *elastic air bubbles* in water, which dynamic deformations (compression and expansion) due to oscillating  $p$  (of the sound) dissipate the sound energy (Meyer and Neumann 1975). As long as the *size of  $\lambda$*  (Table 4.1) is significantly greater than the alveolar size (diameter  $< 1$  mm), the sound losses are relatively low.

---

(Footnote 37 continued)

propagate directly (to the posterior chest surface where a sensor resides) through internal organs (lying between the actuator and sensor). Therefore, any change in the intrathoracic structure would affect the propagation of *high frequencies* through the thorax.

Here the arising losses due to the thermal conduction<sup>38</sup> are considerably larger than those associated with the inner friction (viscous effects) and scattering effects (Wodicka et al. 1989). When the size of  $\lambda$  approaches the alveolar size, i.e., the sound frequency is increasing (4.3), the losses start to increase strongly (Pasterkamp et al. 1997b). However, it is important to observe from Table 4.1 that typical values of  $\lambda$  in the lung parenchyma—despite the relatively low  $\nu$ —are still significantly larger than the alveolar size if the typical frequency range of body sounds (up to 2 kHz) is considered. Provided that  $\nu = 23$  m/s (as the lowest reported value from section “General Issues” in Sect. 4.1.2.1), the resulting size of  $\lambda$  would approach the alveolar size at the earliest at  $f = 23$  kHz.

From an engineering point of view, *low-pass behaviour of the lung* can be expected because damping of sounds in tissue increases with frequency. That is, low frequency components of lung sounds are predominantly transmitted through the lung while high frequency components are filtered out by the lung. As reported in Fachinger (2003), the cut-off frequency of such low-pass behaviour is at about 400 Hz. Interestingly, the *cut-off frequency decreases* with an increasing *accumulation of the air* in the lungs (reduced density of the lungs), which impedes the transmission of lung sounds. On the other hand, increased density of the lungs—in terms of *parenchymal consolidation* as can be caused by *illness*—*increases the cut-off frequency* and thus facilitates the sound transmission (especially, high frequency sound components).

The *consolidated lung* acts as an efficient sound conductor. An increased volumetric portion of tissue in the lungs, e.g., in the congested lungs (compare Footnote 24), favours the transmission of voice sounds to the chest wall, *especially at high sound frequencies* (Wodicka et al. 1989). In fact, the consolidation may cause important changes in the quality of lung sounds recorded on the chest wall. For instance, sounds originating in bronchial and tracheal tracts would be well transmitted to the *chest wall*, a distant sensing site in relation to (centrally located) sound sources, which is a consequence of improved sound transmission through the consolidated parenchyma. In contrast to effects of the *normal lung*—yielding (by definition) *vesicular lung sounds* on the chest—auscultated *sounds on the chest* would be similar in quality to *tracheobronchial lung sounds*, i.e., would be relatively loud and high-pitched (Sect. 4.1.1.2), especially during the expiration phase in which normal vesicular sounds are absent. In addition, *expiratory sounds* would be as loud as *inspiratory sounds*, which is contrary to the quality of vesicular sounds. Likewise, tracheobronchial sounds if heard on the chest instead or in addition to vesicular sounds indicate pathologically consolidated lungs (Loudon and Murphy 1984; Dalmay et al. 1995; Wodicka et al. 1989). Finally, it should be

---

<sup>38</sup> In this case, *thermal losses* arise because *bubble compressions* require greater work performed by the acoustic wave than the work performed by the air in bubbles during *bubble expansions* (Wodicka et al. 1989). The resulting energy difference is conducted into the lung tissue as heat. Interestingly, *enlarged alveoli* tend to increase thermal losses and thus to attenuate more strongly body sounds within the lungs in comparison with *reduced alveoli* (pre-compressed bubbles).

mentioned that an experimental estimation of the transmission characteristics of body sounds in the thorax can even lead to diagnosis and categorization of (respiratory) diseases because different diseases affect the transmission characteristics in a unique way.

### Inhomogeneity Effects

In addition to the geometry-related damping of propagating body sounds (see section “Specific Issues” in Sect. 4.1.2.1) and the sound absorption in terms of the medium-related damping in *homogenous media* (see section “Volume Effects” in Sect. 4.1.2.2), the *heterogeneous structure* of biological tissues impacts strongly the *attenuation of sounds* propagating in a specific direction, e.g., towards the skin surface. A highly heterogeneous structure of the thoracic region is demonstrated in Fig. 4.20a. In general, body sounds interact with such structures in a rather complex way and may experience *spatial redirection*, *accumulated attenuation* with respect to an acoustical sensing device (on the skin), and even *local amplification* because of resonating effects in spatially delimited cavities.

In particular, the following *effects govern the propagation of body sounds* in tissue towards the skin surface and the coupling of sounds into the air above the skin (or into the sensing device, Fig. 4.1):

- scattering,
- diffraction,
- reflection,
- refraction, and
- resonance.

### Scattering and Diffraction

Sound waves are *scattered*, i.e., redirected in random directions from a straight trajectory, when waves encounter inhomogeneities<sup>39</sup> (or obstacles) in the propagation medium; see a detailed discussion on scattering in section “Inhomogeneity effects” in Sect. 5.1.2.2. Such *inhomogeneities* in the thorax are given, for instance, by spatially delimited inner organs, airways, bones, skin, and—on a smaller scale—different types of tissues, porous lung parenchyma, (large) blood vessels. The dimensions of the former *structures are nearly in the range of  $\lambda$*  (Table 4.1) while those of the latter structures are already much smaller than  $\lambda$ .<sup>40</sup>

<sup>39</sup> From an acoustical point of view, *inhomogeneities* or *obstacles* are given by media with different  $Z$  (4.6). That is, fluctuations of the medium *density*  $\rho$  or the varying *propagation velocity*  $v$  of sounds (when entering a different medium, (4.4)) constitute inhomogeneities for the sound wave.

<sup>40</sup> *Inhomogeneities* on an *even smaller scale* such as cellular structures or protein aggregates are unimportant for the scattering of body sounds because the effective  $\lambda$  of sounds is already orders of magnitude larger than the dimensions of these inhomogeneities. However, such small structures are highly relevant for the *optical scattering* (Sect. 5.1).

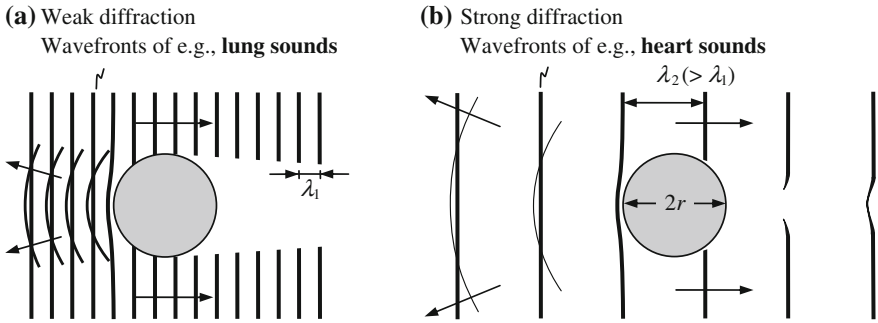


**Fig. 4.25** Scattering and diffraction of body sounds off of an obstacle at (a) relatively high frequencies ( $\lambda_1 < 2r$ , see (4.3)) and (b) relatively low frequencies of sounds ( $\lambda_2 \approx 2r$  and  $\lambda_1 < \lambda_2$ ); compare Sect. 6. Here  $\lambda$  denominates the sound wavelength and  $2r$  the diameter of the obstacle. The *line thickness* of the wavefront indicates the incident, scattered, and diffracted sound intensities, whereas the *arrows* indicate the propagation direction

Generally, some part of the sound wave is *scattered* (or reflected in many directions) off of an obstacle, another part is *absorbed* (see section “Volume Effects” in Sect. 4.1.2.2), whereas the rest of the wave propagates *around the obstacle*, as illustrated in Fig. 4.25. The *bending of the sound wave around small obstacles*—small compared to the size of  $\lambda$  or on the order of  $\lambda$ —is coined as *wave diffraction* (Fig. 4.25b).

- If the size of  $\lambda$  is *large* in relation to the obstacle, only a small part of the wave will be scattered, i.e., only the tiny part that strikes the obstacle; the larger part of this wave will *readily diffract* around the obstacle and remains unaffected (Fig. 4.25b). Likewise, for longer  $\lambda$  the obstacle behaves as a point source of diffracted waves and the resulting *scattering losses* are small, whereas the obstacle’s shape is of little importance. In analogy, the sound can also spread out beyond *small openings*,<sup>41</sup> i.e., small compared to  $\lambda$ ; one could consider them to be anti-obstacles, which then act as localized point sources of sound.
- In contrast to large  $\lambda$ , if the size of  $\lambda$  is *in the same order* of magnitude as the size of the obstacle, the (back) scattering tends to increase while the diffraction (bending towards the obstacle of waves past this obstacle, Fig. 4.25b) becomes less pronounced. The *interference* may arise among diffracted waves creating (alternating)

<sup>41</sup> In fact, every unobstructed point on the *incident wavefront* momentarily present in the *opening* (or slit) acts as a source of a *secondary spherical wave*. The superposition of all spherical waves determines the form of the *resulting transmitted wavefront* at any subsequent time behind the slit, i.e., the *superposition* determines the resulting *diffraction pattern* of the slit. Obviously, not only amplitudes but also relative phases of the individual spherical waves govern their *interference pattern* and thus the resulting transmitted wavefront beyond the opening. Namely,

- *in-phase superposition* leads to *constructive interference* and thus to the maximum of the transmitted intensity at a certain observation point beyond the opening. In contrast,
- *out-of-phase superposition* leads to *destructive interference* and thus to the null in the transmitted intensity at an observation point beyond the opening; for details see Sect. 6.

regions of greater sound intensity (known as constructive interference) and lesser sound intensity (destructive interference); compare Footnote 41.

- For an even *smaller*  $\lambda$  below the size of the obstacle, most of the sound incident on the obstacle is scattered (back) according to the *reflection laws* (4.15), the *diffraction almost disappears*, and a *sound shadow*<sup>42</sup> is formed behind this obstacle (Fig. 4.25a). Likewise, the back scattered energy is much larger for the reflection than diffraction, as illustrated schematically in Fig. 4.25a, b.

Thus obstacles smaller than  $\lambda$  tend to *scatter in all directions* while obstacles bigger than  $\lambda$  tend to *scatter more directional*; compare Fig. 4.25a with Fig. 4.25b (see also Fig. 5.11). In fact, multiple scattering-related redirections—or *multiple scattering events*, compare Fig. 5.10a—contribute to the *overall attenuation* of the propagating sounds when arriving at a distant location, e.g., at a distant sensing device on the skin.

This yields that *high frequency sounds*, with relatively short  $\lambda$  (4.3), do not diffract around obstacles, but are predominantly absorbed (due to their relatively high frequency, section “Volume Effects” in Sect. 4.1.2.2) or reflected instead (see below), which creates the *sound shadow* (Fig. 4.25a). In contrast, *low frequency sounds* have relatively long  $\lambda$  which usually exceeds the dimensions of obstacles in the propagation pathway and thus are bent around these obstacles. These sounds diffract and *pass around obstacles undisturbed* so that the sound wave—already several wavelengths past the obstacle (Fig. 4.25b)—is fully identical with that in front of the obstacle. Likewise, high frequencies scatter much more than low frequencies.

Considering particular body sounds, it can be concluded that *heart sounds*, i.e., low frequency sounds, tend to spread *diffusely* in all directions and diffract more strongly than *lung sounds* or *snoring sounds*, i.e., high frequency sounds, which spread more *directional*. From a practical point of view, it favours the auscultation of heart sounds everywhere on the chest skin.

### Reflection

Provided that the dimensions of the obstacle—in the sound propagation pathway—are larger than  $\lambda$  of the sound wave, the wave is coherently *reflected* off of the obstacle at the *boundary* according to the *reflection laws*. Namely, the *incident angle* to the normal (to the reflective surface at the point of the incidence) equals the *reflection angle* to the normal, whereas all three the incident wave, the reflected wave, and the normal lie in the same plane. Figure 4.26 demonstrates the reflection of inner body sounds—emanating from the body—on the inner skin surface, i.e., on

---

<sup>42</sup> It is interesting to note that the *boundary* between the *sound wave* (i.e., compressions and rarefactions) and the *sound shadow* (i.e., died wave) always extends over a certain number of wavelengths because the mechanical sound wave can not die abruptly due to elastic interactions among adjacent molecules. This effectively determines the spatial extension of the diffraction, which is greater at large  $\lambda$  (or low sound frequency) and less at small  $\lambda$  (or high sound frequency). Likewise, a sound shadow behind an obstacle decreases in size with increasing  $\lambda$ .

the *discontinuity tissue-air*. The equality of the incident angle  $\varphi_T$  and the reflection angle  $\varphi'_T$  can be observed.

The amount of the reflected wave (as related to the incident wave) is determined by the *acoustic reflection factor*  $\Gamma_A$  (compare 2.32) given by

$$\Gamma_A = \frac{P_R}{P_I} = \frac{Z_A - Z_T}{Z_A + Z_T}. \quad (4.15)$$

Here  $P_R$  and  $P_I$  are the respective amplitudes (= peak values) of the reflected and incident (pulsatile) sound pressure; compare Footnote 29. The *characteristic acoustic impedance*  $Z_A$  denotes the air impedance above the skin while  $Z_T$  denotes the tissue impedance below the skin. An approximate estimation of  $\Gamma_A$  with (4.6), data from Table 4.1 and Footnote 24 yields  $Z_A = 343 \text{ kg} \cdot \text{m}^{-2} \cdot \text{s}^{-1}$ ,  $Z_T = 1.5 \cdot 10^6 \text{ kg} \cdot \text{m}^{-2} \cdot \text{s}^{-1}$ , and a very large  $\Gamma_A = -0.99$ . The minus sign of  $\Gamma_A$  indicates that the reflected sound (pressure) wave experiences a *phase reversal* in relation to the incident sound wave. This is because the *air comprises a very soft medium* in comparison with the tissue (i.e.,  $Z_A \ll Z_T$ ); compare Footnotes 29 and 36 in Sect. 5. Consequently, the total sound pressure (=  $p_I + p_R$ ) at the tissue-air interface has to drop to fulfil the boundary condition ( $p_I + p_R \rightarrow 0$ ) so that the resulting reflected wave has to satisfy  $p_R \approx -p_I$ . Figure 4.26 also illustrates the phase reversal by space-shifted incident and reflected wavefronts in the tissue below the skin. The discontinuity tissue-air is partially comparable with the effect of resonance cavity opening in Fig. 4.24a, c; compare also Footnote 36 in Sect. 5.

On the other hand, the high value of  $|\Gamma_A|$  would indicate that more than 99 % of the incident wave is reflected back on the inner skin surface while only 1 % is transmitted through the skin and is then available for the acoustical sensing device. Likewise, the *acoustic impedance mismatch* between different body tissues always accounts for the *sound attenuation* while the associated sound wave crosses boundaries. On the other hand, matched impedances will not yield any attenuation ( $\Gamma_A = 0$  for  $Z_A = Z_T$  in (4.15)). For instance, the impedance mismatch between the lung parenchyma and chest wall can account for a significant decrease in  $p$  by an order of magnitude because the chest wall is much more massive and stiffer than the parenchyma (Pasterkamp et al. 1997b).

However, the above estimation of such high *reflection losses* is of limited validity because the *reflection laws* (including (4.15)) hold only when  $\lambda$  of the sound is relatively small. As already discussed, the latter requirement is hardly met by body sounds in the frequency range up to 2 kHz (Table 4.1), the effective  $\lambda$  being larger or at most equal to the dimensions of inner body structures. In other words, the estimated high reflection losses are rather valid for *high frequency body sounds* with correspondingly short  $\lambda$ . Figure 4.26 signifies the loss in the intensity of body sounds while crossing the simplified tissue-air boundary.

In addition, the above estimation assumes a *simplified tissue-air interface* with a single boundary, whereas the *real skin* constitutes a true *multilayer* consisting of at least three layers, namely, the innermost subcutaneous fat, the dermis, and the outermost epidermis. Thus, there are at least four boundaries for body sounds to

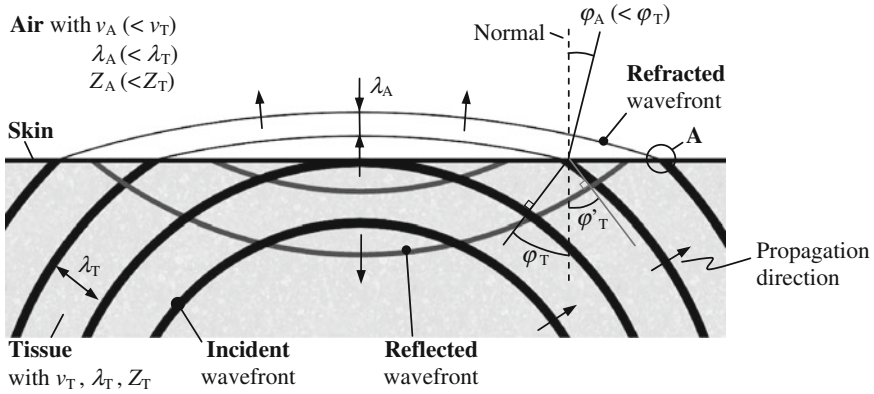


**Fig. 4.26** Reflection and refraction of body sounds on the tissue-air boundary with  $v_T$  and  $v_A$  as the sound propagation velocity in the tissue and air, respectively. Here  $\lambda$  is the corresponding sound wavelength,  $Z$  the corresponding characteristic acoustic impedance,  $\phi_T$  the incident angle in the tissue,  $\phi'_T (= \phi_T)$  the reflection angle in the tissue, and  $\phi_A$  the refraction angle in the air. The *line thickness* of wavefronts indicates roughly the sound intensity

cross while transversing the skin. It can be assumed that *neighbouring layers*—exhibiting similarities in their physical and thus acoustical properties—show *less difference in their  $Z$*  than the difference  $|Z_A - Z_T|$  of the simplified tissue-air interface. Therefore, the effective  $\Gamma$  of boundaries in the multilayer would be less in comparison with the estimated  $\Gamma_A$  of the simplified two-layer system.<sup>43</sup>

*Refraction*

The part of sounds, which was not reflected at the boundary in the propagation pathway, enters another medium behind the boundary (Footnote 39) and usually experiences a redirection (or *bending*) owing to a *change in  $v$* , known as *wave refraction*. In contrast to scattering, diffraction, and reflection, involving spreading and bending of sound waves in a *single medium* with (almost) constant  $v$ , refraction involves bending of sound waves which enter *another medium* with different  $v$ .

<sup>43</sup> For instance, if a *trilayer* is assumed with only one intermediate layer (with  $Z_1$ ) between the tissue ( $Z_T$ ) and the air ( $Z_A$ ), the resulting two *reflection factors*  $\Gamma_M$  (of two reflecting surfaces) for sounds emanating from the body would amount to

$$\Gamma_{M,1} = \frac{Z_1 - Z_T}{Z_1 + Z_T} \quad \text{and} \quad \Gamma_{M,2} = \frac{Z_A - Z_1}{Z_A + Z_1}.$$

Provided that  $Z_A < Z_1 < Z_T$ , the respective magnitudes of  $\Gamma_M$  satisfy  $|\Gamma_{M,1}| < |\Gamma_A|$  and  $|\Gamma_{M,2}| < |\Gamma_A|$ , whereas  $\Gamma_A$  of a simplified *bilayer* tissue-air is given by (4.15). Thus the trilayer shows lower reflection losses in comparison with the *bilayer*.

As illustrated in Fig. 4.26, body sounds in the tissue (*fast medium* with  $v_T$ ) approach the air where their speed  $v_A$  is slower (Table 4.1). As soon as the incident wavefront hits the *slow medium* the wavefront is slowed down at the point of the incidence, for instance, in the region A in Fig. 4.26. Meanwhile, the rest of the wavefront in the tissue, e.g., to the right of the region A, continues to spread with a high speed  $v_T$  until it also hits the slow medium. Consequently, the *wavefront* in the region A is *bend* to the left when the wavefront enters the air; compare depicted propagation directions of the incident and refracted waves. The wavefront in the air seems to be *flattened* in relation to that in the tissue.

It is obvious that not only the direction of the wave propagation changes but also the distance between neighbouring wavefronts decreases, i.e., the *wavelength*  $\lambda$  is decreased in the air related to the incident  $\lambda$  in the tissue (Fig. 4.26). Likewise, a lower  $v$  yields a shorter  $\lambda$  in a medium (4.3) because the sound *frequency*  $f$  does not change from one medium to another (in linear media only); the level of  $f$  is solely determined by the rate of mechanical vibrations in the sound source.

As in the case of reflection, the laws of *acoustic refraction* apply only if the dimensions of the refracting surface are larger than  $\lambda$  of the sound. Namely, the *refraction angle*  $\varphi_A$  (in the air) and the incident angle  $\varphi_T$  (in the tissue) obey *Snell's refraction law*<sup>44</sup>:

$$\frac{v_A}{v_T} = \frac{\sin(\varphi_A)}{\sin(\varphi_T)}, \quad (4.16)$$

whereas the incident wave, the refracted wave, and the normal lie in the same plane (Fig. 4.26). Since the inequality  $v_A < v_T$  applies (Table 4.1), the angle  $\varphi_A$  is smaller than  $\varphi_T$ . Likewise, the refracted wave of inner body sounds is bent towards the normal of the skin, i.e., the air wavefront becomes flattened.

It should be noted that the *flattened wavefront* in the air *favours the auscultation* of body sounds via a (usually) flat acoustical sensing device on the skin (Fig. 4.1). In particular, this advantage is rather applicable for *high frequency body sounds* with correspondingly short  $\lambda$ .

### Resonance

Some *inhomogeneities* in the thorax, especially in the respiratory tract, build *tube-like resonating cavities* such as the *air-filled* upper airways and pulmonary airways. As described in section “Specific Issues” in Sect. 4.1.2.1, cavities act as resonating

<sup>44</sup> Willebrord Snellius (1580–1626) was a Dutch astronomer and mathematician after which *Snell's law* was named. This law relates the degree of the wave bending to the physical properties of materials which surround the bending surface.

acoustic filters. Here *incident waves* reflect at boundaries of a cavity and then interfere with *reflected waves* formed in this way. It leads to *constructive and destructive interference* along the resonating cavity and, in turn, to the phenomenon of *standing waves* in the cavity; compare Fig. 4.24a, b and Footnote 29. It should be noted that such resonating effects are less likely in semi-solid tissues of the body, even though tissues are spatially delimited by e.g., skin or airway walls. The reason for this is that the level of  $\lambda$  in tissues (Table 4.1) is larger than the corresponding dimensions of (homogenous) tissues.

## 4.2 Sensing Aspects

According to Figs. 4.1 and 4.2, *sensing aspects* include

- *coupling* of body sounds from the skin into an acoustical sensing device applied on the skin and
- *conversion* of the sound pressure of coupled sounds into an electric signal within the sensing device.

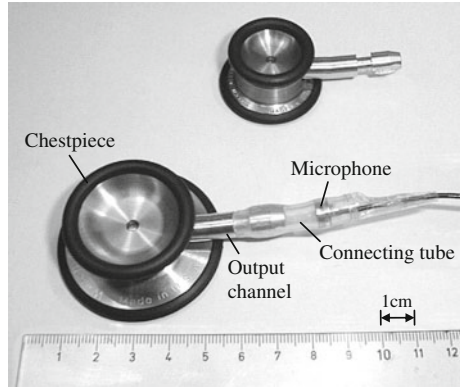
In particular, *body sounds*—mechanical vibrations (and forces) arrived on the skin surface from the inner body—induce mechanical *vibrations of the skin surface*.<sup>45</sup> These vibrations serve as sound sources accessible to the *sensing device* (Fig. 4.1). Profound understanding of diverse coupling aspects offers a solid basis for the *interpretation and diagnostic use of auscultated body sounds*, facilitating also the optimisation of sound auscultation techniques.

As illustrated in Fig. 4.1, a *mixture of body sounds* arrives at the skin level, composed of mainly *heart sounds*, *lung sounds*, and *snoring sounds* (Sects. 4.1.1.1–4.1.1.3). Since different and (almost) independent sound generation mechanisms underlay the different body sounds, it can be assumed that auscultated sounds on the skin represent a mixture of *additive contributions* from the different body sounds. In addition, there are numerous *mutual interrelations* between the different body sounds, as already discussed in Sect. 4.1.1.5.

---

<sup>45</sup> In fact, body sounds cause *skin vibrations* of three different waveform types: *transverse waves* (or shear waves), *longitudinal waves* (or compression waves, compare Fig. 4.19), and a combination of the two types (Ertel et al. 1971). The corresponding *deflection amplitude* of particles involved in the transmission of *acoustic sounds*, e.g., the deflection amplitude of air molecules while transmitting air sounds (Footnote 22), is proportional to the *sound pressure* level and inversely proportional to the *sound frequency*, medium density, and sound velocity (Giancoli 2006). To give a quantitative example, the *deflection in air* at 1 kHz is about 8  $\mu\text{m}$  at the *sound threshold of pain* in humans and less than 0.1 nm (i.e., the approximate size of an atom) at the *threshold of human hearing*.

**Fig. 4.27** Body sound sensors. Small and large stethoscope chestpieces (Fig. 4.31) for the auscultation of high and low frequency sounds, respectively; compare Fig. 4.29



### 4.2.1 Coupling of Body Sounds

It is the *chestpiece* of a standard stethoscope—as illustrated in Fig. 4.27—which forms the basis of the acoustical sensing device<sup>46</sup> (Kaniusas et al. 2005). The chestpiece collects the different *body sounds* by converting mechanical vibrations of *body tissues* of the chest wall (or vibrations of the *skin surface*) into sound vibrations of the *air* within the chestpiece (Fig. 4.1). The airy output of the chestpiece is targeted at a microphone in order to establish an electrical *output signal* proportional to vibrations of the sound pressure at the output.

Body sounds are strongly altered in their properties by *imperfect coupling* from the tissue, throughout the skin, and into the air of the chestpiece. Physical properties of this *acoustical transmission path* have strong implications on the filtering of body sounds; some sound components are attenuated while others are amplified. Dominant *viscoelastic properties* (Footnote 134 in Sect. 2) of the skin render the interaction between tissue-bound body sounds and the resulting skin vibrations even more complex.

It will be shown that the *chestpiece* (Sect. 4.2.1.1) can be considered as an acoustic amplifier with a specific resonance behaviour, whereas the *microphone* (Sect. 4.2.1.2) serves as an (almost ideal) electro-acoustic converter. In addition, the chestpiece is an integrative part of the widely used *stethoscope* (Sect. 4.2.1.3) and thus determines strongly its acoustical transmission.

<sup>46</sup> For the sake of completeness, it should be noted that there are other *acoustical sensing devices*, besides the chestpiece. For instance, piezoelectric sensors shaped as a flat diaphragm can also be used for direct skin attachment and the recording of body sounds.

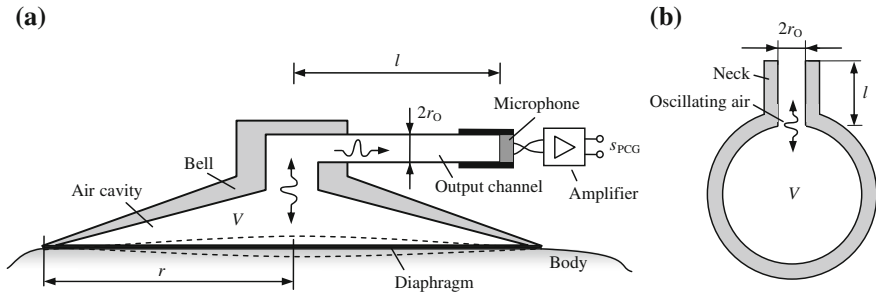


**Fig. 4.28** (a) The structure of the stethoscope chestpiece applied on the skin for the auscultation of body sounds, namely, for the establishment of an acoustic biosignal phonocardiogram  $s_{PCG}$ ; compare Fig. 4.27. (b) The cross section of Helmholtz resonator which resembles the bell of the chestpiece

#### 4.2.1.1 Chestpiece

The *chestpiece* consists of a *circular diaphragm* and a *shallow bell*, as illustrated in Fig. 4.28a. The *acoustic* transmission path of the chestpiece begins with the diaphragm which is in close contact with the skin. The diaphragm follows the *vibration of the skin*<sup>47</sup> which, in turn, follows mechanical forces of inner body sounds. This vibration of the diaphragm creates mechanical *pressure waves* within the air of the bell. The waves travel across the bell towards the output of the chestpiece where a microphone is attached. Consequently, an oscillation of the *microphone membrane* is induced, which finally yields an *electric output signal* (Sect. 4.2.1.2). The diaphragm may also be absent in the chestpiece, as will be discussed later.

#### Diaphragm

The vibration of the circular *diaphragm* (or membrane) exhibits many *vibrational modes* in which all space elements of the membrane oscillate with the same frequency and fixed phase relation. The *fundamental oscillation mode* of the diaphragm is demonstrated in Fig. 4.28a, where the diaphragm's midpoint shows the highest deflection amplitude and the entire diaphragm moves in-phase. In fact, the maximum deflection amplitude (or the maximum sensitivity of the diaphragm) in

<sup>47</sup> The *vibration amplitude of the skin*—may be less than a few  $\mu\text{m}$ , compare Footnote 45—depends strongly on the method of sound recording. For instance, a *massive chestpiece* and a *tight skin contact* would impose a significant mechanical loading on the skin surface. Consequently, the resulting mechanical stress would rise in the skin beneath the chestpiece, which would significantly *limit the mechanical deflection amplitude* of the skin surface; compare with the influence of the *pre-stressed skin* on the acoustic transfer function of the chestpiece (Fig. 4.29 and Footnote 52).

response to an *external excitation* (e.g., to emanating body sounds) occurs at the mechanical *resonance of the diaphragm*, i.e., at the mechanical resonance frequency of the diaphragm. Each mode has its own resonance frequency, known as *eigenfrequency*  $f_{km}$  with  $k$  and  $m$  as mode numbers, according to

$$f_{km} = \frac{c_{km}}{2\pi \cdot r} \cdot \sqrt{\frac{\sigma}{\rho}} = \frac{c_{km}}{2\pi \cdot r} \cdot v. \quad (4.17)$$

Here  $c_{km}$  denotes coefficients for the vibrational mode  $(k, m)$ , whereas  $c_{km}$  is given by the  $m$ th zero of Bessel<sup>48</sup> function of the order  $k$ . Furthermore,  $r$  is the diaphragm radius,  $\rho$  the density of the material the diaphragm is made of,  $v$  the sound propagation velocity along the diaphragm of transverse sound waves, and  $\sigma$  the *mechanical stress* in the diaphragm (due to non-zero surface tension).

It is important to note that  $f_{km}$  represents a series of *non-harmonic eigenfrequencies* while the size of  $f_{km}$  increases with increasing  $k$  and  $m$ . The fundamental oscillation mode  $(0, 1)$  has the lowest  $f_{km} = f_{01}$  with  $c_{km} = c_{01} = 2.4$ . It can be expected that *only the fundamental mode*  $(0, 1)$  is excited in the diaphragm of the chestpiece (Fig. 4.28a), as also indicated in Rappaport and Sprague (1941). This is because of a relatively tight skin contact and, on the other hand, relatively high values of  $f_{km}$  of higher modes, potentially exceeding the frequency range of body sounds (up to 2 kHz). Thus only  $f_{01}$  is practically relevant.

It can be observed from (4.17) that *eigenfrequencies*  $f_{km}$  *increase* with

- *decreasing*  $r$ , i.e., with the diaphragm getting smaller, and, on the other hand, with
- *increasing*  $\sigma$ , i.e., with the rising surface tension (or the pre-stress) of the diaphragm.

Both effects have important *diagnostic consequences*, as will be discussed later.

In fact, the *skin* encompassed by the rim of the bell acts as a *natural diaphragm*, even if the diaphragm of the chestpiece is removed (Fig. 4.28a). The encompassed skin behaves with the properties of a *damped diaphragm* of relatively low  $v$  (from (4.17)). Provided that the *artificial diaphragm* covers the chestpiece, the circular skin region is in tight mechanical contact with this diaphragm and *oscillates concurrently* with the latter. As a result, the *effective diaphragm* consists of

- the artificial diaphragm and
- the natural diaphragm,

---

<sup>48</sup> Friedrich Wilhelm Bessel (1784–1846) was a German astronomer who systematically derived Bessel functions appearing in mathematical descriptions of many physical phenomena, such as the flow of heat or the propagation of electromagnetic waves.

both governing significantly acoustical properties of the chestpiece, especially, of the skin-diaphragm interface (Rappaport and Sprague 1941; Hollins 1971); compare Footnote 52.

## Bell

The diaphragm of the chestpiece is clamped by the *bell* which is usually shaped as a funnel and operates as a *resonating cavity*. In contrast to the resonating cavities from Fig. 4.24, the dimensions of the bell are smaller than the size of  $\lambda$  (in the air, Table 4.1) so that *no standing waves* can be formed in the bell; to be more precise, no dimension of the resonator exceeds  $\lambda/4$ . In fact, the bell serves as a *transducer* which converts the vibration of the diaphragm (i.e., the effective diaphragm or the natural only) into longitudinal sound waves propagating through the air within the cavity (Ertel et al. 1971). Likewise, the resonating cavity is *excited by the diaphragm, absorbs* best a band of sound frequencies around its resonating frequency, and transmits the absorbed sounds towards its output channel (Fig. 4.28a).

As illustrated in Fig. 4.28, the bell with its output channel resembles *Helmholtz*<sup>49</sup> *resonator*, a container of air (or cavity) with a short small-diameter open neck.<sup>50</sup> As long as the dimensions of Helmholtz resonator are smaller than  $\lambda/4$ , i.e., there is no significant pressure variation inside the cavity, a single *resonance frequency*  $f_{HR}$  dominates:

$$f_{HR} = \frac{v}{2\pi} \cdot \sqrt{\frac{A}{V \cdot l'}}. \quad (4.18)$$

Here  $v$  is the sound propagation velocity in the air,  $A$  the cross sectional area of the opening port (or the output channel), i.e.,  $A = \pi \cdot r_O^2$  with  $r_O$  as the radius of the opening port,  $V$  the inner volume of the resonator, and  $l'$  the effective length the oscillating air column has in the opening port. The size of  $l'$  depends on  $r_O$  and is usually approximated as  $l' = l + \pi/2 \cdot r_O$  (Veit 1996) with  $l$  as the geometrical length of the opening port (Fig. 4.28).

<sup>49</sup> Hermann von Helmholtz (1821–1894) was a German scientist and philosopher whose groundbreaking investigations occupied almost the whole field of science, including physiology, physics, electricity, and chemistry.

<sup>50</sup> The function of *Helmholtz resonator* can be summarised as follows. A volume of the air in and near the neck—compare Fig. 4.28b—starts to vibrate in response to *external excitation*. For instance, pushing extra air down the neck into the cavity creates an overpressure in the cavity. After release of the external force, the air rushes out due to the *springiness* (or compressibility) of the air within the cavity. Shortly afterwards, the air pressure inside the cavity undershoots the equilibrium level (i.e., the atmospheric pressure, Footnote 26) because the air in the neck has mass and thus possesses *momentum* when it rushes out. A slight vacuum occurs in the cavity, which then sucks some air back into the cavity. It results in a (damped) oscillation of the air (in and near the neck) into and out of the cavity at a specific *natural frequency*, known as the *resonance frequency*  $f_{HR}$ .

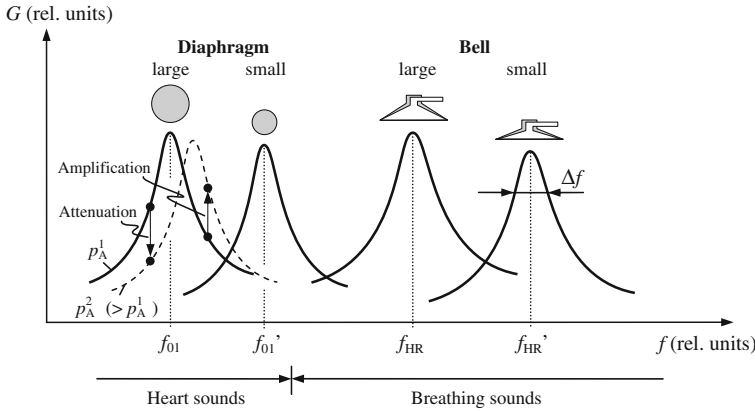


**Fig. 4.29** Contributions of the chestpiece bell (Helmholtz resonator) and the chestpiece diaphragm (Fig. 4.28a) to the acoustic transfer function  $G$  of the chestpiece; compare Fig. 4.32. Large and small bells are compared with each other as well as large and small diaphragms (considering only the fundamental oscillation mode with the eigenfrequency  $f_{01}$ , see (4.17)). The impact of increased application pressure  $p_A$  of the chestpiece (with the diaphragm) on the skin is also indicated for  $p_A^1 < p_A^2$ . Approximate frequency regions of heart sounds and breathing sounds are depicted for comparison

It can be observed from (4.18) that the frequency  $f_{HR}$  increases with

- *increasing*  $A$  because a larger opening accelerates the escape (and the inflow) of the air out of (and into) the cavity, leading to a higher  $f_{HR}$ ;
- *decreasing*  $V$  because less air must move out (and into) the cavity to relieve (and build up) the sound pressure within the cavity towards (and away from) the atmospheric pressure (Footnote 26), leading to faster response times; and
- *decreasing*  $l$  (or  $l'$ ) because a shorter opening port induces less resistance to the oscillating air flow and decreases momentum (inertia) of the oscillating air in the port, leading to a higher  $f_{HR}$ .

Figure 4.29 depicts schematically the *acoustic transfer functions* (or frequency response curves) of the chestpiece *diaphragm and bell*. It is obvious that the diaphragm transmits optimally body sounds into the bell at its  $f_{01}$  (4.17). Sound components below and above  $f_{01}$  are damped because the diaphragm is excited at these frequencies to a lesser extent. Since the *vibration of the diaphragm* is damped, the corresponding resonance curve is widened around  $f_{01}$ , whereas the widening is quantitatively described by the *quality factor*.<sup>51</sup> It can be observed in Fig. 4.29 that

<sup>51</sup> The *quality factor* represents the degree to which an *oscillatory system* is undamped. It is defined as the ratio of the *resonance frequency* (e.g.,  $f_{HR}$  from (4.18)) to the *bandwidth*  $\Delta f$  of the sound oscillation. Here the bandwidth  $\Delta f$  is determined as the difference of two frequencies (above  $f_{HR}$  and below  $f_{HR}$ ) at which the acoustical power left (or dissipated) in the oscillatory system is one-half (or 3 dB less than) its maximum value at  $f_{HR}$ , compare Fig. 4.29. The quality factor  $> 0.5$  represents an *underdamped system* in which oscillations can arise in response to an *external*

the resonance curve moves towards higher sound frequencies with decreasing  $r$  (or increasing  $\sigma$ ). This means that smaller diaphragm or an increased *application pressure*<sup>52</sup> of the chestpiece on the skin facilitates attenuation of lower frequencies ( $< f_{01}$ , Fig. 4.29) and amplification of higher frequencies ( $> f_{01}$ ). In analogy, increased mounting surface tension of the diaphragm (clamped by the bell) or a static excursion (*pre-bending*) of the diaphragm while applied on the skin increases  $\sigma$  and thus raises  $f_{01}$ , e.g., the eigenfrequency  $f_{01}$  moves toward  $f_{01}'$  (Fig. 4.29). Likewise, the auscultation of *high frequency body sounds* or, in analogy, the reduction of *low frequency body sounds*, is favoured by small  $r$  and high  $\sigma$ , which is highly significant in diagnosis<sup>53</sup> of body sounds. In addition, the reduction of low frequency body sounds tends to unmask high frequency body sounds. Usually low frequency sounds are relatively loud and are audible in the first place, *masking*<sup>54</sup> the informative high frequency sounds (usually faint but pathologic) when presented together.

This means that the *attenuation of low frequencies* or *unmasking of high frequencies* is favoured by *decreasing  $r$* ; compare Fig. 4.29 and (4.17). In addition, the efficiency of a deliberately reinforced unmasking by an increased application pressure improves with decreasing  $r$ . This is because the tendency of the application

---

(Footnote 51 continued)

*disturbance* displacing the system from its equilibrium state. Otherwise, the factor  $< 0.5$  represents an *overdamped system* and implies an exponential decay back to the equilibrium state in response to a temporal external disturbance. In other words, lossy materials have lower quality factor and make the response curve (transfer function) wider and lower; i.e.,  $\Delta f$  increases while  $G$  decreases in Fig. 4.29.

<sup>52</sup> The *application pressure of the chestpiece* on the skin is a relevant issue because the varying pressure alters sound filtering characteristics of the diaphragm (Fig. 4.28). In fact, the chestpiece must be used with the principles of a *damped diaphragm* in mind, namely,

- the *lightest* possible application for the auscultation of *low frequency sounds* and
- the *firmest* possible application for the auscultation of *high frequency sounds*.

It is important to note here that increasing application pressure increases not only the pre-stress of the artificial diaphragm but also the *mechanical stress of the skin* region under the diaphragm, the skin encompassed by the rim of the bell. As a result, increased stress of the skin—or increased pre-stress of the *natural diaphragm* so formed (4.17)—contributes to the auscultation of high frequency sound components because the natural diaphragm oscillates concurrently with the *artificial diaphragm*.

<sup>53</sup> From a diagnostic point of view, the effect of the *attenuation of lower frequencies* ( $< f_{01}$ , Fig. 4.29) by simply increasing the *application pressure of the chestpiece* on the chest wall is deliberately used by physicians (Hollins 1971; Ertel et al. 1966b; Abella et al. 1992); compare Footnote 52. That is, increased application pressure favours the detection of high frequency sounds ( $> f_{01}$ , Fig. 4.29) which usually indicate *pathology* (see section “Volume Effects” in Sect. 4.1.2.2) and possess *localising properties* (Footnote 36).

<sup>54</sup> *Masking of body sounds* is important in two respects (Rappaport and Sprague 1941),

- masking of a sound in the presence of other sounds and
- masking of a sound following another sound of considerably large intensity.

In the first case, as a sound mixture becomes more intense, the low pitched sound components (e.g., *heart sounds*) start to dominate because the high pitched components (e.g., *lung sounds*) are masked by peculiar characteristics of human hearing. In the second case, a preceding sound of a comparably great intensity tends to temporarily fatigue the ear, thereby masking a following low intensity sound.

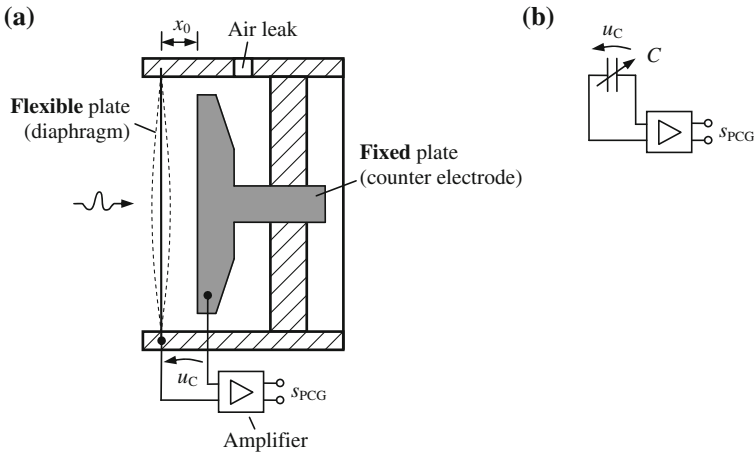


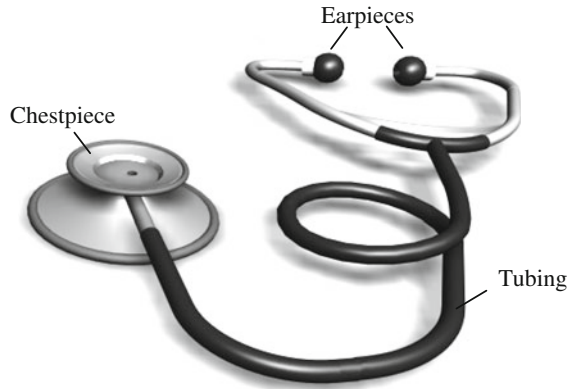
**Fig. 4.30** Condenser microphone as an acousto-electric converter. (a) The principle set-up. (b) The corresponding electrical circuit model

pressure to stretch the skin beneath the diaphragm—the skin operating as a damped *natural diaphragm* (Footnote 52)—increases with decreasing  $r$ . Likewise, this makes the eigenfrequency  $f_{01}$  of the diaphragm of *low  $r$  highly susceptible* to a variation of the *application pressure* (Rappaport and Sprague 1941). Similarly, thick diaphragms and diaphragms with relatively high  $f_{01}$  (in the resting state of the diaphragm) are also very susceptible to the variation of the application pressure. However, a pronounced attenuation of low frequencies also causes a pronounced attenuation of the *total sound intensity* passing through the diaphragm (Rappaport and Sprague 1941), which is a disadvantageous issue in the sound auscultation.

In analogy, the resonance curve of the bell, namely, of *Helmholtz resonator*, moves towards higher frequencies with decreasing volume  $V$  (4.18), facilitating *absorption and transmission* of high frequency body sounds; compare Fig. 4.29. The width of the resonance curve remains almost unchanged; likewise, the *quality factor* (Footnote 51) of Helmholtz resonator—with respect to the sound absorption—increases with decreasing  $V$ .

As shown in Rappaport and Sprague (1941), especially below 200 Hz the bell shows increasing transmission efficiency with increasing  $V$  and increasing (input) diameter of the bell. The authors in Ertel et al. (1966b) demonstrate that the response of the bell to the frequencies above approximately 100 Hz strongly deteriorates with the *bell getting shallow*, whereas the response to lower frequencies below 100 Hz remains almost unchanged. It is likely that, while the bell gets shallow, the resonance frequency  $f_{HR}$  moves to a higher value because of decreasing  $V$ , the *quality factor* of the resonator decreases, and thus the *resonance curve* widens due to increasing frictional losses in the flattened resonator. As reported in Hollins (1971), Ertel et al. (1971), *deep trumpet-shaped bells* provide amplification of body sounds at low frequencies (below approximately 100 Hz) and

**Fig. 4.31** Typical binaural stethoscope including a single chestpiece, flexible tubing, and two earpieces



may also provide amplification at high frequencies (above 100 Hz). In contrast, *shallow bells* provide amplification at low frequencies and predominantly attenuate high frequencies; compare Fig. 4.32. It should be stressed that the latter *amplification* was reported for the combination of the *bell* with a *tubing* connecting to *earpieces* (as intrinsic parts of the standard stethoscope, Fig. 4.31), i.e., the amplification means higher sound intensity at the output of earpieces in comparison with the input of the bell. That is, the reported amplification was also significantly influenced by the sound *transmission pathway in the tubing*, as discussed in Sect. 4.2.1.3. In addition, *bell materials* of moderate density favour the auscultation of low sound frequencies (Hollins 1971).

Furthermore, the larger is the *entrance area of the bell* for the incoming body sounds, the more efficient is the bell at lower frequencies of sounds (Rappaport and Sprague 1941). This behaviour can be attributed to the circular skin region encompassed by the rim of the bell, which was previously referred to as the *natural diaphragm*. That is, increasing  $r$  of the bell (Fig. 4.28a) yields lower  $f_{01}$  of this natural diaphragm (4.17) and thus manifests in higher efficiency of a widely open bell for the recording of low frequency body sounds.

After the discussion of the resonance behaviour of the chestpiece, the *transmission efficiency of the bell* in terms of the resulting *magnitude of acoustic waves* within the bell should be addressed (Hollins 1971; Ertel et al. 1966b; Rappaport and Sprague 1941). Provided a constant excitation of the bell by body sounds at the skin surface, the magnitude of sound in the bell is

- proportional to the *entrance area of the bell*, i.e., to the surface area ( $= \pi \cdot r^2$ ) of the diaphragm, and
- inversely proportional to the *volume*  $V$  to a certain extent (compare Fig. 4.28a).

In fact, the *first criterion* results from the effort to gather body sounds from the largest possible area on the skin. However, increasing surface area is limited by the problem of obtaining a good acoustic seal at the (usually curved) surface of the chest wall. The *second criterion* related to  $V$  follows from the consideration that

body sounds are to be transmitted from the large-area diaphragm (for sound collection) to the small-area output channel (for sound recording); i.e., the inequality  $r \gg r_O$  applies (Fig. 4.28a). Thus an infinitely small  $V$  would produce a maximum variation in the sound pressure (or maximum sound intensity) within the bell because the *spring constant of the air* (such as the effective stiffness of the air) in the bell is inversely proportional to  $V$ . As discussed in Hollins (1971), Rappaport and Sprague (1941), *small internal volumes* of transmission pathways increase the sound magnitude and thus favour the transmission efficiency. In other words, the vibration magnitude of the air in the region of the diaphragm is much less than the vibration magnitude in the region of the output channel, given the inequality  $r \gg r_O$  from above (Fig. 4.28a). However, too small values of  $V$  yield high *frictional resistance* during oscillatory movements of the enclosed air and thus introduce additional transmission losses within the bell (compare Sect. 4.2.1.3).

It is interesting to conclude that the above criteria are optimally met if the inner cavity of the bell has a *shape of a funnel* which shows simultaneously a *minimum*  $V$  and a *maximum*  $\pi \cdot r^2$ . In general, other physical factors also contribute to the transmission losses in the bell such as the *surface hardness* of the bell cavity and *air leaks* between the bell and the clamped diaphragm (Abella et al. 1992; Rappaport and Sprague 1941), as discussed later.

## Diaphragm and Bell

The *interplay between the diaphragm and bell* should be discussed in terms of the transmission acoustics of the chestpiece. In general, the diaphragm attenuates the *entire transmission pattern* of the chestpiece when compared to the same chestpiece with removed diaphragm (Ertel et al. 1966b); compare Fig. 4.32. In particular, the *bell alone* favours the transmission of *low frequency sounds*, whereas these sounds are suppressed by the *diaphragm* which favours the transmission of *high frequency sounds*. Obviously, the difference between the transmission acoustics of the diaphragm and bell results from the different resonance characteristics of the diaphragm and bell; in particular, it results from the differing values of  $f_{01}$  (4.17) and  $f_{HR}$  (4.18) and from the differing quality factors; compare Fig. 4.29.

Rigid *diaphragms* attenuate lower frequencies and thereby accentuate faint, high frequency murmurs (Ertel et al. 1971; Rappaport and Sprague 1941). The diaphragms act as *high-pass filters* within the relevant range of body sounds up to 2 kHz and *unmask* high pitched sounds (Footnote 54). As discussed in Welsby and Earis (2001), Hollins (1971), Ertel et al. (1966b), Rappaport and Sprague (1941), the presence of the diaphragm reduces the magnitude of *masking low frequency sounds* (Footnote 54) and thus allows better characterization and *identification of high frequency sounds*, i.e., of informative and usually pathologic body sounds (Footnote 36). However, as already mentioned, the deliberate unmasking can not be attained without lowering the sensitivity of the chestpiece throughout its entire frequency range (Rappaport and Sprague 1941), as can also be observed in Fig. 4.32.

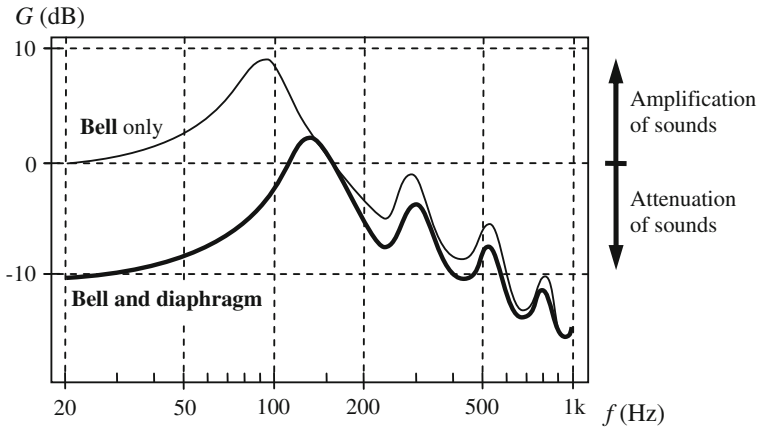


**Fig. 4.32** Acoustic transfer function  $G$  of the stethoscope which includes the chestpiece (with a shallow bell), rubber tubes, and earpieces (Fig. 4.31). The response is defined as the ratio of the sound pressure at the earpiece output to the sound pressure at the chestpiece entrance. The depicted experimental data are taken from Ertel et al. (1966b)

The authors in Hollins (1971), Rappaport and Sprague (1941) show that the *bell alone* is superior to the *bell with the diaphragm* as sound transmitter in the frequency range up to about 400 Hz, whereas the superiority is best at about 300 Hz (Welsby et al. 2003). For sound frequencies above 400 Hz, the reverse is true. The sound *amplification* of the chestpiece (with the diaphragm) was also reported in Kaniusas (2006). According to Abella et al. (1992), in the low frequency range 37–112 Hz typical *chestpieces with the bell alone amplify* body sounds by about 2 up to 12 dB,<sup>55</sup> whereby *chestpieces with the diaphragm attenuate* the sound transmission in most cases by about 5 up to 20 dB; compare Fig. 4.32. In the high frequency range 125–1,000 Hz, *all chestpieces* (with and without the diaphragm) *attenuate* by about 10 dB on average and the attenuation increases with the sound frequency. It should be stressed that the reported quantitative data from Abella et al. (1992) is related to the combination of the chestpiece, tubing, and earpieces (Fig. 4.31), including a strong influence of the tubing on the transmission acoustics (Sect. 4.2.1.3).

Although the *diaphragm* filters out only relatively low frequencies, it is the transmission pattern of the *bell* which predominantly determines whether there is sufficient sound level for high frequencies of sound to be audible (Rappaport and Sprague 1941). Admittedly, there is a trade-off between

<sup>55</sup> Surprisingly, the original *Laennec's stethoscope* (Fig. 1.9), i.e., a simple wooden cylinder, has been shown to amplify body sounds by about 18 dB at the sound frequency of 200 Hz, as noted in Ertel et al. (1966b), Hollins (1971). Surprisingly, this *high amplification* value is comparable with those of modern chestpieces, which makes it difficult to espouse an optimistic view of continuing acoustical improvement of the chestpiece over nearly two centuries (Sect. 1.2.1) aside from the convenience and aesthetic of the modern chestpiece (Fig. 4.31).

- the *detection sensitivity* of body sounds, i.e., the sensitivity is best *with the bell only* and thus without the diaphragm-related losses of sound, and, on the other hand,
- the *characterization* of body sounds (or their identification), i.e., the characterization is best *with the diaphragm* in place.

It follows from the above that physical properties of the chestpiece influence strongly the transmission properties of the different *body sounds* (Sect. 4.1.1). The auscultation of *heart sounds* requires a bell-shaped, open-ended chestpiece (without the diaphragm) which favours the transmission of low frequency body sounds. In contrast, the auscultation of *breathing sounds* such as lung sounds requires a semi-rigid diaphragm covering the flat chestpiece and favouring the identification of high frequency sounds. In the latter case, the *low intensity and high frequency breathing sounds* are unmasked in view of the *high intensity and low frequency heart sounds* (Sect. 4.2.2.3); likewise, high frequency breathing sounds appear to be amplified. In addition, *heart sounds*, i.e., low frequency components of body sounds, can be suppressed by applying *firm application pressure* on the chestpiece bell (Footnote 52). Similarly, *breathing sounds*, i.e., high frequency sound components, are more readily heard with the firmly applied bell or with the diaphragm in use.

### Air Leaks

Finally, it should be noted that *air leaks* between

- the chest wall and the rim of the bell or, in analogy, the chest wall and the diaphragm clamped by the bell,
- the bell and the clamped diaphragm, as well as
- the output channel and the microphone

increase not only the *transmission losses* along the sound propagation pathway but also *reshape the acoustic transfer function* of the chestpiece. Likewise, *leak tightness* (good sealing) favours the transmission efficiency of the chestpiece and, in particular, favours the *auscultation of low frequency body sounds*. That is, air leaks act as *high-pass filters*<sup>56</sup> (Rappaport and Sprague 1941) which reduce the amount of low frequency sound components. In addition, air leaks deteriorate the immunity of the chestpiece to external *sound interferences*.

---

<sup>56</sup> An *air leak*—if there is one in the chestpiece—behaves as a *high-pass filter*. In general, the larger is the air leak the more balanced are the sound pressures inside and outside of the chestpiece because of leaking air down the pressure gradient. While the *frequency of sound* gets lower, there is more time for the air to leak out or in, which equalises the latter pressures to a larger extent. As a result, the transmission of low frequency sounds deteriorates provided that an air leak is present. Conclusively, the air leak acts as a high-pass filter. It is interesting to note that some stethoscopes had even an *adjustable leak valve*, i.e., an adjustable high-pass filter. This valve was used to regulate the amount of (low frequency) *heart sounds* reaching the output of the stethoscope (Rappaport and Sprague 1941).

### 4.2.1.2 Microphone

The *microphone* terminates the *output channel of the chestpiece bell*, as shown in Fig. 4.28a. The microphone is an *acousto-electric converter*. It converts the *sound pressure* variation at the end of the output channel, i.e., at the open neck of Helmholtz resonator (Fig. 4.28b), into an electric signal. This signal serves as the input to a subsequent *signal amplifier*. The output of the amplifier is the *acoustic biosignal phonocardiogram* which instantaneous amplitude is proportional to the instantaneous sound pressure.

The microphone—as illustrated in Fig. 4.30—is usually realised as a *capacitor*, known as the *condenser microphone*. It comprises a metallic diaphragm, i.e., a *flexible plate*, spaced at a short distance from a parallel (massive) *fixed plate*. Both plates act as electrodes of the capacitor. The *sound pressure* variation at the flexible plate bends this plate, which changes the microphone capacitance  $C$ .<sup>57</sup> Likewise, the phase front of the acoustic pressure wave—but not the phase front of the wave of the sound particle velocity—modulates the momentary size of  $C$ . Since the electric charge accumulated on the capacitor plates is nearly constant, the *voltage*  $u_C$  across the capacitor (Fig. 4.30) varies instantaneously in response to the change of  $C$ ,<sup>58</sup>

<sup>57</sup> The *capacitance*  $C$  of the *condenser microphone* from Fig. 4.30b can be approximated as

$$C = \frac{\varepsilon \cdot A}{x_0 + \Delta x},$$

where  $\varepsilon$  is the dielectric permittivity of the air between the plates,  $A$  the cross sectional area of the fixed plate,  $x_0$  the distance between the plates, and  $\Delta x$  the change of this distance due to the sound pressure wave; compare Sect. 6. The above *approximation* holds only if the inequality  $\Delta x \ll x_0$  applies and  $\Delta x$  is constant over the entire  $A$ . It should be noted that the size of  $A$  is nearly equal to the cross sectional area of the flexible plate and that of the output channel, see Fig. 4.28a. For instance, if a *harmonic oscillation* of the flexible plate is assumed (Fig. 4.30a) in response to the sound pressure variation at the flexible plate then  $\Delta x = X \cdot \cos(\omega t)$  with  $X$  as the amplitude of this oscillation.

<sup>58</sup> The *voltage*  $u_C$  across the *capacitor* which carries the *electric charge*  $Q$  is given by

$$u_C = \frac{Q}{C} = \frac{Q}{\varepsilon \cdot A} \cdot (x_0 + \Delta x);$$

compare Footnotes 33 in Sect. 2 and 57. For the sound frequencies

$$f \gg \frac{1}{2\pi \cdot R \cdot C},$$

the level of  $Q$  *remains nearly constant*. Here  $R$  denotes the resistance of the RC circuit within the signal amplifier operating the condenser microphone (Fig. 4.30b). In other words, if the time constant  $R \cdot C$  is much larger than the oscillation period of the sound, i.e., the *operating circuit* is too inert to follow instantaneously the changes in the sound pressure, then the current  $dQ/dt$  through the capacitor is almost zero and  $Q$  *changes* are negligible. The latter condition is fulfilled for typical frequencies of *body sounds*, which yields that the voltage  $u_C$  is a function of  $\Delta x$  only, to be more precise,  $\Delta u_C$  is (approximately) linearly dependent on  $\Delta x$ .

i.e., possible discharge of the capacitor is much slower than the oscillatory change of  $C$  with the sound frequency. In qualitative terms, increasing sound pressure at the flexible plate decreases the distance between the plates, increases the size of  $C$  (Footnote 57) and thus decreases the instantaneous level of  $u_C$  (Footnote 58).

The *waveform of  $u_C$*  follows the *sound pressure* waveform at the flexible plate with a high *waveform and phase fidelity*, provided that the corresponding change of  $C$  is relatively small. In fact, the voltage  $u_C$  goes above and below the bias voltage ( $= u_C$  at  $\Delta x = 0$ , Footnote 58) in synchrony with the momentary sound pressure. The condenser microphone typically shows an *acoustic transfer function* which is practically linear in the frequency range 20–20,000 Hz (within 3 dB range). *Air leaks* in the microphone casing—as shown in Fig. 4.30a—are deliberately used to adjust the acoustic transfer function; compare Footnote 56.

The microphone within the chestpiece applied on the chest wall (Fig. 4.28a), which will be referred to as the *skin microphone*, should be put into perspective with an ambient *room microphone*, i.e., an air-coupled condenser microphone for the registration of body sounds. Obviously, there are strong differences in the *sound coupling*. In order to reach the *skin microphone*, body sounds must pass through the lung parenchyma (as applicable e.g., for *lung sounds*), solid tissues of the mediastinum (applicable for *heart sounds*), pharynx, tracheal and bronchial airways (applicable for *snoring sounds*), and lastly cross the chest skin. Specific filtering effects apply on the transmitted body sounds, as described in Sect. 4.1.2.1.

In contrast, the *room microphone* registers only those body sounds which can be heard by the naked human ear and, to be more precise, which have passed *airway-bound routes* (Fig. 4.23), the pharynx and the nose or mouth cavity (Fig. 4.10). Conclusively, the *room microphone* is applicable for the auscultation of only *lung sounds and snoring sounds*. *Heart sounds* (i.e., low frequency sounds) are not expected to enter respiratory airways—with an aperture towards the room microphone—during their propagation through solid tissue of the mediastinum (Fig. 4.23). Only sounds leaving the pharynx out of the nose or mouth can reach the room microphone; compare also with the effect of small openings on the sound diffraction (see section “Inhomogeneity Effects” in Sect. 4.1.2.2). The latter airy pathway has also a major filtering effect on the transmitted body sounds, amplifying some frequency components and damping others (Fig. 4.24).

Provided the increasing *sound absorption coefficient* with increasing sound frequency (see section “Volume Effects” in Sect. 4.1.2.2) and the dependence of the sound *propagation pathway* on the frequency (see section “Specific Issues” in Sect. 4.1.2.1), it can be concluded that

- *high frequency sounds* tend to dominate in the *room microphone* while
- *low frequency sounds* tend to dominate in the *skin microphone*.

In particular, recording of *heart sounds* requires the *skin microphone* (within the chestpiece). In contrast, *lung and snoring sounds* can be auscultated by both the *room microphone* and the *skin microphone*. The sound sources of breathing sounds (i.e., high frequency sounds) reside in relatively large airways, whereas the

associated sounds induced tend to propagate along (branched) airways outwards from the body towards both microphones.

However, the room microphone is strongly influenced by *environmental noise* and *position of the subject* (namely, position of the subject's airways) relative to the room microphone. In contrast, the skin microphone within the chestpiece (affixed on the chest wall) ideally receives only body sounds emitted by the skin. It is assumed that the chestpiece does not move with respect to the skin, i.e., acoustical *movement artefacts* can be neglected, and there is a *sound-proof isolation* of the skin microphone from ambient noise.

### 4.2.1.3 Stethoscope

The *transmission acoustics of the stethoscope* will be discussed, whose basic component is the chestpiece (Sect. 4.2.1.1). In fact, the stethoscope is acoustically a unique device, in that it accounts for acoustical properties of the human ear<sup>59</sup> (Rappaport and Sprague 1941; Ertel et al. 1966b). A *typical stethoscope*—with a modern realisation illustrated in Fig. 4.31 and its precursor, the original Laennec' stethoscope, illustrated in Fig. 1.9—includes

- the bell-type *chestpiece* for *coupling and amplification* of body sounds (compare Fig. 4.27),
- the (rubber) *tubing* as an intermediate connecting element for sound *transmission*, and
- *earpieces* for sound *delivery* into human ears.

As demonstrated in Fig. 4.32, the transmission and filtering pattern of the stethoscope in the frequency domain, namely, the *acoustic transfer function*, does not show a linear sound amplification but almost *regular amplification peaks* (or weak attenuation peaks) alternating with troughs of attenuation (or troughs of strong attenuation). In particular, the amplitudes of the dominant amplification peaks vary with the sound frequency, which indicates the influence of the transmission acoustics of the *chestpiece*, i.e., the bell only or the bell with the clamped diaphragm (Fig. 4.29). Such acoustic transfer functions have been discussed and published in Ertel et al. (1966a, b, 1971) with their critical review in Hollins (1971) and a follow-up study in Abella et al. (1992).

It can be observed in Fig. 4.32 that the *bell with the diaphragm* strongly attenuates low frequency sounds below more than 100 Hz, contrary to the *bell without the diaphragm*. In the latter case, the first (primary) amplification peak

---

<sup>59</sup> For instance, *human ears* alter the performance of the whole *stethoscope* because earpieces of the stethoscope are terminated with the acoustical impedance of ears and, on the other hand, the latter impedance varies with the sound frequency. As a practical consequence, an *artificial ear*, i.e., a mechanical ear analog with the acoustics of human ears, should be incorporated into experimental systems for the assessment of the objective acoustic transfer functions of stethoscopes (Ertel et al. 1966a, b); compare Fig. 4.32.

occurs at about 100 Hz, the second one occurs at about 300 Hz, whereas other peaks follow at a multiple of about 200 Hz. The presence of the diaphragm lowers the first amplification peak (from about +9 to +2 dB) and shifts this peak to higher frequencies (from about 90 to 130 Hz).

The *undulating pattern* suggests that the *standing waves* within the tubing contribute significantly to the acoustic transfer function of the stethoscope; compare section “Specific Issues” in Sect. 4.1.2.1. In fact, the acoustic propagation lumen within the *tubing* can be approximated as an *open resonating cavity*, compare with Fig. 4.24a. This resonating cavity is *acoustically sealed* at its end with the chestpiece—in analogy with the closed end in Fig. 4.24a—and is *acoustically open* at its end with earpieces—in analogy with the mouth opening in Fig. 4.24a. Consequently, the standing waves arise only when the axial extension of the tubing matches  $\lambda/4$ ,  $3 \cdot \lambda/4$ , or  $5 \cdot \lambda/4$  of sound waves passing through the tubing. A node of the sound pressure and a node of the sound particle velocity result at the opposite ends of the tubing lumen. The resulting *non-harmonic eigenfrequencies* can be calculated according to (4.9), i.e., the sound frequencies at which *body sounds*—more precisely, components of body sounds—are best transmitted through the *tubing* (and even amplified within it) from the chestpiece to earpieces (Fig. 4.31).

In *quantitative terms*, the observed peaks in Fig. 4.32 for the bell without the diaphragm yield—in the context of (4.9)—an axial *extension of the open resonating cavity* of about 86 cm. In particular, the frequencies  $f_F^1 = 100$  Hz and  $f_F^2 = 300$  Hz are assumed to correspond with  $\lambda/4$  and  $3 \cdot \lambda/4$  extensions of the cavity, respectively. This estimated axial extension is the approximate axial length of the typical tubing, which strongly indicates that the acoustic resonating lumen is the lumen of the tubing.

In general, the circular *skin* region beneath the diaphragm, already referred to as the *natural diaphragm* (Sect. 4.2.1.1), should be taken into consideration regarding the *acoustic transfer function* of the chestpiece and, consequently, of the whole stethoscope (Rappaport and Sprague 1941; Hollins 1971). For instance, the *primary amplification peak* in the frequency range of about 100 Hz—as illustrated in Fig. 4.32—can not be expected to arise in praxis, since the depicted experimental data from Ertel et al. (1966b) do not consider this natural diaphragm. In fact, the *eigenfrequency*  $f_{01}$  (4.17) of the natural diaphragm can be even higher than that of the artificial diaphragm clamped by the bell, despite the lightest application of the chestpiece on the skin (Footnote 52). Likewise, the *resonance curve* of the natural diaphragm is located at a relatively high  $f_{01}$  and thus damps the relatively low sound frequencies (at around 100 Hz) which are normally amplified by the bell only. However, it is very difficult to assess quantitatively the behaviour of the natural diaphragm in an experimental way.

As already discussed in Sect. 4.2.1.1, the length and inner diameter of the *tubing* (connecting to earpieces, Fig. 4.31) should be as small as possible because the *inner volume* of the tubing is inversely proportional to the magnitude of the acoustic pressure wave within the tubing. However, the smaller is the inner diameter of the tubing, the higher is the local *frictional resistance*—to which the oscillating air column in the tubing is subjected—and thus the lower is the resulting magnitude of the *pressure wave*. In other words, a *compromise* should be reached between the

inner volume (inner diameter) and the frictional resistance of the tubing. Authors in Rappaport and Sprague (1941), Hollins (1971), Abella et al. (1992) prove experimentally that a *longer tubing* and a *smaller diameter* tend to yield *greater sound reduction*. For instance, an increase in the tubing length from about 8 to 66 cm contributes about 15 dB attenuation of the sound pressure at the sound frequency of 200 Hz. The above effect of the varying tubing length dominates above 100 Hz, whereas the tubing length minimally affects the sound attenuation at frequencies below 100 Hz (Rappaport and Sprague 1941).

Furthermore, the *wall of the tubing* should be sufficiently rigid and the *interior surface* sufficiently smooth to attain maximum transmission efficiency of the tubing (Abella et al. 1992; Rappaport and Sprague 1941). This is because any wall motion and increased frictional resistance reduce the effective variation of the sound pressure in the tubing. In addition, *air leaks* in the tubing also contribute to the sound attenuation (Abella et al. 1992), as discussed in Footnote 56.

## 4.2.2 Registration of Body Sounds

As soon as *body sounds* have been coupled into the *chestpiece* (Sect. 4.2.1.1) and converted into an acoustic biosignal *phonocardiogram* (Sect. 4.2.1.2), body sounds are available for signal analysis and *diagnostic purposes*. That is, the phonocardiogram reflects inner body sounds which, in principle, are *mechanical waves* echoing the *mechanical function* of

- *cardiac system* and
- *respiratory system*.

The following sections will demonstrate *experimental phonocardiograms* recorded from the *heart region on the chest*, as illustrated in Fig. 4.33. *Numerous physiological parameters* and events related to the cardiac and respiratory systems will be derived out of phonocardiograms. Likewise, *multiparametric data* (Sect. 1.4) will be derived from a *single* acoustical sensing device. In particular, the *sensing*

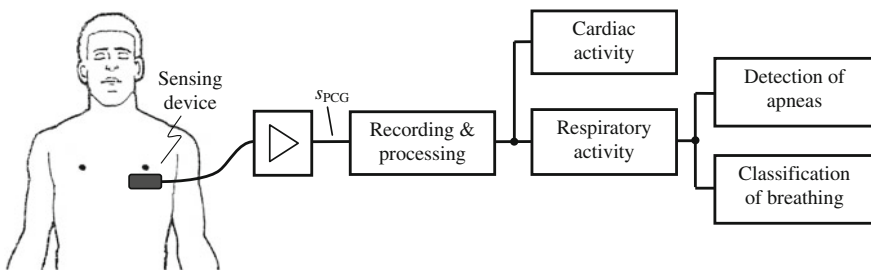


**Fig. 4.33** Registration of body sounds on the chest wall and their multiparametric processing in order to extract various cardiorespiratory parameters; compare Fig. 4.1

*device*, i.e., the chestpiece with a microphone at its output (Fig. 4.28a), was affixed to the chest skin with a double-sided adhesive tape.

The *dynamic nature* of body sounds reveals cardiorespiratory activity. It will be shown that *different frequency ranges* of the different *body sounds* are highly useful for the multiparametric evaluation. For the *chest region*, as summarized in Sect. 4.1.1.5,

- *heart sounds* reside in the frequency range up to 100 Hz,
- *vesicular lung sounds* in the range 100–500 Hz,
- *normal snoring sounds* in the range 100–800 Hz, and
- *obstructive snoring sounds* in the range 100–2,000 Hz.

In particular, *signal power* of the phonocardiogram—compare Footnote 193 in Sect. 3—will be estimated in the different frequency ranges to uncover cardiac and breathing activity. That is,

- signal power  $P_L$  in the low frequency range up to 100 Hz, accounting for *heart sounds* and thus for *cardiac activity*, will be used; as well as
- signal power  $P_W$  in the wide frequency range 100–2,000 Hz, accounting for *vesicular lung sounds* and (normal and obstructive) *snoring sounds* and thus for the *breathing activity*.

Besides the use of the signal power, there are many other (direct and indirect) methods to extract cardiac and breathing activity out of the mixed body sounds (Sect. 3.2.1) emanating from the depths of the body (Fig. 4.1).

### 4.2.2.1 Cardiac Activity

*Heart sounds* arise in the course of cardiac activity, as discussed in Sect. 4.1.1.1 and exemplified in Figs. 4.5, 4.9 and 4.13. An important (vital) physiological parameter of cardiac activity is the heart rate  $f_C$  (Sect. 3.1.1).

Figure 4.34 demonstrates the *registration of  $f_C$*  out of heart sounds during an obstructive *sleep apnea*. In the *time domain* (Fig. 4.34a), heart sounds can clearly be distinguished. Obstructive snoring sounds—surrounding the obstructive sleep apnea (Sect. 4.1.1.4)—yield larger deflection amplitudes than heart sounds (compare Fig. 4.14). In the *frequency domain*, the *signal power  $P_L$*  was estimated, which time course is depicted in Fig. 4.34b. The oscillation of  $P_L$  clearly follows the periodic occurrence of both heart sounds as a unit,<sup>60</sup> as expected from Sect. 4.1.1.1.

---

<sup>60</sup> It should be noted that the *course of  $P_L$*  from Fig. 4.34b does not follow the individual *heart sounds*, i.e., the first or second heart sound, but rather the assembly of both heart sounds as a unit. This is because time intervals for  $P_L$  estimation (of 256 ms duration, Fig. 4.34) are larger than individual durations of heart sounds (usually < 140 ms, Sect. 4.1.1.1). Consequently, the instantaneous level of  $P_L$  is a sliding average over both heart sounds.

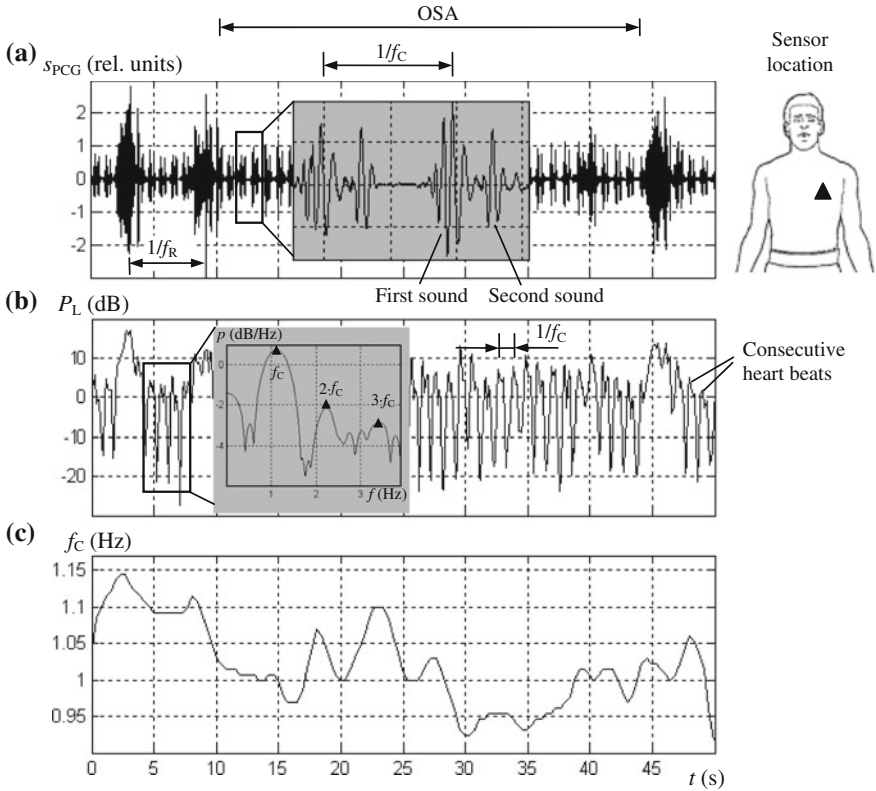


**Fig. 4.34** Assessment of cardiac activity by body sounds in the course of an obstructive sleep apnea (OSA). (a) Acoustic biosignal phonocardiogram  $s_{PCG}$  from the heart region on the chest. (b) Signal power  $P_L$  of  $s_{PCG}$  in the low frequency range up to 100 Hz (calculated for time intervals of 0.256 s duration with 50 % overlap). (c) The heart rate  $f_C$  derived from the time course of  $P_L$  (calculated for time intervals of 4 s duration with 90 % overlap) using signal processing methods in the frequency domain (Footnote 61). The power spectral density  $p$  of  $P_L$  is depicted in (b) for the time interval 3.8–7.8 s, demonstrating multiple peaks at  $f_C$ ,  $2 \cdot f_C$ , and  $3 \cdot f_C$ . The respiratory rate  $f_R$  is also indicated in (a)

Thus, the oscillation rate of  $P_L$  is actually the heart rate  $f_C$  which estimated time course<sup>61</sup> is shown in Fig. 4.34c. It can be observed that  $f_C$  temporarily decreases

<sup>61</sup> In general, the heart rate  $f_C$  can be estimated from the time course of  $P_L$  in different ways:

- In the *time domain*, detection of peaks in  $P_L$  (or, alternatively, zero crossings in  $P_L$ ) could be performed, whereas the difference between the corresponding neighbouring timestamps of peaks (or zero crossings) yields the *instantaneous level* of  $1/f_C$ ; compare Figs. 5.31 and 5.33.
- In the *frequency domain*, peaks in the *power spectral density* of  $P_L$  could be detected, especially those peaks which reside at multiple frequencies. These multiple frequencies would most likely correspond to *multiple harmonics* of  $f_C$ , i.e.,  $f_C$ ,  $2 \cdot f_C$ , ...  $k \cdot f_C$  with  $k$  as the integer index. Since a time interval (window) of  $P_L$  is used for the calculation of the power spectral

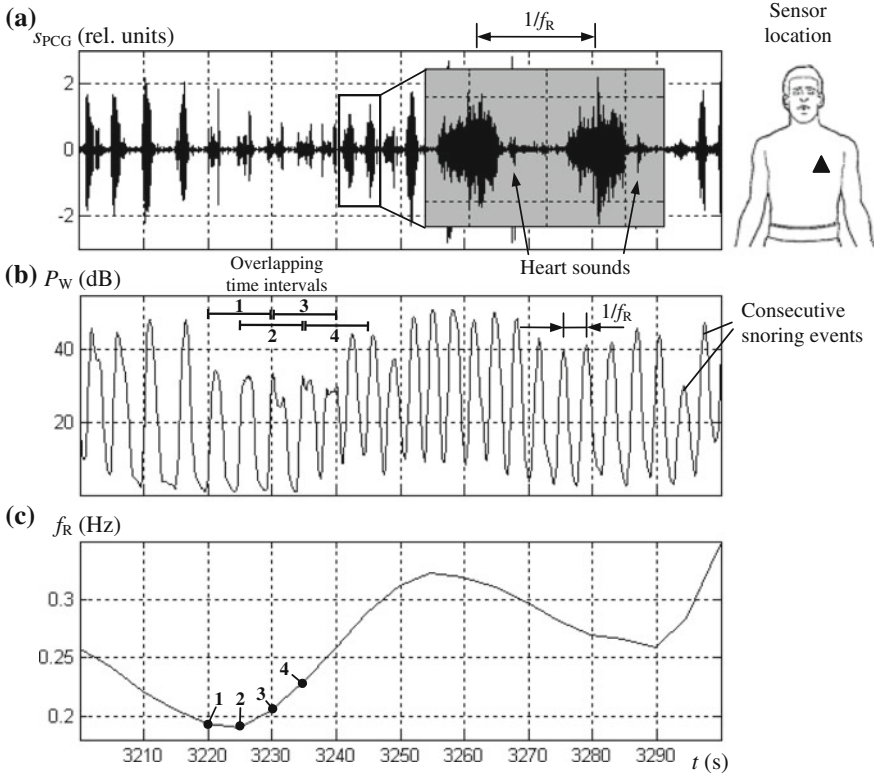


**Fig. 4.35** Assessment of respiratory activity by body sounds in the course of obstructive snoring. **(a)** Acoustic biosignal phonocardiogram  $s_{PCG}$  from the heart region on the chest. **(b)** Signal power  $P_W$  of  $s_{PCG}$  in the wide frequency range 100–2,000 Hz (calculated for time intervals of 0.256 s duration with 50 % overlap). **(c)** The respiratory rate  $f_R$  derived from the time course of  $P_W$  (calculated for time intervals of 10 s duration with 50 % overlap) using signal processing methods in the frequency domain (Footnote 61). Four consecutive time intervals are indicated in **(b)** while the corresponding values of  $f_R$  are indicated in **(c)**

during the apnea, which confirms physiological discussions in section “Ceased Respiration” in Sect. 3.2.1.1 and polysomnographic observations in Fig. 3.9.

(Footnote 61 continued)

density and thus the estimation of  $f_c$ , this method yields only an *average level* of  $f_c$  within this particular time interval (window). The corresponding examples are demonstrated in Figs. 4.34b and 4.35.

### 4.2.2.2 Respiratory Activity

*Breathing sounds*, i.e., lung and snoring sounds, arise in the course of respiratory activity, as discussed in Sects. 4.1.1.2–4.1.1.4 and exemplified in Figs. 4.9, 4.13 and 4.14. An important (vital) physiological parameter of respiratory activity is the respiratory rate  $f_R$  (Sect. 3.1.2).

Figure 4.35 demonstrates the *registration of  $f_R$*  out of breathing sounds during *obstructive snoring*. In the *time domain* (Fig. 4.35a), obstructive snoring sounds can clearly be distinguished (compare Fig. 4.14) with their obvious dominance over heart sounds. In the *frequency domain*, the signal power  $P_W$  was estimated, which time course is depicted in Fig. 4.35b. The consecutive snoring events are clearly visible in the oscillating course of  $P_W$ , whereas the oscillation rate of  $P_W$  is actually the rate  $f_R$ . The estimated time course<sup>62</sup> of  $f_R$  (Fig. 4.35c) reflects clearly the regions of accelerated and decelerated oscillations of  $P_W$  (Fig. 4.35b).

Figure 4.36 demonstrates the course of  $P_W$  during two different *sleep apneas*, namely, an obstructive sleep apnea (Fig. 4.36a) and obstructive sleep hypopnea (Fig. 4.36b). In the case of the *obstructive apnea*—this particular apnea is also demonstrated in Fig. 4.15a—large peaks of  $P_W$  surround this apnea, whereas these peaks correspond to snoring events. In addition, two minor peaks, i.e., *apneic respiratory efforts* (Sect. 3.1.2), reside directly within this apnea. A *residual cardiac component* can be recognized in  $P_W$  (Fig. 4.36a), which oscillates with  $f_C$  and indicates minor contributions of heart sounds above 100 Hz to the power  $P_W$ . In the case of the *obstructive hypopnea* (Fig. 4.36b)—this particular hypopnea is also demonstrated in Fig. 4.16—the amplitude of  $P_W$  peaks is temporarily reduced. This confirms that the intensity of snoring events is diminished during the hypopnea. In fact, *waveform analysis* of  $P_W$  allows for the detection of apneas<sup>63</sup> (Kaniusas 2006); compare Fig. 4.33.

<sup>62</sup> In analogy with Footnote 61, the respiratory rate  $f_R$  can be estimated from the time course of  $P_W$  in the *time domain* (by detecting peaks or zero crossings) and the *frequency domain* (by detecting multiple harmonics of  $f_R$ ).

<sup>63</sup> There are numerous methods to *detect sleep apneas* by *acoustical means*. However, strong variability of snoring sounds—or, in general, variability of breathing sounds—within single subjects and even from one breath to another complicates matters (Sect. 4.1.1.3). In fact, apneas are characterised by

- *increased total intensity of breathing sounds* which surround apneas because of deteriorated pharyngeal dynamics (Itasaka et al. 1999; Pasterkamp et al. 1997b). Thus, intensity thresholds and time interval measurements can be applied for *apnea detection* (Brunt et al. 1997). In addition, obstructive snoring shows increased amount of high frequency components (Sect. 4.1.1.3), so that
- *increased partial intensity of breathing sounds* within a limited (specific) frequency range favours *apnea detection* (McCombe et al. 1995; Penzel et al. 1990; Rauscher et al. 1991; Verse et al. 2000).

Usually, an overestimation of the number of apneas is reported, which were detected by acoustical means. The reliability of apnea detection typically increases with the apnea severity (or with the airway obstruction severity) and with respiratory disturbance index (Sect. 3.1.2). Provided that the *waveform of  $P_W$*  serves as a basis for apnea detection—as illustrated in Fig. 4.36—

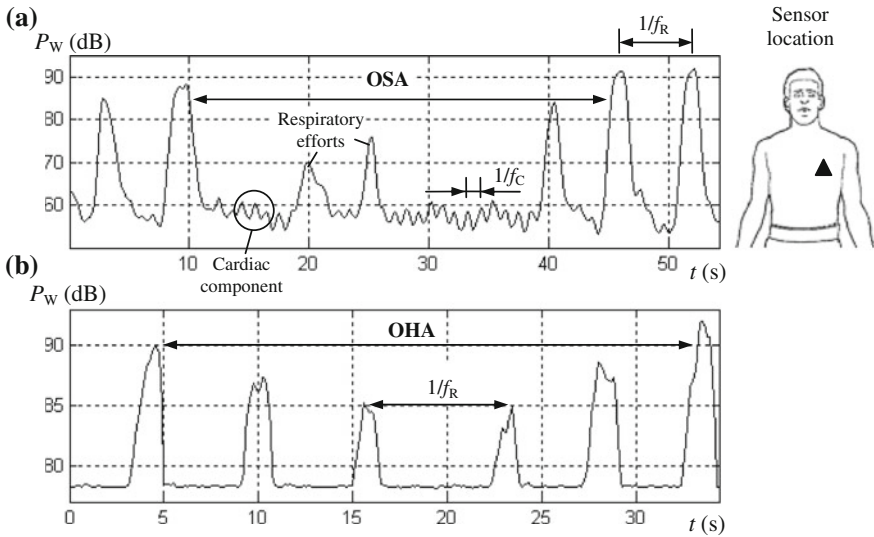


**Fig. 4.36** Detection of apneas by the use of body sounds; in particular, by the use of the acoustic biosignal phonocardiogram  $s_{PCG}$  from the heart region on the chest. **(a)** Signal power  $P_W$  of  $s_{PCG}$  in the wide frequency range 100–2,000 Hz (calculated for time intervals of 0.256 s duration with 50 % overlap) in the course of an obstructive sleep apnea (OSA) which is also illustrated in Fig. 4.15a. **(b)** Signal power  $P_W$  in the course of an obstructive sleep hypopnea (OHA) which is also illustrated in Fig. 4.16. The respiratory rate  $f_R$  and heart rate  $f_C$  are indicated

A simplified *classification of breathing* into

- normal breathing,
- normal snoring, and
- obstructive snoring

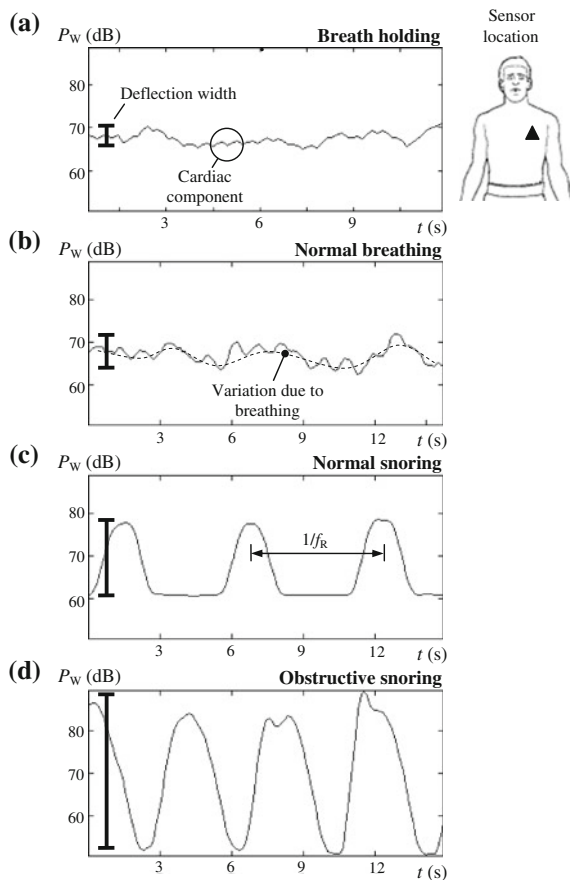
is highly relevant for diagnosis of respiratory diseases (Sects. 3.1.2 and 4.1.1) and can be addressed by body sounds (Fig. 4.33). However, the above classification is not straightforward because of *strong variability of breathing sounds* (i.e., high dispersion of sound characteristics), *fluent transition* from one breathing type to another, and *missing standards* in the classification of breathing.

In fact, the *frequency range* of body sounds extends *beyond 100 Hz* with the *onset of breathing*; compare the frequency range of heart sounds only with that of breathing sounds (Sect. 4.2.2). Furthermore, the effective frequency range of body sounds widens towards *higher frequencies* while breathing becomes progressively *obstructive*; compare the frequency range of normal snoring sounds with that of

(Footnote 63 continued)

adaptive and time-dependent power *thresholds* can be used. The resulting intervals in combination with time limits facilitate apnea detection (Kaniusas 2006).

**Fig. 4.37** Classification of breathing by the use of body sounds; in particular, by the use of the acoustic biosignal phonocardiogram  $s_{PCG}$  from the heart region on the chest. (a) Signal power  $P_W$  of  $s_{PCG}$  in the wide frequency range 100–2,000 Hz (calculated for time intervals of 0.256 s duration with 50 % overlap) during breath holding. (b) Signal power  $P_W$  during normal breathing. (c) Normal snoring. (d) Obstructive snoring. The respiratory rate  $f_R$  is also indicated



obstructive sounds.<sup>64</sup> Thus, it can be expected that the *signal power*  $P_W$  in the wide frequency range 100–2,000 Hz accounts for the different breathing types.

Figure 4.37 demonstrates the course of  $P_W$  for *different types of breathing*. In particular, during breath holding (Fig. 4.37a), the *residual cardiac component*

<sup>64</sup> The appearance of high frequencies in body sounds is a clear indication for approaching *obstruction*. For instance, as discussed in Kaniusas et al. (2005),

- *normal breathing* shows a predominance of low frequency sound power according to  $P_L' > P_M > P_H$ ,
- *normal snoring* yields  $P_L' \geq P_M > P_H$ , and
- *obstructive snoring* shows a predominance of high frequency power corresponding to  $P_L' \geq P_H \geq P_M$ .

Here  $P_L'$  is the signal power of the phonocardiogram in the extended low frequency range up to 300 Hz,  $P_M$  the signal power in the medium frequency range 300–800 Hz, and  $P_H$  the signal power in the high frequency range 800–2,000 Hz; see Sect. 4.1.1.3.

dominates. *Normal breathing* yields a slight superimposed oscillation with  $f_R$  (Fig. 4.37b). In contrast, *normal snoring* causes clear peaks (Fig. 4.37c), whereas *obstructive snoring* induces an even higher peak amplitude (Fig. 4.37d). Likewise, the deflection width of  $P_W$  increases from breath holding to normal breathing, from normal breathing to normal snoring, and, finally, from normal snoring to obstructive snoring.

Since the deflection width of  $P_W$  during *normal breathing* is relatively small (Fig. 4.37b), i.e., lung sounds and silent snoring sounds are almost masked by heart sounds (Figs. 4.9 and 4.13a), it can be expected that here the *registration of  $f_R$*  is more challenging than during normal (or obstructive) snoring. Snoring yields large oscillations of  $P_W$  (Fig. 4.37c, d) and dominates clearly over heart sounds in the time domain, which facilitates the registration of  $f_R$ , as exemplified in Fig. 4.35.

### 4.2.2.3 Spatial Distribution of Body Sounds

It can be expected that the *intensity of body sounds* is unevenly distributed inside the body as well as on the skin surface. This is of high importance if an *optimal auscultation region* for particular body sounds has to be used.

The *uneven spatial distribution* of body sounds is due to the facts that

- *sources* of body sounds usually *lack spatial symmetry* with respect to the body axis. The special asymmetry is primarily given by the massive mediastinum on the left side of the thorax; compare Fig. 4.20 (Sect. 4.1.1). In addition,
- *sound propagation paths* from sound sources to the skin surface cross *heterogeneous tissues* (such as blood, muscles, bones, air, and lung tissue). This yields a highly heterogeneous sound transmission in the body or, broadly speaking, *varying sound absorption* as a function of space (Table 4.1, Sect. 4.1.2). Furthermore,
- *spatial propagation paths* in the body even depend on the characteristic *properties of propagating sounds* (such as sound frequency, Fig. 4.23).

The spatial distribution of the intensity of *heart sounds* was investigated by Kompis et al. (1998). The authors demonstrated that *hypothetical sound sources* (estimated sources) of the *first heart sound* are *spatially limited* to the location of the heart itself. Indeed, given the generation mechanisms of heart sounds (from Sect. 4.1.1.1), the sound sources of the first heart sound can be expected to reside in a constricted space within the heart. This is because atrioventricular valves—the origin site of the first heart sound—are located inside the heart and thus the corresponding sound sources are almost *isolated from outside* the heart (compare Fig. 4.3).

In contrast, the *second heart sound* gives rise to a *spatially scattered* pattern of *hypothetical sound sources*. This pattern shows multiple sound sources which are close to the heart region but are spatially separated from each other. It can be explained by the distal location of semilunar valves, the origin site of the second heart sound. Semilunar valves act as output valves which closure induces vibrations of blood *outside the heart*; these vibrations, in turn, contribute to the scattering of multiple sound sources.

The spatial distribution of the intensity of (vesicular) *lung sounds* on the chest wall is consistent with the origin of these sounds (Sect. 4.1.1.2), as proven by many authors (Pasterkamp et al. 1997a; Kompis et al. 1998, 2001; Loudon and Murphy 1984; Fachinger 2003). During inspiration, *hypothetical sound sources of inspiratory sounds* are widely distributed in terms of *diffuse sources* and reside predominantly in the periphery of the lung (distal airways). In contrast, *expiratory sounds* if heard on the chest wall are rather generated by a *point source* of sound residing in the upper proximal airways. Likewise, expiratory sounds on the chest are similar in quality to tracheobronchial lung sounds.

In addition, the distribution of vesicular *lung sounds* is *asymmetric* on the chest wall (Pasterkamp et al. 1997a, b; Jones et al. 1999; Fachinger 2003). The intensity of surface sounds lateralizes with the *right-over-left dominance* at the anterior upper chest and with the *left-over-right dominance* at the posterior upper chest. This lateralization dominates during *expiration* and for *low frequency sounds*,<sup>65</sup> i.e., for sounds below 300 Hz (Pasterkamp et al. 1997b) or below 600 Hz (Wodicka et al. 1989). In addition, anterior sites show higher intensity of lung sounds than posterior sites.

It is likely that the latter asymmetries are related to

- the *asymmetric* localization of inner *cardiovascular structures* on the left side of the major airways and, on the other hand, related to
- the *asymmetric* morphology and asymmetric distribution of bronchial *airways*.

That is, the preferential coupling of *inspiratory sounds* (i.e., vesicular lung sounds) into the right anterior upper chest could be explained by the massive *mediastinum on the left* side because the mediastinum tends to *attenuate strongly* the propagating sounds towards the left anterior upper chest. In analogy, *expiratory sounds* which propagate towards the left anterior upper chest are also damped by the mediastinum adjacent to the left side of the major airways; expiratory sounds towards the right anterior upper chest are damped to a lesser extent. The effect of the *asymmetric bronchial airways* can be exemplified by the fact that some major left bronchi are directed more posteriorly compared with the right bronchi, which is due to the anterior position and required space of the heart. Obviously, the asymmetric airways favour the left-over-right dominance of the sound intensity at the posterior upper chest because areas of sound generation are closer to the chest wall (or to the skin surface) at posterior sites on the left. It can be observed that the *lateralization* of breathing sounds is compatible with the discussed *concepts* of a

---

<sup>65</sup> It should be noted that *sound frequencies* which *lateralize* best coincide well with sound frequencies which tend to be *coupled* from the airy respiratory airways into the semi-solid mediastinum (or into the lung parenchyma); compare with the frequency dependent propagation of body sounds in Fig. 4.23 and Section “Specific Issues” in Sect. 4.1.2.1. Thus, it can be expected that *heterogeneous tissues* contribute significantly to the *asymmetric transmission* of vesicular lung sounds at relatively *low sound frequencies*. At relatively *high frequencies*, the asymmetry of the sound transmission is weaker because sounds predominantly prefer airway-bound routes and their pathways are more direct, bypassing the damping effect of the *asymmetric mediastinum*.

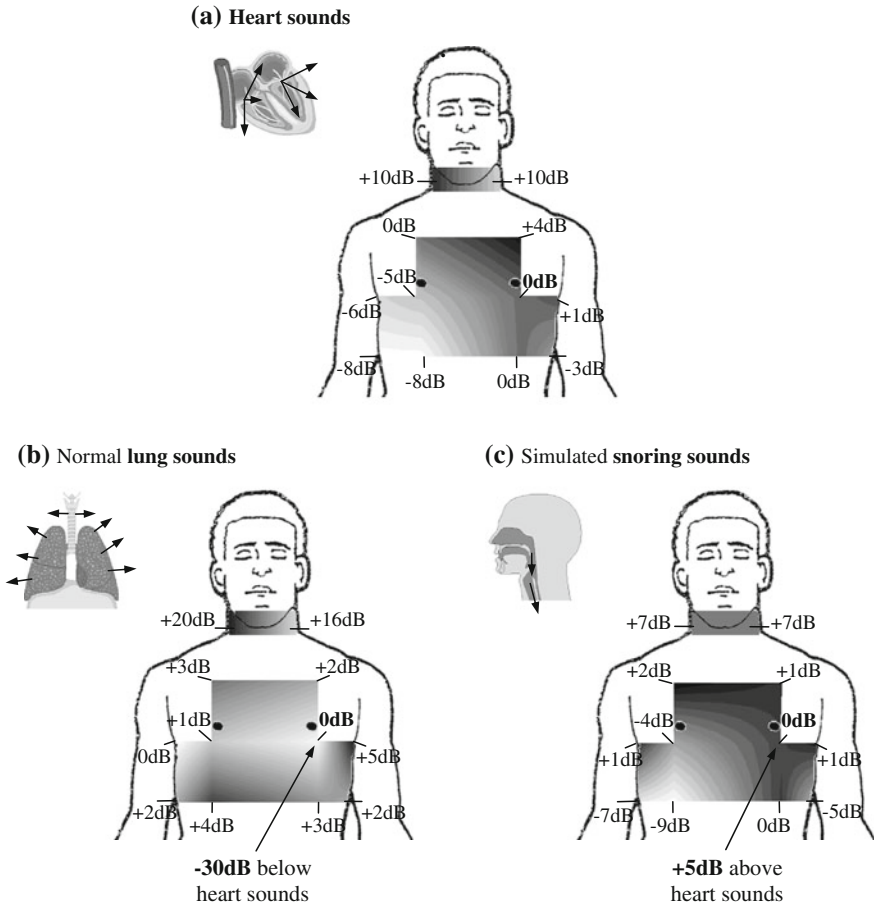


**Fig. 4.38** Spatial distributions of body sounds on the upper body of two healthy male subjects. Local variations of the relative sound intensity are shown, whereas the (averaged) intensity level is given in dB in relation to the heart region on the chest (with the local intensity level of 0 dB). Intensity values between the measured points (denoted by explicit numbers) are generated using bilinear interpolation and are indicated through *grey tones*. (a) Spatial distribution of heart sounds. (b) Distribution of normal lung sounds. In the heart region, the corresponding sound intensity is 30 dB below the local intensity of heart sounds. (c) Distribution of simulated snoring sounds. In the heart region, the corresponding sound intensity is 5 dB above the local intensity of heart sounds

*central origin of expiratory sounds* and a *distributed origin of inspiratory sounds*, when sounds are auscultated on the chest wall (Sect. 4.1.1.2).

The spatial distribution of the intensity of *snoring sounds* on the chest wall can be expected to follow the aforementioned pattern of *expiratory sounds* lateralization because sources of snoring sounds (and those of expiratory breathing sounds, Sect. 4.1.1.2) reside close to the upper airways (Sect. 4.1.1.3). Likewise, this spatial distribution of snoring sounds could be derived from the observed lateralization of

*artificial sounds* introduced at the mouth (close to the pharyngeal airway, the origin site of snoring sounds); i.e., derived from the *passive transmission* of sounds from the mouth to the chest wall (Pasterkamp et al. 1997a). Given the above analogies, it can be expected that *snoring sounds* would lateralize with the *right-over-left dominance* at the anterior upper chest. At the posterior upper chest, snoring sounds can be expected to be only slightly louder on the left, which is similar to the lateralisation of vesicular lung sounds due to the asymmetry of bronchial airways. In addition, anterior sites can be expected to show higher intensity of snoring sounds than posterior sites.

As illustrated in Fig. 4.38, intensities of *body sounds* were assessed on ten different *regions on the thorax*; in particular, at around the 3rd, 5th, and 7th intercostal space anterior left and right, respectively, and around the 5th and 7th intercostal space lateral left and right, respectively (Kaniusas et al. 2005). In addition, sound intensities on the neck, collateral to the trachea, were assessed for comparison. Each subfigure in Fig. 4.38 includes data on the *relative sound intensity* in relation to the heart region on the chest (around the 5th intercostal space anterior left). Thus, the relative sound intensity in this heart region amounts to 0 dB.

In comparison with the heart region, the following *tendencies* can be observed within the spatial distributions of Fig. 4.38:

- *Heart sounds* (Fig. 4.38a)—the sound intensity decreases with increasing distance from the heart, i.e., the intensity shows minimum values of about  $-8$  dB in the lower right thorax region. Conversely, the intensity yields a  $10$  dB maximum at the neck.
- *Lung sounds* (Fig. 4.38b)—the sound intensity shows only slight local differences at the thorax without any evident lateralization, which results from widely distributed sound sources. Strongly enhanced sounds arise at the neck (up to  $+20$  dB) because tracheobronchial sounds (with near sources) are more intense than vesicular sounds (with distant sources); see Sect. 4.1.1.2.
- (Simulated) *snoring sounds* (Fig. 4.38c)—the sound intensity shows a maximum of about  $+7$  dB at the neck because of closely located sources of snoring sounds. The intensity tends to decrease with increasing distance from the neck.

When the discussed distributions of the different body sounds are compared with each other, it can be observed that—in the heart region on the chest—the intensity of *lung sounds* is about  $30$  dB below that of *heart sounds*. *Snoring sounds* in the heart region are stronger by about  $5$  dB than local heart sounds. From a practical point of view, it means that *simultaneous auscultation* of a mixture of the different body sounds *disadvantages (faint) lung sounds*; compare Footnotes 53 and 54. The *heart region* on the chest yields a ratio  $0$  dB:  $-30$  dB:  $+5$  dB (relative intensities of heart: lung:snoring sounds). A more *optimal region* for the simultaneous auscultation of all three body sounds would be the lower right thorax region (around the 7th intercostal space anterior right); it yields a ratio  $-8$  dB:  $-26$  dB:  $-4$  dB or, related to the heart region,  $0$  dB:  $-18$  dB:  $+4$  dB. Another attractive region would be the neck, whereas its right side yields a ratio  $+10$  dB:  $-10$  dB:  $+12$  dB or  $0$  dB:  $-20$  dB:  $+2$  dB, respectively. In any case, lung sounds are at a disadvantage.

The *use of spatial distributions* of the different body sounds may lead to advanced diagnostic methods beyond a simple single spot sound auscultation. This has already been proposed for heart sounds (Leong-Kon et al. 1998) and lung sounds (Kompis et al. 2001). For instance, *acoustic images* of a pathologically consolidated lung—by the use of the spatial distribution of the intensity of lung sounds—differ substantially from images of a healthy lung and thus help to localize abnormalities; compare section “Volume Effects” in Sect. 4.1.2.2. Obviously, the *spatial resolution* of acoustic images can not be expected to resolve differences below approximately 2 cm while localising sound sources. This is because the resolution is determined by the size of  $\lambda$  whose lowest reported values are about 2.3 cm (at  $v = 23$  m/s and  $f = 1$  kHz, see (4.3) and section “General Issues” in Sect. 4.1.2.1).

## References

- M. Abella, J. Formolo, D.G. Penney, Comparison of the acoustic properties of six popular stethoscopes. *J. Acoust. Soc. Am.* **91**(4), 2224–2228 (1992)
- G. Amit, K. Shukha, N. Gavriely, N. Intrator, Respiratory modulation of heart sound morphology. *Am. J. Physiol. Heart Circ. Physiol.* **296**(3), 796–805 (2009)
- R. Beck, M. Odeh, A. Oliven, N. Gavriely, The acoustic properties of snores. *Eur. Respir. J.* **8**(12), 2120–2128 (1995)
- N. Brooks, G. Leech, A. Leatham, Factors responsible for normal splitting of first heart sound. High-speed echophonocardiographic study of valve movement. *Br. Heart J.* **42**(6), 695–702 (1979)
- D.L. Brunt, K.L. Lichstein, S.L. Noe, R.N. Aguillard, K.W. Lester, Intensity pattern of snoring sounds as a predictor for sleep-disordered breathing. *Sleep* **20**(12), 1151–1156 (1997)
- A. Bulling, F. Castrop, J.D. Agneskirchner, W.A. Ovtsharoff, L.J. Wurzinger, M. Gratzl, *Body Explorer. An Interactive Program on the Cross-Sectional Anatomy of the Visible Human Male* (Springer, Berlin, 1997)
- D. Chamier, Unpublished ball pen drawing, Institute of Art and Design, Vienna University of Technology (2014)
- F. Cirignota, Classification and definition of respiratory disorders during sleep. *Minerva Med. Rev.* **95**(3), 177–185 (2004)
- F. Dalmay, M.T. Antonini, P. Marquet, R. Menier, Acoustic properties of the normal chest. *Eur. Respir. J.* **8**(10), 1761–1769 (1995)
- J. Earis, Lung sounds. *Thorax* **47**(9), 671–672 (1992)
- K.R. Erikson, F.J. Fry, J.P. Jones, Ultrasound in medicine—a review. *IEEE Trans. Sonic Ultrason.* **21**(3), 144–170 (1974)
- P.Y. Ertel, M. Lawrence, R.K. Brown, A.M. Stern, Stethoscope acoustics I. The doctor and his stethoscope. *Circulation* **34**(5), 889–898 (1966a)
- P.Y. Ertel, M. Lawrence, R.K. Brown, A.M. Stern, Stethoscope acoustics II. Transmission and filtration patterns. *Circulation* **34**(5), 899–909 (1966b)
- P.Y. Ertel, M. Lawrence, W. Song, Stethoscope acoustics and the engineer: concepts and problems. *J. Audio Eng. Soc.* **19**(3), 182–186 (1971)
- P. Fachinger, Computer based analysis of lung sounds in patients with pneumonia—Automatic detection of bronchial breathing by Fast-Fourier-Transformation (in German: Computerbasierte Analyse von Lungengeräuschen bei Patienten mit Pneumonie—Automatische Detektion des Bronchialatmens mit Hilfe der Fast-Fourier-Transformation). Dissertation, Philipps-University Marburg, (2003)
- D.C. Giancoli, *Physics* (in German: Physik). Pearson Studium (2006)

- L.J. Hadjileontiadis, S.M. Panas, in *Nonlinear Separation of Crackles and Squawks from Vesicular Sounds Using Third-Order Statistics*. Proceedings of the 18th Annual EMBS International Conference, vol. 5, (1996), pp. 2217–2219
- L.J. Hadjileontiadis, S.M. Panas, Adaptive reduction of heart sounds from lung sounds using fourth-order statistics. *IEEE Trans. Biomed. Eng.* **44**(7), 642–648 (1997a)
- L.J. Hadjileontiadis, S.M. Panas, Separation of discontinuous adventitious sounds from vesicular sounds using a wavelet-based filter. *IEEE Trans. Biomed. Eng.* **44**(12), 1269–1281 (1997b)
- W. Hohenhorst, Unpublished image data, Clinic of Otolaryngology, Alfried Krupp Hospital, Germany (2000)
- P.J. Hollins, The stethoscope. Some facts and fallacies. *Br. J. Hosp. Med.* **5**, 509–516 (1971)
- K. Ishikawa, T. Tamura, Study of respiratory influence on the intensity of heart sound in normal subjects. *Angiology* **30**(11), 750–755 (1979)
- Y. Itasaka, S. Miyazaki, K. Ishikawa, K. Togawa, Intensity of snoring in patients with sleep-related breathing disorders. *Psychiatry Clin. Neurosci.* **53**(2), 299–300 (1999)
- V.K. Iyer, P.A. Ramamoorthy, Y. Ploysongsang, Autoregressive modeling of lung sounds: characterization of source and transmission. *IEEE Trans. Biomed. Eng.* **36**(11), 1133–1137 (1989)
- A. Jones, R.D. Jones, K. Kwong, Y. Burns, Effect of positioning on recorded lung sound intensities in subjects without pulmonary dysfunction. *Phys. Ther.* **79**(7), 682–690 (1999)
- E. Kaniusas, Multiparametric physiological sensors. Habilitation theses, Vienna University of Technology, 2006
- E. Kaniusas, in *Acoustical Signals of Biomechanical Systems*, ed. by C.T. Leondes. Biomechanical Systems Technology, vol. 4 (World Scientific Publishing, Singapore, 2007), pp. 1–44
- E. Kaniusas, H. Pfützner, B. Saletu, Acoustical signal properties for cardiac/respiratory activity and apneas. *IEEE Trans. Biomed. Eng.* **52**(11), 1812–1822 (2005)
- T. Koch, S. Lakshmanan, K. Raum, M. Wicke, D. Mörlein, S. Brand, in *Sound Velocity and Attenuation of Porcine Loin Muscle, Backfat and Skin*. Proceedings of the International Federation for Medical and Biological Engineering, vol. 25, issue 13 (2010), pp. 96–99
- M. Kompis, H. Pasterkamp, Y. Oh, Y. Motai, G.R. Wodicka, in *Spatial Representation of Thoracic Sounds*. Proceedings of the 20th Annual EMBS International Conference, vol. 20, issue 3 (1998), pp. 1661–1664
- M. Kompis, H. Pasterkamp, G.R. Wodicka, Acoustic imaging of the human chest. *Chest* **120**, 1309–1321 (2001)
- D. Leong-Kon, L.G. Durand, J. Durand, H. Lee, in *A System for Real-Time Cardiac Acoustic Mapping*. Proceedings of the 20th Annual EMBS International Conference, vol. 20, issue 1 (1998), pp. 17–20
- C. Lessard, M. Jones, Effects of heart valve sounds on the frequency spectrum of respiratory sounds. *Innov. Technol. Biol. Med.* **9**(1), 116–123 (1988)
- G. Liistro, D. Stanescu, C. Veriter, Pattern of simulated snoring is different through mouth and nose. *J. Appl. Physiol.* **70**(6), 2736–2741 (1991)
- R. Loudon, R.L.H. Murphy, Lung sounds. *Am. Rev. Respir. Dis.* **130**(4), 663–673 (1984)
- A.W. McCombe, V. Kwok, W.M. Hawke, An acoustic screening tool for obstructive sleep apnoea. *Clin. Otolaryngol.* **20**(4), 348–351 (1995)
- E. Meyer, E.G. Neumann, *Physical and Technical Acoustics* (in German: Physikalische und technische Akustik) (Friedrich Vieweg & Sohn, Braunschweig, 1975)
- R. Mikami, M. Murao, D.W. Cugell, J. Chretien, P. Cole, J. Meier-Sydow, R.L. Murphy, R.G. Loudon, International Symposium on lung sounds. Synopsis of proceedings. *Chest* **92**(2), 342–345 (1987)
- M. Moerman, M. De Meyer, D. Pevernagie, Acoustic analysis of snoring: review of literature. *Acta Otorhinolaryngol. Belg.* **56**(2), 113–115 (2002)
- A.K. Ng, T.S. Koh, E. Baey, T.H. Lee, U.R. Abeyratne, K. Puvanendran, Could formant frequencies of snore signals be an alternative means for the diagnosis of obstructive sleep apnea? *Sleep Med.* **9**(8), 894–898 (2008)

- W.W. Nichols, M.F. O'Rourke, *McDonald's Blood Flow in Arteries: Theoretical, Experimental and Clinical Principles* (Hodder Arnold Publication, London, 2005)
- H. Pasterkamp, S. Patel, G.R. Wodicka, Asymmetry of respiratory sounds and thoracic transmission. *Med. Biol. Eng. Comput.* **35**(2), 103–106 (1997a)
- H. Pasterkamp, S.S. Kraman, G.R. Wodicka, Respiratory sounds, advances beyond the stethoscope. *Am. J. Respir. Crit. Care Med.* **156**(3), 974–987 (1997b)
- Y. Peng, Z. Dai, H.A. Mansy, R.H. Sandler, R.A. Balk, T.J. Royston, Sound transmission in the chest under surface excitation: an experimental and computational study with diagnostic applications. *Med. Biol. Eng. Comput.* **52**, 695–706 (2014)
- T. Penzel, G. Amend, K. Meinzer, J.H. Peter, P. Wichert, MESAM: a heart rate and snoring recorder for detection of obstructive sleep apnea. *Sleep* **13**(2), 175–182 (1990)
- J.R. Perez-Padilla, E. Slawinski, L.M. Difrancesco, R.R. Feige, J.E. Remmers, W.A. Whitelaw, Characteristics of the snoring noise in patients with and without occlusive sleep apnea. *Am. Rev. Respir. Dis.* **147**(3), 635–644 (1993)
- R.M. Rangayyan, *Biomedical Signal Analysis: A Case-Study Approach*. IEEE Press Series in Biomedical Engineering (Wiley Interscience, New York, 2002)
- M.B. Rappaport, H.B. Sprague, Physiologic and physical laws that govern auscultation, and their clinical application. The acoustic stethoscope and the electrical amplifying stethoscope and stethograph. *Am. Heart J.* **21**(3), 257–318 (1941)
- H. Rauscher, W. Popp, H. Zwick, Quantification of sleep disordered breathing by computerized analysis of oximetry, heart rate and snoring. *Eur. Respir. J.* **4**(6), 655–659 (1991)
- D.A. Rice, Sound speed in pulmonary parenchyma. *J. Appl. Physiol.* **54**(1), 304–308 (1983)
- T.D. Rossing, *Springer Handbook of Acoustics* (Springer, New York, 2007)
- B. Saletu, M. Saletu-Zyhlarz, *What You Always Wanted to Know About the Sleep* (in German: Was Sie schon immer über Schlaf wissen wollten). (Ueberreuter, Vienna, 2001)
- J. Schäfer, A simple procedure for quantitative and time coded detection of snoring sounds in apnea and snoring patients (in German: Ein einfaches Verfahren zur quantitativen und zeitcodierten Erfassung von Schnarchgeräuschen bei Apnoikern und Schnarchern). *Laryngol. Rhinol. Otol.* **67**(9), 449–452 (1988)
- J. Schäfer, *Snoring, Sleep Apnea, and Upper Airways* (in German: Schnarchen, Schlafapnoe und obere Luftwege) (Georg Thieme, Stuttgart, 1996)
- M. Sergi, M. Rizzi, A.L. Comi, O. Resta, P. Palma, A. De Stefano, D. Comi, Sleep apnea in moderate-severe obese patients. *Sleep Breath.* **3**(2), 47–52 (1999)
- F. Series, I. Marc, L. Atton, Comparison of snoring measured at home and during polysomnographic studies. *Chest* **103**(6), 1769–1773 (1993)
- S. Silbernagl, A. Despopoulos, *Pocket-Atlas of Physiology* (in German: Taschenatlas Physiologie) (Georg Thieme, Stuttgart, 2007)
- F. Trendelenburg, *Introduction into Acoustics* (in German: Einführung in die Akustik) (Springer, Berlin, 1961)
- I. Veit, *Technical Acoustics* (in German: Technische Akustik) (Vogel, Würzburg, 1996)
- T. Verse, W. Pirsig, B. Junge-Hülsing, B. Kroker, Validation of the POLY-MESAM seven-channel ambulatory recording unit. *Chest* **117**(6), 1613–1618 (2000)
- H.K. Walker, W.D. Hall, J.W. Hurst, *Clinical Methods: The History, Physical, and Laboratory Examinations* (Butterworth, Boston, 1990)
- P.D. Welsby, J.E. Earis, Some high pitched thoughts on chest examination. *Postgrad. Med. J.* **77**, 617–620 (2001)
- P.D. Welsby, G. Parry, D. Smith, The stethoscope: some preliminary investigations. *Postgrad. Med. J.* **79**, 695–698 (2003)
- Wikipedia, Free encyclopedia (2010), <http://en.wikipedia.org>
- K. Wilson, R.A. Stoohs, T.F. Mulrooney, L.J. Johnson, C. Guillemainault, Z. Huang, The snoring spectrum: acoustic assessment of snoring sound intensity in 1139 individuals undergoing polysomnography. *Chest* **115**, 762–770 (1999)
- G.R. Wodicka, K.N. Stevens, H.L. Golub, E.G. Cravalho, D.C. Shannon, A model of acoustic transmission in the respiratory system. *IEEE Trans. Biomed. Eng.* **36**(9), 925–934 (1989)



<http://www.springer.com/978-3-662-45105-2>

Biomedical Signals and Sensors II  
Linking Acoustic and Optic Biosignals and Biomedical  
Sensors  
Kaniusas, E.  
2015, XVII, 217 p. 75 illus., 8 illus. in color., Hardcover  
ISBN: 978-3-662-45105-2